Operant EEG-based BMI:

Learning and consolidating device control with brain activity

Nuno João Machado Loureiro

Dissertation presented to obtain the Ph.D degree in Neuroscience

Instituto de Tecnologia Química e Biológica António Xavier | Universidade Nova de Lisboa

Oeiras,
December, 2019

UNIVERSIDADE NOVA DE LISBOA

Operant EEG-based BMI:

Learning and consolidating device control with brain activity

Nuno João Machado Loureiro

Dissertation presented to obtain the
Ph.D degree in Neuroscience
Instituto de Tecnologia Química e Biológica António Xavier | Universidade Nova de Lisboa

Research work coordinated by:

Oeiras, December, 2019

Operant EEG-Based BMI: Learning And Consolidating Device Control With Brain Activity

Nuno João Machado Loureiro

A Dissertation
Presented To The Faculty
Of Universidade Nova De Lisboa
In Candidacy For The Degree
Of Doctor Of Philosophy

Supervised By: Rui M. Costa And José Del R. Millán

International Neuroscience Doctoral Programme
Champalimaud Research
Lisbon, Portugal

2019

ACKNOWLEDGEMENTS

And here we are! This has been a long road and I am grateful for all the amazing people that made this journey so much more enjoyable and meaningful. I am happy that the time to thank them has finally arrived.

To my Ph.D. advisors, Rui and José, thank you for accepting me as your student and for welcoming me into your labs.

José, my visits to your lab were invaluable for this work. Thank you for your guidance on the design of the experiments and all the support throughout my Ph.D. Thank you to the CNBI lab at EPFL, and in particular to Simis, I truly appreciate the help you gave me during my visits.

Rui, I admire your superhuman talent to always find the bright side of the road, and to point it out to everyone who listens. You are a true example in life and in science and I am lucky to have you as a mentor and a friend. I will keep many fond memories of your wise, inspirational words, always said at just the right moment. As a new door opens, I look forward to the next adventure and to many more of those moments.

Special thanks to Vitor, for being there in every twist and turn, this work would not exist without you. Thank you for always being available and willing to help searching for the answers (yes, I know the answer is $\pi/2$). I had a lot of fun during these years, and you were certainly responsible for a big part of it.

To the Costa lab mates, for making the work environment feel like home. For all the discussions and all the wisdom but mostly for being a family. You are an amazing group of human beings! In particular, I have to single out a few people from the lab. I have to thank Cris, for all the *galões* in the early mornings, when everyone else was still asleep. For teaching me how to navigate the waters, always making sure that my compass was pointing in the right direction. To Ana, for being *"mais do que uma mãe para mim"*. Thank you for your unlimited generosity and for all the help. To Ivo, Ricardo and Andreas for the exciting discussions and timely advice. To Vivek, for the engineering exchanges, and the silly dances in the office. To Fernando for the countless arguments about technology vs product. To Marcelo and Joaquim, for teaching me about the brain, helping me understand my results better and overall for making me a better scientist.

To Tim, for the collaboration with the aircraft simulator and for taking us to the best *Schweinshaxe* in town. Multiple times.

To my thesis committee, Christian and Noam, for their suggestions and comments on my work, and for pushing me to graduate!

To Teresa Dias and Teresa Carona, for patiently fixing the problems when I was less than diligent with bureaucracy. To Mariana, for always finding a way to squeeze a time slot in the boss' agenda.

To Albino and the Neuropsychiatry unit, for the discussions and guidance on conducting research with humans. In particular to Gonçalo for the last minute save.

To the software (Baúto, Cachitas, Luís and Ricardo) and hardware (Artur, Dário, Filipe and Paulo) platforms, for the environment you created when we moved into your floor. Probably not so productive, but definitely much more enjoyable.

To Antonia and Madalena, for bringing joy when I most needed it. For being confidants over many coffee breaks.

To my INDP classmates, for sharing the pain and joy of going through this journey together. To Nuno and Ritinha, for the puzzles and laughs. To Marina and Michael for broadening my horizons, and for always making the time to help me. To Hedi, for all the conversations over pizzas, and for partnering in a parallel journey that consumed many weekends and may help many fellow scientists.

To the CNP community, for providing the perfect balance between seriousness and fun, making it the best possible environment a Ph.D. student can hope for.

To Gil, Moita and Alves, for the philosophical discussions that often extended well into the late nights and for making sure I wouldn't get rusty in my Physics and Engineering.

To my family, for always making me feel welcomed even after I disappear for long periods at a time. To my uncle Miguel for encouraging my pursuit of a Ph.D.

To my sisters, Inês e Carolina, for your support, the silly games and for putting up with me during the stressful times.

To my parents, for their unconditional support and love. Your values and your education are why I can write this thesis today. I owe you who I am.

To Louise for making me happy during all these years and for patiently bearing with me, always with a smile :)

... This work would not exist without you. Thank you all!

“For the things we have to learn before we can do them,
we learn by doing them.”

— Aristotle In Nicomachean Ethics (350 B.C.E)

RESUMO

Os animais têm uma capacidade notável de se adaptar ao ambiente que os rodeia e que está em constante mudança. Como animais, fazemo-lo aprendendo novas ações motoras e aperfeiçoando-as através de tentativa e erro, selecionando ações que anteriormente originaram resultados favoráveis em detrimento de ações que geraram resultados negativos. Está bem estabelecido que a aprendizagem de novas ações físicas é acompanhada por mudanças na atividade neuronal no córtex e no estriado. Milhões de pessoas em todo o mundo sofrem de condições que limitam a sua mobilidade e capacidade de produzir ações físicas. As Interfaces Cérebro-Máquina (ICM) transformam diretamente a atividade neuronal em sinais de controlo para dispositivos, sem a necessidade de comandos motores, podendo ajudar a restaurar ou substituir a função perdida desses pacientes. Importantes estudos em ICMs demonstraram que os animais são capazes de usar feedback para modular a atividade neuronal e que aprender a controlar novos padrões de ICM requer plasticidade cortical e no estriado, semelhante ao que acontece durante aprendizagem motora. No entanto, está ainda por demonstrar que uma abordagem de aprendizagem operante possa ser usada para controlar um padrão complexo e de múltiplas bandas de atividade de EEG. Aprender a controlar um padrão complexo de EEG, não relacionado com atividade motora, exigiria estabelecer uma nova ligação entre a atividade neuronal e as ações numa tarefa, ligação essa que teria que ser aprendida *de novo,* e seria, portanto, uma conexão natural à ação desejada.

Na primeira parte desta dissertação, desenvolvemos um novo paradigma de aprendizagem operante com uma tarefa de ICM baseada em EEG para testar se sujeitos são capazes de controlar um complexo padrão de EEG.

O ICM implementa um transcodificador constante, dependente de um rácio de quatro bandas de EEG, que converte a atividade neuronal na posição de um cursor num ecrã e que os sujeitos precisam de controlar continuamente. Como o transcodificador é independente de qualquer plano motor preexistente, os sujeitos têm que aprender *de novo* uma nova ligação entre o padrão de EEG e a posição do cursor. Nesta tese mostramos que os sujeitos aprendem rapidamente a modular a atividade de EEG para aumentar o desempenho na tarefa, e que essa atividade é refinada ao longo do treino. Observamos ainda que a aprendizagem é consolidada ao longo do tempo e pode ser facilmente recuperada em cada dia de treino, bem como após um intervalo longo de três semanas no treino.

Num segundo projeto, investigamos a aplicação da aprendizagem operante da ICM num cenário real: demonstramos a implementação bem-sucedida de uma ICM operante no controlo de um simulador de aeronave.

Por fim, descrevemos o desenvolvimento de um novo *headset* de ICM baseado em EEG, capaz de gravar sinais de alta qualidade com elétrodos secos e ativos. Este *headset* é o primeiro sistema capaz de gravar, processar e transmitir sinais para uma ICM operante, permitindo a extensão desta tecnologia a um público-alvo mais alargado.

Em suma, a ICM proposta nesta tese, baseada numa aprendizagem operante de sinais de EEG, juntamente com as suas aplicações práticas, oferece uma alternativa aos métodos de descodificação de atividade neuronal predominantes no campo. A capacidade de aprendizagem dos sujeitos tem um papel central nesta abordagem. Aqui, demostramos pela primeira vez que os sujeitos conseguem aprender a estabelecer um novo vínculo entre um padrão de EEG complexo e comandos para controlar um dispositivo.

SUMMARY

Animals have a striking capacity to adapt to their surrounding, ever-changing environment. As animals, we do this by learning new motor actions and perfecting them through trial and error, selecting actions that previously led to positive outcomes over actions that did not. It is well established that the learning of new physical actions is accompanied by changes in neural activity in the cortex and the striatum.

Millions of patients worldwide suffer from conditions that limit their mobility and capacity to produce physical actions. Brain-Machine Interfaces (BMI) have the capability to bypass motor impairment and can help restore or substitute the lost function of these patients. BMIs directly translate neural activity into control signals for external devices. Prominent studies in BMIs, have demonstrated that animals are capable of relying on feedback to shape neural activity and that learning a new BMI pattern requires cortical and striatal plasticity, similarly to what is seen during motor learning.

It remains to be demonstrated that feedback and an operant learning approach can be used for control of a complex, multiband pattern of EEG activity. Learning to control a complex EEG pattern, unrelated to motor activity, would require establishing a new link between the activity and task actions. This link would need to be learned *de novo* and would provide a natural connection to the desired task action.

In the first part of this thesis, we developed a novel operant learning approach with a EEG-based BMI task to test whether subjects can learn to control a complex, multiband EEG pattern. The BMI implements a fixed transcoder, dependent on a ratio of four EEG bands, that converts neural activity into cursor position on a screen, which the subjects need to continuously control. Because the transcoder is independent of a pre-existent motor plan, a link between the EEG pattern and cursor position needs to be learned *de novo*. We demonstrated that users can rapidly learn to modulate their neural activity to more frequently produce a rare EEG-pattern in order to increase success in task, and that the EEG activity is refined with training. We further showed that the learning is consolidated over time and can be readily recalled during each training day as well as after a long intermission in training.

In a second project, we investigated the application of the operant learning BMI in a real-world scenario. We demonstrated the successful implementation of the operant BMI in the control of an aircraft simulator. Finally, we described the development of a novel, standalone EEG-based headset, capable of recording high-quality signals with active dry-electrodes. This headset fully records, processes, and transmits signals for operant BMI applications, allowing for a more extensive reach of this technology.

Taken together, our novel operant EEG-based BMI, along with its practical applications, offers an alternative to the prevalent decoder methods. The learning capabilities of the users are given a central role in this approach, and we show for the first time, to our knowledge, that subjects can learn to establish a new link between a complex, multiband EEG pattern and an effector.

CONTENTS

ABBREVIATIONS LIST

AP Action Potential

BCI Brain Computer Interface

BMI Brain-Machine Interface

ECOG Electrocorticography

EMG Electromyography

EOG Electrooculography

EPFL École Polytechnique Fédérale de Lausanne

ERP Event-Related Potentials

ErrP Error-Related Potentials

FES Functional Electrical Stimulation

FFT Fast Fourier Transform

fMRI functional Magnetic Resonance Imaging

LFP Local Field Potentials

LIS Locked-in Syndrome

MEA Multi electrode array

MI Motor Imagery

PSD Power Spectral Density

RL Reinforcement Learning

SCP Slow Cortical Potentials

SMR Sensorimotor Rhythms

SNR Signal-to-Noise Ratio

SSVEP Steady-State Visually Evoked Potentials

TOBI Tools for Brain-Computer Interaction

1

INTRODUCTION

Whether you are reading this thesis on paper or screen, it is easy to take for granted all the highly specialized movements you are doing at this very moment just to go through each page. Just to turn a page, you have to reach for and grasp it, turn it and let go at the precise moment not to rip it. If you're reading on a screen, you have to scroll through with the mouse or keyboard. The actions of scrolling through this document took you days or even months to master until you could perform them, almost flawlessly and unconsciously, every time. It is indeed fascinating to think about how we start with somehow uncontrollable movements in early life (motor babbling) and, by trial and error, we learn to tailor them to meet our intentions (Costa, 2011). We repeat more frequently the actions that lead to positive reinforcements (Skinner, 1938; Thorndike, 1898), and these actions become more stereotyped to achieve the desired outcomes (Cohen and Sternad, 2009; Santos et al., 2015; Shmuelof et al., 2012; Todorov and Jordan, 2002; Venkatraman et al., 2010; Wolpert et al., 1995), just like the ones you are using now. Fundamental discoveries in neuroscience made in the last century have shed light on our understanding of how motor learning happens and what brain structures are involved, such as the motor cortex, the striatum and the thalamus (Díaz-Hernández et al., 2018;

Georgopoulos et al., 1993; Jin and Costa, 2010; Karni et al., 1998; Serruya et al., 2002; Yin et al., 2009). Furthermore, the stereotyping of actions with training is accompanied by plastic changes in the motor cortex and striatum, showing a refinement of behavior-specific neural activity (Barnes et al., 2005; Cao et al., 2015; Costa et al., 2004; Jin and Costa, 2010; Santos et al., 2015). These changes in neural activity during motor learning suggest that the brain selects and refines the neural patterns that lead to successful behavior (Costa, 2011). Therefore, similar neural processes could be used learning to operantly control external devices. Indeed, animals can learn to increase performance in operant learning tasks, by re-entering more often specific patterns of neural activity (Athalye et al., 2018; 2017; Carmena et al., 2003; Clancy et al., 2014; Fetz, 1969; Ganguly and Carmena, 2009; Koralek et al., 2012).

In this dissertation, we expand on these animal findings and focus on the development of a novel system that can bypass motor actions and exploit human subjects' neural activity to directly control an external device just by thinking about it, independently of movement. Just as if we were controlling a new external thumb to scroll a thesis with. For that, we need a Brain-Machine Interface (BMI), which is the topic of the work presented here and what we will be discussing in this dissertation.

Generally speaking, a Brain-Machine Interface (BMI) can be divided into two main classes. It can either be a system 1) that reads outputs from the brain into a machine, or 2) that writes inputs to the brain, from a machine. The latter is in itself an exciting field of research that has led to significant medical applications and scientific discoveries, such as the cochlear implant (Wilson and Dorman, 2008), the deep brain stimulation (DBS) technique (Perlmutter and Mink, 2006) and transcranial magnetic stimulation (TMS) (Hallett, 2000). Given the subject of this dissertation and the work in the following chapters, we will focus this introduction on the first class of BMIs, the ones that record outputs from the brain. Hereafter, we shall refer to them merely as BMIs. In particular, we will focus on interfaces that can be used to control neuroprosthetic devices or communication interfaces.

In this introduction, we will describe how the brain signals that are used for BMI are generated and summarize the techniques available to record them. We will then review some of the pioneering work in the BMI field and present the state of the art of several BMI approaches used both in humans and animal models. We will discuss the distinction between the operant learning and the decoder approaches to BMI, giving examples of significant works with both approaches. We will then summarize some of the clinical and research applications of BMIs. Finally, we will present a short description of what you will find in the next chapters of this dissertation.

Brain signals that can be used for BMIs

The performance of BMIs depends on the electrical activity recorded from neurons, most commonly from the brain. This electrical activity is primarily generated by neurons capable of firing stereotyped electrical impulses, i.e., action potentials, to communicate within a vast neural network. It is the balanced activity of this neural network that allows us to control all our conscious and subconscious functions. Depending on where and how we measure the neural activity, we may be detecting different types of signals. When measuring activity intra-cortically with implanted microelectrode arrays, for example, we can capture the fast action potentials (~1 ms) representing the largest potential changes that we can notice in the brain. However, for distant techniques, such as electroencephalography and electrocorticography, to be able to detect these electrical changes, it requires the synchronous activity of many action potentials, which happens only at slower timescales (Buzsáki et al., 2012). Furthermore, in these cases, the origin of the signal comes also from slower (and smaller) changes in postsynaptic potentials. Neurons communicate with neighboring cells forming synapses at their dendrites. At the synapses, the signal is transferred chemically via neurotransmitters, generating slower changes in the membrane potential. The postsynaptic potentials can either be excitatory (EPSP) or inhibitory (IPSP), depending on the kind of neurotransmitter involved. In the cases of EPSPs, current moves inward generating a sink in the extracellular medium, whereas in IPSPs, the current moves from the cell to the outside medium, thus generating a source on the outside (Lopes da Silva, 2010). Because many individual sources must overlap in time to induce a measurable signal far from its origin, e.g., EEG recording on the scalp, this overlap is mostly generated from slower events, such as postsynaptic potentials (Buzsáki et al., 2012).

Methods to record neural activity for BMI

Several methods are currently used to record neural activity. Each of these methods has advantages and disadvantages which need to be taken into account when comparing their performances. **Fig.1.1** exemplifies one of the trade-offs between the different available techniques for neural recordings, in this case, the temporal-spatial resolution of the method.

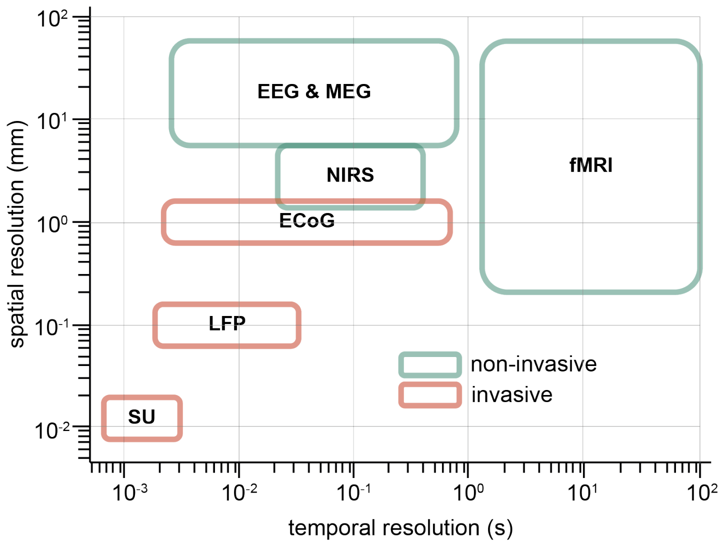

Fig. 1.1 | Overview of the spatial and temporal resolution of BMI recording methods. Invasive (red): single unit (SU), local field potentials (LFP), electrocorticography (ECoG); Non-invasive (green): electroencephalography (EEG), magnetoencephalography (MEG), near infrared spectroscopy (NIRS), functional magnetic resonance imaging (fMRI). Figure adapted from (Sejnowski et al., 2014).

One of the primary trade-offs of the different methods is whether it requires surgery and, thus, how safe they are to use. Invasive neuronal recordings use electrodes that are implanted in the brain and can provide the best recording signal of all techniques, being able to measure signals ranging from action potentials (AP) up to local field potentials (LFP) (Collinger et al., 2013; Hochberg et al., 2012). Despite their unmatched low signal to noise ratio, invasive techniques are generally only implemented as a last resort in patients. The implantation of these electrodes requires open-skull surgery with all its associated risks and may lead to problems like biocompatibility and biostability in long-term applications (Waldert, 2016).

Invasive methods also involve high costs and long waiting times for surgery. An alternative to invasive methods that have gained popularity in recent years is Electrocorticography (ECoG) (Benabid et al., 2019; Leuthardt et al., 2004; Wang et al., 2013). By being semi-invasive, this technique does not carry many of the burdens of the fully-invasive methods mentioned above (e.g., long-term signal stability, biocompatibility) while still offering high spatial resolution LFP recordings that can be beneficial to many BMIs. Despite these advantages, ECoG still requires a medical procedure making it impractical for most BMI applications.

Although offering much higher signal quality, invasive techniques are undesirable due to the intrinsic risks for the subject. For this reason, invasive techniques, such as the ones described above, are not suitable to be used with healthy subjects. Non-invasive techniques have thus dominated the number of publications in the BMI field and, in particular, EEG has been the most adopted recording technique (Hwang et al., 2013).

Given its high temporal resolution, wide brain surface coverage, and lower costs, EEG is highly used in BMI applications. Despite their lower spatial resolution, EEG systems offer higher portability and ease of use. Other techniques such as Near-Infrared Spectroscopy (NIRS) (Reich, 2005; Sitaram et al., 2007b) , functional Magnetic Resonance Imaging (fMRI) (Sitaram et al., 2007a) and Magnetoencephalography (MEG) (Cohen, 1972) have also been used for BMIs, but these still represent a very small fraction of the studies conducted with non-invasive techniques(Hwang et al., 2013).

In this thesis, we use an EEG-based BMI. EEG is a non-invasive technique, initially discovered by Hans Berger, who published the reports on the first experiments in 1929 (Birbaumer, 2006). EEGs record the synchronous activity of tens of thousands of neurons at a time (both action potentials and synaptic potentials), by placing electrodes on the subjects' scalp, **Fig. 1.2**. This activity largely corresponds to the summation of EPSPs and IPSPs at the synapses of cortical neurons (Lopes da Silva, 2013). In particular, cortical pyramidal neurons contribute the most to the EEG signal(Kirschstein and Köhling, 2009). These neurons typically receive their inputs from corticocortical and thalamocortical nerve fibers. Due to pyramidal neurons' characteristic long apical dendrites when a postsynaptic signal spreads electronically in the dendrite, it creates an extracellular dipole perpendicular to the cortex. This dipole is the main contributor to the signal measured on the scalp. Typically, neurons that are located on the top of the gyri contribute more to the EEG signal than apical neurons located in the gyral walls forming horizontal dipoles or at a depth of the sulci due to their distance to the scalp (Kirschstein and Köhling, 2009).

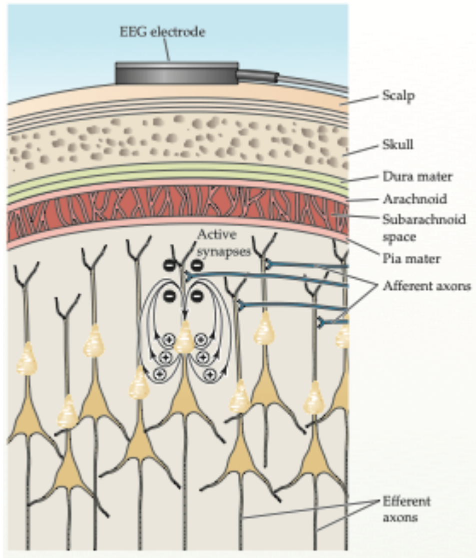

Fig. 1.2 | An EEG electrode measures the synchronous activity of a large number of neurons in the underlying regions of the brain, image from (Purves et al., 2012).

The EEG detects the difference in potential of the signal measured in each specific electrode compared to a particular reference. The oscillatory activity, i.e. waves, measured in the EEG thus reflect the rhythmic fluctuation PSPs of the underlying neural populations. Particular frequency ranges have been consistently recognized in different behavioural and cognitive processes (Buzsáki, 2006; Schomer and Lopes da Silva, 2012). These waves are typically designated by Greek letters such as delta (0-4Hz), theta (4-8Hz), alpha (8-12Hz), beta (14-30Hz) and gamma (>30Hz), and are commonly used in BMIs to detect users' intention and processed to send control commands to external devices.

Brain-Machine Interfaces

A BMI is a system capable of translating neural activity into control signals for effectors, like computers, neuroprosthetics, or muscles. Because movement is not required to operate these devices, they have been proposed to help rehabilitate/restore or substitute lost function in patients with motor disabilities and neurological disorders (Elbert et al., 2012; Sterman, 1977). This technology has demonstrated profound results in allowing patients with such disorders to re-establish communication with the people around them and interact with their surrounding world (Ajiboye et al., 2017; Benabid et al., 2019; Birbaumer et al., 1999; Collinger et al., 2013; Hochberg et al., 2012; Pandarinath et al., 2017). In the last decades, research in the BMI field with humans and animal models has helped us understand how neural activity is reorganized when the brain has to deal with controlling external devices (Carmena et al., 2003; Ganguly and Carmena, 2009; Ganguly et al., 2011) and how animals are able to learn to modulate it voluntarily (Clancy et al., 2014; Koralek et al., 2012; Neely et al., 2018). These findings may hold the key to the development of high-performing BMIs for patients and to the adoption of this technology in healthy individuals in the near future.

Pioneering works in BMI

We can pinpoint the first invasive BMI demonstrations in animals to half a century ago with the pioneering studies of Eberhard Fetz, in 1969. In his work, monkeys learned to control an auditory or a visual feedback signal by modulating the activity of a single neuron in the motor cortex (Fetz, 1969; Fetz and Baker, 1973; Fetz and Finocchio, 1971). The monkeys were given a task to increase the firing rate of single neurons above a certain threshold in order to receive food rewards. After several training sessions, the animals learned to increase these cells' activity up to 5 times above their normal levels. These findings demonstrated, for the first time, the animals' capacity to learn to regulate neural activity directly in order to achieve behavioral outcomes. The same year, Joe Kamiya published the first report showing that healthy human subjects could self-control alpha waves recorded with EEG in real-time. The control could be modulated when given continuous sensory feedback of their activity, such as a rising or falling tone (Kamiya, 1969). These studies laid the groundwork for experiments in humans and animal models, using a diversity of invasive and non-invasive techniques that have shown that BMIs' can be used to voluntarily modulate neural activity and control external devices.

Closed-Loop Motor Brain-Machine Interface Systems

A BMI is characterized by three main components, **Fig. 1.3**: 1) an acquisition system or sensors used to record the brain activity; 2) a processor or mathematical algorithm that translates the recorded neural activity into a control command for an effector; and 3) a device or effector that is to be controlled by the user's intended actions (e.g., computer, neuroprosthetic or our muscles).

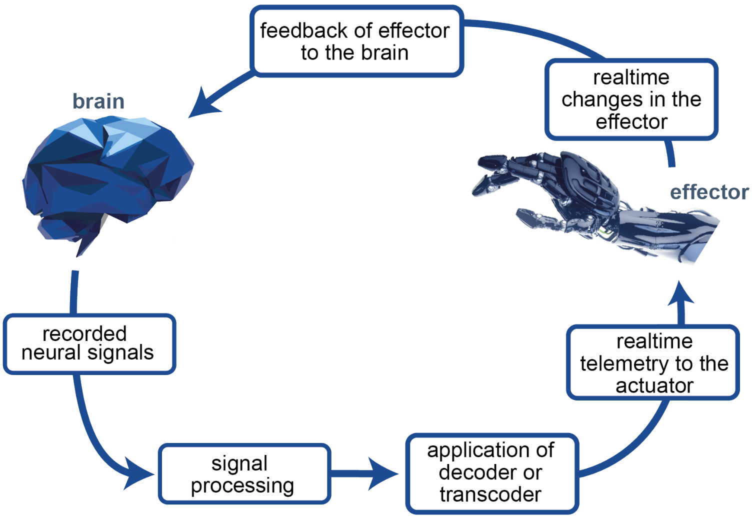

Fig. 1.3 | Schematic representation of a Brain Machine Interface (BMI) closed loop. Neural signals are recorded from the brain and the signals are processed and transformed in realtime. The result of the transformation is sent as an input command to actuate on the effector. Changes in the state or movement of the effector and fed back to the brain, closing the BMI loop.

In most cases, the BMI is part of a closed feedback loop, which is established by providing the subject with visual or sensory feedback of the changes in the effector in near-real-time (Carmena et al., 2003). For a closed-feedback BMI loop to operate correctly, there needs to be adaptation within the control loop. This is a critical step of a BMI to guarantee that the subject's intentions are matched with the appropriate control changes on the device. Within the control loop, there are two places where the adaptation can occur: the algorithm and the brain. Depending on where in the control loop the adaptation happens, we can either have a decoder (adaptation of the algorithm) or a learning (adaptation of the brain) approach to the BMI (Carmena, 2013). Each of these approaches can have advantages and disadvantages, and we will review them in more detail below.

The decoder approach

During the last decades and with the rise of the field of machine learning, the development of brain-machine interfaces has mostly focused on the decoder approach. The goal of this approach is to decode a natural plan in the subject's neural signals. A mathematical model is trained to decode and categorize the subject's brain activity of pre-existing natural plans and relate it to specific control actions on a device. Early invasive studies developed decoder approaches that were able to offline reconstruct an animal's movement, only based on the recorded neural activity (Georgopoulos et al., 1986). Expanding on these results, further studies demonstrated that the decoder approach could be used online to reconstruct movement and that the decoded neural activity could be applied in the control a neuroprosthetic skill (Carmena et al., 2003; Chapin et al., 1999; Hochberg et al., 2006; Serruya et al., 2002; Taylor et al., 2002). The decoder approach has been used with notable results in human patients, leveraging the use of invasive microelectrode arrays (Aflalo et al., 2015; Ajiboye et al., 2017; Collinger et al., 2013; Gilja et al., 2015; Hochberg et al., 2006; 2012; Kim et al., 2008; Pandarinath et al., 2017).

For example in two of these studies, patients with tetraplegia were implanted with one (Hochberg et al., 2012) or two (Collinger et al., 2013) microelectrode arrays in the motor cortex (MI), capable of recording single- and multi-unit activity . The activity from MI was initially recorded while the subjects observed a robotic arm moving in several dimensions. A decoder was then used to relate the recorded activity to the corresponding state of the robotic arm. The decoder was then used online to translate the subject's neural activity into commands to the arm. Subjects were able to successfully move the robotic arm in several degrees of freedom to reach for objects and to grasp those same objects.

The decoder approach has also been widely implemented in human EEG studies. The execution and imagination of particular motor commands/limb movements are typical examples of natural plans used for BMI (Blefari et al., 2015; McFarland et al., 2000; Meyer et al., 2014; Millan et al., 2004a; Pfurtscheller et al., 1997). In such cases, EEG records changes over the sensorimotor cortex, while the subject is, for example, imagining the movement of the left or right arm. A decoder is used to classify the activity and relate it to the intended action. The outcome of the decoder is then used to link the activity to specific commands to control a device.

Other implementations of the decoder approach have been proposed, which are not motor related. BMIs focused on the exploitation of Visual Evoked Potentials (VEP), and in particular Steady-State VEPs, rely on the decoding of the photic driving response over the visual cortex at a specific frequency when a subject looks at a stimulus that is blinking at that particular frequency (Vialatte et al., 2010; Yijun Wang et al., 2008).

Also, very commonly exploited are Event-Related Potential (ERP), which rely on evoked potentials time-locked to cognitive or sensory/motor events. The P300 application of ERPs, typically used for spellers, for example, is a response to a stimulus that can be decoded from a positive peak of EEG activity over the parietal cortex. These peaks can be seen to occur about 300ms after the presentation of infrequent stimuli in oddball paradigm tasks (Fazel-Rezai et al., 2012). Other implementations of cognitive ERPs seen in Error-Related Potentials (ErrP), which are evoked when the subject realizes an error (Chavarriaga et al., 2010) and Contingent Negative Variation (CNV), which are typically linked to attention and anticipation (Walter et al., 1964).

With the extensive development of ever more sophisticated algorithms to implement decoder approaches (Lotte et al., 2018; 2007), many times these applications end up neglecting the subject in the BMI loop and their capacity to learn (Lotte et al., 2013; McFarland and Wolpaw, 2018; Perdikis et al., 2018).

The learning approach

In contrast to the decoder approach described above, the learning approach uses a mathematical transformation, which is mostly kept fixed throughout the training, and that needs to be learned by the brain. In this thesis, we propose the term *transcoder* for the mathematical transformation of neural activity with the operant learning approach, thus differentiating from the conventional decoder approaches. The transcoder is a new pathway between activity and the device to be controlled. In these cases, there is not an *a priori* natural motor plan that can solve the task, and the brain needs to adapt to the transcoder, much like having a new spinal cord directing the transformed brain activity to a new limb. The transformation needs to be learned *de novo* (Carmena, 2013; Costa, 2011). Several studies have shown that animals can learn a fixed transcoder (Athalye et al., 2018; Clancy et al., 2014; Fetz, 1969; Fetz and Baker, 1973; Ganguly and Carmena, 2009; Koralek et al., 2012) when trained through a closed-loop operant learning task to increase rewards (Skinner, 1938; Thorndike, 1898). During operant BMI learning, cortico-striatal plasticity is shown to be necessary for learning to re-enter specific motor cortex activity (Koralek et al., 2012; 2013). Neurons in cortex that are directly controlling the BMI develop coherence with dorsal striatum spiking (Koralek et al., 2013), while coherence is not observed for task-unrelated neurons. The striatum seems to be critical during the learning phases of BMI when subjects learn to re-enter target cortical patterns, but not required to execute the same entrance after learning (Koralek et al., 2012; Neely et al., 2018). Moreover, task-relevant cortical neural activity is refined (Athalye et al., 2018). Neurons directly implicated in the BMI task progressively increase and align their covariance to the target pattern, while the variability of neural activity uncorrelated with the BMI task decreases with training (Athalye et al., 2018; 2017). Similarly, the refinement of activity is also seen during motor skill learning (Costa et al., 2004; Jin and Costa, 2010; Rioult-Pedotti et al., 2000; Santos et al., 2015). The operant learning approach expands on the range of possible sources of control signals that the BMI can achieve when compared to decoding pre-existent natural plans, as described before.

In human studies, an implementation of the operant learning approach has explored Slow Cortical Potentials (SCPs) (Roberts et al., 1989). In such systems, subjects modulate the excitation or inhibition of local cortical networks voluntary, which can be noticed in the EEG as potential shifts that occur over 0.5–10.0s. Such an application was a major breakthrough in the field of BMI, allowing patients to control a cursor and type letters on a screen (Birbaumer et al., 1999). Besides this significant application, most human studies that have implemented the operant learning approach have used it during regulation of one band decoder that can be linked to particular mental states (e.g., meditative, relaxed or excited states). Operant learning is also commonly implemented as a training method to generate a natural pattern more consistently. Often referred to as neurofeedback training in the literature, this approach has been shown to help subjects disrupt or enhance particular behaviors. Studies have showed that neurofeedback can improve selective visual attention (Schafer and Moore, 2011), decrease the onset of movement execution (Khanna et al., 2017) and even decrease seizure frequency in epilepsy patients (Tan et al., 2009). Neurofeedback has also been successfully used for the modulation of neural activity in patients with Parkinson's disease (PD) implanted with an Activa PC neurostimulator. In this study, PD patients were showed to be able to learn to modulate beta frequencies in order to control a cursor to hit 4 different targets.

The modulation of a more consistent pattern through the operant learning approach is also valuable for the decoder approaches described previously. For example, in motor imagery, the subject is fed back the output of the decoder so that they can produce consistent and stable signals that the decoder is able to classify (Lotte et al., 2013).

Despite these implementations, it still remains to be demonstrated that the operant learning approach can be used for control of a complex, multiband pattern of EEG activity. Learning to control a complex EEG pattern, unrelated to motor activity, would require establishing a new link between the activity and task actions. This link needs to be learned *de novo,* and provides a natural connection to the desired task action.

The two-learner system

Recent studies have proposed an emerging paradigm that relies on the online adaptation of the decoder to rapidly increase the initial performance in BMI control. Known as the closed-loop decoder adaptation (CLDA), this paradigm adapts the parameters of the decoder by taking into consideration relevant information about task goals, while the subjects perform the BMI task (Dangi, et al. 2014; Gilja et al., 2012; Orsborn, et al. 2012). This approach may lead to a better representation of the link between the neural activity controlling the task and the subjects' intended actions. The difficulty in this approach is to understand how and when to change the decoder parameters without hindering the subject's capacity to learn to modulate their neural activity. In other words, how to minimize the moving-target problem, where the decoder is constantly changing while the subjects are also learning it. Co-designing an optimal decoder that is able to co-exist with the corresponding engagement of neural activity will be one of the major challenges to achieve a high-performing, robust and generalizable BMIs (Shenoy and Carmena, 2014). Studies have implemented CLDA approaches by first initializing the parameters of the decoder from arm reaching movements (Gilja et al., 2012), or through visual feedback of cursor movements (Orsborn, et al. 2012). Once the decoder parameters are set, the subjects have to select the corresponding brain activity to control the BMI task. At every timestep the algorithm estimates intention, by rotating the cursor's decoded velocity vector towards the target while keeping its magnitude unchanged, and by equating it to zero when reaching the target. Taking into account the estimated intention, a maximum-likelihood technique is used to change the decoder parameters converging them to a better solution (Dangi, et al. 2014; Gilja et al., 2012; Orsborn, et al. 2012). This technique can be used to adapt the decoder parameters during early training phases of closed-loop control and until a specified level of performance is reached. Once these criteria are achieved, the parameters are can be fixed during training allowing for neural adaptation similar to the methods described in the *learning approach* section above.

The CLDA method has also been implemented in non-human primates in the control of a 2D continuous BMI task, using an LFP-based decoder (So, et al. 2014), as opposed to spike-based BMIs. This study showed that monkeys were able to learn arbitrary transforms of selective LFP frequency bands. Here, the CLDA approach was used initially to adapt the decoder to subject-specific modulations of different LFP frequency bands in order to increase task performance. Given the similarities between LFP and EEG signal sources, the demonstration of the CLDA approach in LFP-based BMIs, suggests that such methodology could also play an important role in future EEG-based BMI work.

Clinical and research implementation of BMIs

Given the characteristics of BMIs mentioned above, this technology has naturally found its most essential role in applications for disabled people, helping in the restoration and substitution of a lost motor ability or communication capacity. However, BMIs have been tested extensively in the control of diverse applications with populations of healthy subjects and patients alike. A boom of interest in the field since the 1990s has showcased the effectiveness of BMI systems in numerous applications and paradigms.

One of the most widely used applications of BMI has been in cursor control, with studies showing control of one (Buch et al., 2008; Wolpaw et al., 1991), two (Leuthardt et al., 2004; Wolpaw and McFarland, 2004), and three degrees of freedom (McFarland et al., 2010). Spellers have also been an essential application of BMI systems with which disabled patients were able to communicate and write messages (Birbaumer et al., 1999; Millan and Mourino, 2003; Nijboer et al., 2008; Pandarinath et al., 2017). Control of moving robots (Bell et al., 2008; Millan et al., 2004b) as well as wheelchairs (Galán et al., 2008) have also been demonstrated. Perhaps one of the most impressive applications of BMI to date has been regarding prosthetic control, where BMIs have been used for reaching and grasping control of robotic limbs (Collinger et al., 2013; Hochberg et al., 2012), full exoskeletons (Benabid et al., 2019) and for the stimulation and control of muscles of the subject's natural limb (Ajiboye et al., 2017; Biasiucci et al., 2018; Ethier et al., 2012; Pfurtscheller et al., 2000; Shaikhouni et al., 2016).

Clinical applications for motor control have been tested in individuals with different neurological disorders. In general, the implementation of BMIs in a clinical setting is done in patients whose lesions or injuries have rendered parts of or all of the PNS system and muscles dysfunctional. However, these patients should still have intact or otherwise not fully compromised brain functions to be able to control the BMI. The main clinical applications for BMI have been demonstrated in patients with amyotrophic lateral sclerosis (ALS) (Birbaumer et al., 1999; Nijboer et al., 2008), high levels of spinal cord injury (SCI) (Leeb et al., 2007; Müller-Putz et al., 2005), severe cerebral palsy (CP) (Neuper et al., 2003), Duchenne Muscular Dystrophy (DMD) and Spinal Muscular Atrophy type II (SMA II) (Cincotti et al., 2008), and stroke (Buch et al., 2008). For many of these patients, their disabilities still allow the use of other assistive technologies (AT) such as eye trackers or recordings of EMG. In such cases, BMIs can be viewed as supplementary or supportive technology. However, BMIs are currently the only available option for patients with complete paralysis of all voluntary muscles, including eye movements (CLIS).

WHY KEEP READING THIS THESIS?

In this thesis, we expand on the existent studies from animal models and human subjects described above, implementing an operant learning approach to an EEG-based BMI task. The BMI uses a fixed transcoder that converts neural activity into cursor position. The success in the task depends on re-entering more often rare states of EEG activity which are converted by the transcoder to uncommon target cursor positions on screen. Because the transcoder is not selected for its relation to a mental state or motor action, a link between the EEG pattern and cursor position needs to be learned *de novo*. The complex pattern of activity depends on a ratio of four EEG bands, making it less likely to be controllable by simple changes of mental states, such as relaxed or excited states. Implementing a ratio of four bands also makes the transcoder more robust to muscular and ocular activity, as well as external noise, than a single band transcoder. This main reasons are that the 1) noise affecting bands in the numerator and denominator of the ratio will be evened out and 2) if the muscular or ocular activity affects a specific band, this will have a lower impact on the overall result of the transcoder when compared to a transcoder composed of only that particular band.

In this dissertation, we describe in detail the experiments conducted with this approach and the subsequent findings. We show that subjects are able to rapidly learn to modulate the EEG activity in order to increase performance in the task. The EEG activity is refined throughout training, which can be seen by the distribution of the overall EEG patterns becoming closer to the optimal pattern to reach the target, even for period when target has not been reached. We also show that all EEG bands of the fixed transcoder are used during target reach. The learning is consolidated, and when tested after three weeks of training intermission, we show that the learning is retained and can be readily recalled.

We present a "real world" implementation of the BMI paradigm described in the previous chapter. We show that the BMI can be used for the control of the horizontal displacement of an aircraft. We also briefly discuss the on-going development of a novel EEG headset. The headset uses active, dry-EEG sensors that record and process the signal locally to be used with the operant learning BMI paradigm. This EEG headset fully records, processes and transmits a signal that can be used for operant BMI tasks, opening up a range of applications and allowing a wider reach of the technology.

We humans have mastered the use of our bodies and muscles to interact with the world. However, in a world where computers and electronic devices have become the norm, our muscles may not be the most efficient way to communicate with these new devices. Brain-Machine Interfaces, offer us a key to by-pass muscular activity, directly interfacing these devices with the brain and allowing us to expand the ways to interact with the world.

REFERENCES

Aflalo, T., Kellis, S., Klaes, C., Lee, B., Shi, Y., Pejsa, K., Shanfield, K., Hayes-Jackson, S., Aisen, M., Heck, C., et al. (2015). Decoding motor imagery from the posterior parietal cortex of a tetraplegic human. Science *348*, 906–910.

Ajiboye, A.B., Willett, F.R., Young, D.R., Memberg, W.D., Murphy, B.A., Miller, J.P., Walter, B.L., Sweet, J.A., Hoyen, H.A., Keith, M.W., et al. (2017). Restoration of reaching and grasping movements through brain-controlled muscle stimulation in a person with tetraplegia: a proof-of-concept demonstration. The Lancet *389*, 1821–1830.

Athalye, V.R., Santos, F.J., Carmena, J.M., and Costa, R. (2018). Evidence for a neural law of effect. Science *359*, 1024–1029.

Athalye, V.R., Ganguly, K., Costa, R.M., and Carmena, J.M. (2017). Emergence of Coordinated Neural Dynamics Underlies Neuroprosthetic Learning and Skillful Control. Neuron *93*, 955–970.e955.

Barnes, T.D., Kubota, Y., Hu, D., Jin, D.Z., and Graybiel, A.M. (2005). Activity of striatal neurons reflects dynamic encoding and recoding of procedural memories. Nature *437*, 1158–1161.

Bell, C.J., Shenoy, P., Chalodhorn, R., and Rao, R.P.N. (2008). Control of a humanoid robot by a noninvasive brain–computer interface in humans. J. Neural Eng. *5*, 214–220.

Benabid, A.L., Costecalde, T., Eliseyev, A., Charvet, G., Verney, A., Karakas, S., Foerster, M., Lambert, A., Morinière, B., Abroug, N., et al. (2019). An exoskeleton controlled by an epidural wireless brain–machine interface in a tetraplegic patient: a proof-of-concept demonstration. The Lancet Neurology 1–11.

Biasiucci, A., Leeb, R., Iturrate, I., Perdikis, S., Al-Khodairy, A., Corbet, T., Schnider, A., Schmidlin, T., Zhang, H., Bassolino, M., et al. (2018). Brain-actuated functional electrical stimulation elicits lasting arm motor recovery after stroke. Nat Commun *9*, 2421.

Birbaumer, N., Ghanayim, N., Hinterberger, T., Iversen, I., Kotchoubey, B., Kübler, A., Perelmouter, J., Taub, E., and Flor, H. (1999). A spelling device for the paralysed. Nature *398*, 297–298.

Birbaumer, N. (2006). Breaking the silence: brain-computer interfaces (BCI) for communication and motor control. Psychophysiology *43*, 517–532.

Blefari, M.L., Sulzer, J., Hepp-Reymond, M.-C., Kollias, S., and Gassert, R. (2015). Improvement in precision grip force control with self-modulation of primary motor cortex during motor imagery. Frontiers in Behavioral Neuroscience *9*, 18.

Buch, E., Weber, C., Cohen, L.G., Braun, C., Dimyan, M.A., Ard, T., Mellinger, J., Caria, A., Soekadar, S., Fourkas, A., et al. (2008). Think to Move: a Neuromagnetic Brain-Computer Interface (BCI) System for Chronic Stroke. Stroke *39*, 910–917.

Buzsáki, G. (2006). Rhythms of the Brain (Oxford University Press).

Buzsáki, G., Anastassiou, C.A., and Koch, C. (2012). The origin of extracellular fields and currents--EEG, ECoG, LFP and spikes. Nat Rev Neurosci *13*, 407–420.

Cao, V.Y., Ye, Y., Mastwal, S., Ren, M., Coon, M., Liu, Q., Costa, R.M., and Wang, K.H. (2015). Motor Learning Consolidates Arc-Expressing Neuronal Ensembles in Secondary Motor Cortex. Neuron *86*, 1385–1392.

Carmena, J.M. (2013). Advances in neuroprosthetic learning and control. PLoS Biol *11*, e1001561.

Carmena, J.M., Lebedev, M.A., Crist, R.E., O'Doherty, J.E., Santucci, D.M., Dimitrov, D.F., Patil, P.G., Henriquez, C.S., and Nicolelis, M.A.L. (2003). Learning to control a brain-machine interface for reaching and grasping by primates. PLoS Biol *1*, E42.

Chapin, J.K., Moxon, K.A., Markowitz, R.S., and Nicolelis, M.A. (1999). Real-time control of a robot arm using simultaneously recorded neurons in the motor cortex. Nat. Neurosci. *2*, 664–670.

Chavarriaga, R., Biasiucci, A., Forster, K., Roggen, D., Troster, G., and Millan, J.D.R. (2010). Adaptation of hybrid human-computer interaction systems using EEG error-related potentials. (IEEE), pp. 4226–4229.

Cincotti, F., Mattia, D., Aloise, F., Bufalari, S., Schalk, G., Oriolo, G., Cherubini, A., Marciani, M.G., and Babiloni, F. (2008). Non-invasive brain–computer interface system: Towards its application as assistive technology. Brain Research Bulletin *75*, 796–803.

Clancy, K.B., Koralek, A.C., Costa, R.M., Feldman, D.E., and Carmena, J.M. (2014). Volitional modulation of optically recorded calcium signals during neuroprosthetic learning. Nature Publishing Group *17*, 1–4.

Cohen, D. (1972). Magnetoencephalography: Detection of the Brain's Electrical Activity with a Superconducting Magnetometer. Science *175*, 664–666.

Cohen, R.G., and Sternad, D. (2009). Variability in motor learning: relocating, channeling and reducing noise. Exp Brain Res *193*, 69–83.

Collinger, J.L., Wodlinger, B., Downey, J.E., Wang, W., Tyler-Kabara, E.C., Weber, D.J., McMorland, A.J.C., Velliste, M., Boninger, M.L., and Schwartz, A.B. (2013). High-performance neuroprosthetic control by an individual with tetraplegia. Lancet *381*, 557–564.

Costa, R.M. (2011). A selectionist account of de novo action learning. Curr. Opin. Neurobiol. *21*, 579–586.

Costa, R.M., Cohen, D., and Nicolelis, M.A.L. (2004). Differential corticostriatal plasticity during fast and slow motor skill learning in mice. Curr. Biol. *14*, 1124–1134.

Dangi, S., Gowda, S., Moorman, H.G., Orsborn, A.L., So, K., Shanechi, M., and Carmena, J.M. (2014). Continuous closed-loop decoder adaptation with a recursive maximum likelihood algorithm allows for rapid performance acquisition in brain-machine interfaces. Neural Comput 26, 1811–1839.

Dangi, S., Orsborn, A.L., Moorman, H.G., and Carmena, J.M. (2013). Design and Analysis of Closed-Loop Decoder Adaptation Algorithms for Brain-Machine Interfaces. Neural Comput 25, 1693–1731.

Díaz-Hernández, E., Contreras-López, R., Sánchez-Fuentes, A., Rodríguez-Sibrían, L., Ramírez-Jarquín, J.O., and Tecuapetla, F. (2018). The Thalamostriatal Projections Contribute to the Initiation and Execution of a Sequence of Movements. Neuron *100*, 739–752.e5.

Elbert, T., Rockstroh, B., Lutzenberger, W., and Birbaumer, N. (2012). Self-Regulation of the Brain and Behavior (Springer Science & Business Media).

Ethier, C., Oby, E.R., Bauman, M.J., and Miller, L.E. (2012). Restoration of grasp following paralysis through brain-controlled stimulation of muscles. Nature *485*, 368–371.

Fazel-Rezai, R., Allison, B.Z., Guger, C., Sellers, E.W., Kleih, S.C., and Kübler, A. (2012). P300 brain computer interface: current challenges and emerging trends. Front. Neuroeng. *5*.

Fetz, E.E. (1969). Operant Conditioning of Cortical Unit Activity. Science *163*, 955–958.

Fetz, E.E., and Baker, M.A. (1973). Operantly conditioned patterns on precentral unit activity and correlated responses in adjacent cells and contralateral muscles. Journal of Neurophysiology *36*, 179–204.

Fetz, E.E., and Finocchio, D.V. (1971). Operant Conditioning of Specific Patterns of Neural and Muscular Activity. Science *174*, 431–435.

Galán, F., Nuttin, M., Lew, E., Ferrez, P.W., Vanacker, G., Philips, J., and Millán, J.D.R. (2008). A brain-actuated wheelchair: Asynchronous and non-invasive Brain–computer interfaces for continuous control of robots. Clinical Neurophysiology *119*, 2159–2169.

Ganguly, K., and Carmena, J.M. (2009). Emergence of a stable cortical map for neuroprosthetic control. PLoS Biol *7*, e1000153.

Ganguly, K., Dimitrov, D.F., Wallis, J.D., and Carmena, J.M. (2011). Reversible large-scale modification of cortical networks during neuroprosthetic control. Nature Publishing Group *14*, 662–667.

Georgopoulos, A.P., Schwartz, A.B., and Kettner, R.E. (1986). Neuronal population coding of movement direction. Science *233*, 1416–1419.

Georgopoulos, A., Taira, M., and Lukashin, A. (1993). Cognitive neurophysiology of the motor cortex. Science *260*, 47–52.

Gilja, V., Nuyujukian, P., Chestek, C.A., Cunningham, J.P., Yu, B.M., Fan, J.M., Ryu, S.I., and Shenoy, K.V. (2012). A brain-machine interface control algorithm designed from a feedback control perspective. Conf Proc IEEE Eng Med Biol Soc 2012, 1318–1322.

Gilja, V., Pandarinath, C., Blabe, C.H., Nuyujukian, P., Simeral, J.D., Sarma, A.A., Sorice, B.L., Perge, J.A., Jarosiewicz, B., Hochberg, L.R., et al. (2015). Clinical translation of a high-performance neural prosthesis. Nat Med *21*, 1142–1145.

Hallett, M. (2000). Transcranial magnetic stimulation and the human brain. Nature *406*, 147–150.

Hochberg, L.R., Bacher, D., Jarosiewicz, B., Masse, N.Y., Simeral, J.D., Vogel, J., Haddadin, S., Liu, J., Cash, S.S., van der Smagt, P., et al. (2012). Reach and grasp by people with tetraplegia using a neurally controlled robotic arm. Nature *485*, 372–375.

Hochberg, L.R., Serruya, M.D., Friehs, G.M., Mukand, J.A., Saleh, M., Caplan, A.H., Branner, A., Chen, D., Penn, R.D., and Donoghue, J.P. (2006). Neuronal ensemble control of prosthetic devices by a human with tetraplegia. Nature *442*, 164–171.

Hwang, H.-J., Kim, S., Choi, S., and Im, C.-H. (2013). EEG-Based Brain-Computer Interfaces: A Thorough Literature Survey. International Journal of Human-Computer Interaction *29*, 814–826.

Jin, X., and Costa, R.M. (2010). Start/stop signals emerge in nigrostriatal circuits during sequence learning. Nature *466*, 457–462.

Kamiya, J. (1969). Operant control of EEG alpha rhythm and some of its reported effects on consciousness. In Allered States of Consciousness, C.T. Tart, pp. 507–517.

Karni, A., Meyer, G., Rey-Hipolito, C., Jezzard, P., Adams, M.M., Turner, R., and Ungerleider, L.G. (1998). The acquisition of skilled motor performance: Fast and slow experience-driven changes in primary motor cortex. Proceedings of the National Academy of Sciences *95*, 861–868.

Khanna, P, JM C. Elife, 2017. 2017a. "Beta Band Oscillations in Motor Cortex Reflect Neural Population Signals That Delay Movement Onset." elifesciences.org 6:555.

Khanna, Preeya et al. 2017b. "Neurofeedback Control in Parkinsonian Patients Using Electrocorticography Signals Accessed Wirelessly with a Chronic, Fully Implanted Device." IEEE Transactions on Neural Systems and Rehabilitation Engineering 25(10):1715–24.

Kim, S.-P., Simeral, J.D., Hochberg, L.R., Donoghue, J.P., and Black, M.J. (2008). Neural control of computer cursor velocity by decoding motor cortical spiking activity in humans with tetraplegia. J. Neural Eng. *5*, 455–476.

Kirschstein, T., and Köhling, R. (2009). What is the source of the EEG? Clin EEG Neurosci *40*, 146–149.

Koralek, A.C., Costa, R.M., and Carmena, J.M. (2013). Temporally precise cell-specific coherence develops in corticostriatal networks during learning. Neuron *79*, 865–872.

Koralek, A.C., Jin, X., Long, J.D., Costa, R.M., and Carmena, J.M. (2012). Corticostriatal plasticity is necessary for learning intentional neuroprosthetic skills. Nature *483*, 331–335.

Leeb, R., Friedman, D., Müller-Putz, G.R., Scherer, R., Slater, M., and Pfurtscheller, G. (2007). Self-Paced (Asynchronous) BCI Control of a Wheelchair in Virtual Environments: A Case Study with a Tetraplegic. Computational Intelligence and Neuroscience *2007*, 1–8.

Leuthardt, E.C., Schalk, G., Wolpaw, J.R., Ojemann, J.G., and Moran, D.W. (2004). A brain–computer interface using electrocorticographic signals in humans. J. Neural Eng. *1*, 63–71.

Lopes da Silva, F. (2010). EEG: Origin and Measurement. In EEG-fMRI, C. Mulert, and L. Lemieux, eds. (content.schweitzer-online.de).

Lopes da Silva, F. (2013). EEG and MEG: relevance to neuroscience. Neuron *80*, 1112–1128.

Lotte, F., Bougrain, L., Cichocki, A., Clerc, M., Congedo, M., Rakotomamonjy, A., and Yger, F. (2018). A review of classification algorithms for EEG-based brain–computer interfaces: a 10 year update. J. Neural Eng. *15*, 031005–031029.

Lotte, F., Congedo, M., Lécuyer, A., Lamarche, F., and Arnaldi, B. (2007). A review of classification algorithms for EEG-based brain–computer interfaces. J. Neural Eng. *4*, R1–R13.

Lotte, F., Larrue, F., and Mühl, C. (2013). Flaws in current human training protocols for spontaneous Brain-Computer Interfaces: lessons learned from instructional design. Front Hum Neurosci *7*, 568.

McFarland, D.J., Miner, L.A., Vaughan, T.M., and Wolpaw, J.R. (2000). Mu and beta rhythm topographies during motor imagery and actual movements. Brain Topogr *12*, 177–186.

McFarland, D.J., and Wolpaw, J.R. (2018). Brain–computer interface use is a skill that user and system acquire together. PLoS Biol *16*, e2006719.

McFarland, D.J., Sarnacki, W.A., and Wolpaw, J.R. (2010). Electroencephalographic (EEG) control of three-dimensional movement. J. Neural Eng. *7*, 036007.

Meyer, T., Peters, J., Zander, T.O., Schölkopf, B., and Grosse-Wentrup, M. (2014). Predicting motor learning performance from Electroencephalographic data. J Neuroeng Rehabil *11*, 24.

Millan, J.D.R., and Mourino, J. (2003). Asynchronous bci and local neural classifiers: an overview of the adaptive brain interface project. IEEE Trans. Neural Syst. Rehabil. Eng. *11*, 159–161.

Millan, J.D.R., Renkens, F., Mouriño, J., and Gerstner, W. (2004a). Brain-actuated interaction. Artificial Intelligence *159*, 241–259.

Millan, J.D.R., Renkens, F., Mouriño, J., and Gerstner, W. (2004b). Noninvasive brain-actuated control of a mobile robot by human EEG. IEEE Trans Biomed Eng *51*, 1026–1033.

Müller-Putz, G.R., Scherer, R., Pfurtscheller, G., and Rupp, R. (2005). EEG-based neuroprosthesis control: A step towards clinical practice. Neuroscience Letters *382*, 169–174.

Neely, R.M., Koralek, A.C., Athalye, V.R., Costa, R.M., and Carmena, J.M. (2018). Volitional Modulation of Primary Visual Cortex Activity Requires the Basal Ganglia. Neuron *97*, 1356–1368.e4.

Neuper, C., Müller, G.R., Kübler, A., Birbaumer, N., and Pfurtscheller, G. (2003). Clinical application of an EEG-based brain–computer interface: a case study in a patient with severe motor impairment. Clinical Neurophysiology *114*, 399–409.

Nijboer, F., Sellers, E.W., Mellinger, J., Jordan, M.A., Matuz, T., Furdea, A., Halder, S., Mochty, U., Krusienski, D.J., Vaughan, T.M., et al. (2008). A P300-based brain–computer interface for people with amyotrophic lateral sclerosis. Clinical Neurophysiology *119*, 1909–1916.

Orsborn, A.L., Dangi, S., Moorman, H.G., and Carmena, J.M. (2012). Closed-Loop Decoder Adaptation on Intermediate Time-Scales Facilitates Rapid BMI Performance Improvements Independent of Decoder Initialization Conditions. IEEE Trans. Neural Syst. Rehabil. Eng. 20, 468–477.

Pandarinath, C., Nuyujukian, P., Blabe, C.H., Sorice, B.L., Saab, J., Willett, F.R., Hochberg, L.R., Shenoy, K.V., and Henderson, J.M. (2017). High performance communication by people with paralysis using an intracortical brain-computer interface. eLife *6*, 336–27.

Perdikis, S., Tonin, L., Saeedi, S., Schneider, C., and Millan, J.D.R. (2018). The Cybathlon BCI race: Successful longitudinal mutual learning with two tetraplegic users. PLoS Biol *16*, e2003787–28.

Perlmutter, J.S., and Mink, J.W. (2006). Deep Brain Stimulation. Annu. Rev. Neurosci. *29*, 229–257.

Pfurtscheller, G., Guger, C., Müller, G., Krausz, G., and Neuper, C. (2000). Brain oscillations control hand orthosis in a tetraplegic. Neuroscience Letters *292*, 211–214.

Pfurtscheller, G., Neuper, C., Flotzinger, D., and Pregenzer, M. (1997). EEG-based discrimination between imagination of right and left hand movement. Electroencephalogr Clin Neurophysiol *103*, 642–651.

Purves, D., Augustine, G.J., Fitzpatrick, D., and Hall, W.C. (2012). Neuroscience. Massachusetts (Elsevier).

Reich, G. (2005). Near-infrared spectroscopy and imaging: basic principles and pharmaceutical applications. Adv. Drug Deliv. Rev. *57*, 1109–1143.

Rioult-Pedotti, M.S., Friedman, D., and Donoghue, J.P. (2000). Learning-induced LTP in neocortex. Science *290*, 533–536.

Roberts, L.E., Birbaumer, N., Rockstroh, B., Lutzenberger, W., and Elbert, T. (1989). Self-Report During Feedback Regulation of Slow Cortical Potentials. Psychophysiology *26*, 392–403.

Santos, F.J., Oliveira, R.F., Jin, X., and Costa, R.M. (2015). Corticostriatal dynamics encode the refinement of specific behavioral variability during skill learning. eLife.

Schafer, R.J., and Moore, T. (2011). Selective attention from voluntary control of neurons in prefrontal cortex. Science 332, 1568–1571

Schomer, D.L., and Lopes da Silva, F. (2012). Niedermeyer's Electroencephalography (Lippincott Williams & Wilkins).

Sejnowski, T.J., Churchland, P.S., and Movshon, J.A. (2014). Putting big data to good use in neuroscience. Nat. Neurosci. *17*, 1440–1441.

Serruya, M.D., Hatsopoulos, N.G., Paninski, L., Fellows, M.R., and Donoghue, J.P. (2002). Instant neural control of a movement signal. Nature *416*, 141–142.

Shaikhouni, A., Annetta, N.V., Bockbrader, M.A., Friedenberg, D.A., Nielson, D.M., Sederberg, P.B., Glenn, B.C., Mysiw, W.J., Morgan, A.G., Deogaonkar, M., et al. (2016). Restoring cortical control of functional movement in a human with quadriplegia. Nature *533*, 1–13.

Shenoy, K.V., and Carmena, J.M. (2014). Combining decoder design and neural adaptation in brain-machine interfaces. Neuron 84, 665–680.

Shmuelof, L., Krakauer, J.W., and Mazzoni, P. (2012). How is a motor skill learned? Change and invariance at the levels of task success and trajectory control. Journal of Neurophysiology *108*, 578–594.

Sitaram, R., Caria, A., Veit, R., Gaber, T., Rota, G., Kuebler, A., and Birbaumer, N. (2007a). fMRI Brain-Computer Interface: A Tool for Neuroscientific Research and Treatment. Computational Intelligence and Neuroscience *2007*, 1–10.

Sitaram, R., Zhang, H., Guan, C., Thulasidas, M., Hoshi, Y., Ishikawa, A., Shimizu, K., and Birbaumer, N. (2007b). Temporal classification of multichannel near-infrared spectroscopy signals of motor imagery for developing a brain–computer interface. NeuroImage *34*, 1416–1427.

Skinner, B.F. (1938). The Behavior of Organisms (D. Appleton & Company).

So, K., Dangi, S., Orsborn, A.L., Gastpar, M.C., and Carmena, J.M. (2014). Subject-specific modulation of local field potential spectral power during brain–machine interface control in primates. J. Neural Eng. *11*, 026002.

Sterman, M.B. (1977). Sensorimotor EEG operant conditioning: experimental and clinical effects. Pavlov J Biol Sci *12*, 63–92.

Taylor, D.M., Tillery, S.I.H., and Schwartz, A.B. (2002). Direct cortical control of 3D neuroprosthetic devices. Science *296*, 1829–1832.

Thorndike, E.L. (1898). Animal Intelligence, an Experimental Study of the Associative Processes in Animals, by Edward L. Thorndike,...

Todorov, E., and Jordan, M.I. (2002). Optimal feedback control as a theory of motor coordination. Nat. Neurosci. *5*, 1226–1235.

Venkatraman, S., Jin, X., Costa, R.M., and Carmena, J.M. (2010). Investigating Neural Correlates of Behavior in Freely Behaving Rodents Using Inertial Sensors. Journal of Neurophysiology *104*, 569–575.

Vialatte, F., Maurice, M., Dauwels, J., and Cichocki, A. (2010). Steady-state visually evoked potentials: Focus on essential paradigms and future perspectives. Progress in Neurobiology *90*, 418–438.

Waldert, S. (2016). Invasive vs. Non-Invasive Neuronal Signals for Brain-Machine Interfaces: Will One Prevail? Front Neurosci *10*, 5696.

Walter, W.G., Cooper, R., Akdridge, V.J., McCallum, W.C., and Winter, A.L. (1964). Contingent negative variation: an electric sign of sensorimotor association and expectancy in the human brain. Nature *203*, 380–384.

Wang, W., Collinger, J.L., Degenhart, A.D., Tyler-Kabara, E.C., Schwartz, A.B., Moran, D.W., Weber, D.J., Wodlinger, B., Vinjamuri, R.K., Ashmore, R.C., et al. (2013). An Electrocorticographic Brain Interface in an Individual with Tetraplegia. PLoS ONE *8*, e55344.

Wilson, B.S., and Dorman, M.F. (2008). Cochlear implants: A remarkable past and a brilliant future. Hearing Research *242*, 3–21.

Wolpaw, J.R., and McFarland, D.J. (2004). Control of a two-dimensional movement signal by a noninvasive brain-computer interface in humans. Proceedings of the National Academy of Sciences *101*, 17849–17854.

Wolpaw, J.R., McFarland, D.J., Neat, G.W., and Forneris, C.A. (1991). An EEG-based brain-computer interface for cursor control. Electroencephalogr Clin Neurophysiol *78*, 252–259.

Wolpert, D., Ghahramani, Z., and Jordan, M. (1995). An internal model for sensorimotor integration. Science *269*, 1880–1882.

Yijun Wang, Xiaorong Gao, Bo Hong, Chuan Jia, and Shangkai Gao (2008). Brain-Computer Interfaces Based on Visual Evoked Potentials. IEEE Eng. Med. Biol. Mag. *27*, 64–71.

Yin, H.H., Mulcare, S.P., Hilário, M.R.F., Clouse, E., Holloway, T., Davis, M.I., Hansson, A.C., Lovinger, D.M., and Costa, R.M. (2009). Dynamic reorganization of striatal circuits during the acquisition and consolidation of a skill. Nat. Neurosci. *12*, 333–341.

2

OPERANT LEARNING OF A COMPLEX, MULTIBAND EEG PATTERN

SUMMARY

Most non-invasive Brain-Machine Interfaces (BMI) for control use online decoder approaches. Despite the constant development of high-performing classification algorithms, these studies overlook the users' capabilities to learn. In this study we introduce a novel EEG-based BMI using an operant learning approach. The BMI implements a fixed transcoder, i.e. a new pathway between activity and the device to be controlled. The choice of the transcoder is unrelated to *a priori* natural plans, requiring the brain to establish a new link between the activity and task performance, much like having a new spinal cord directing the transformed brain activity to a new limb. We show that users can modulate their neural activity to learn to more frequently produce a rare, complex EEG-pattern to increase success in task. The specific pattern depends on the continuous modulation of four EEG frequency bands and is selected with increasing accuracy throughout training. We observe that users rapidly learn the new transformation and that the EEG activity is refined with training. The

learning is consolidated and can be readily recalled during each training day, as well as after a three-week training intermission. The approach proposed in this chapter offers an alternative to the prevalent decoder approaches used for non-invasive BMI. Our results suggest that this approach can be useful for BMI control extending possible applications of this technology, since the subjects are not constrained by pre-existent links between neural activity and movements.

All data discussed in this chapter is currently in preparation as the following manuscript: Nuno Loureiro, Vitor B. Paixão, José Carmena, José Del R. Millán, Rui M. Costa, *Operant learning, refinement, and consolidation of a complex EEG pattern controlling an actuator*

INTRODUCTION

Millions of patients worldwide suffer from conditions that limit their mobility e.g. stroke, spinal cord injury, amyotrophic lateral sclerosis, or amputation. BMIs have been proposed as a promising way to improve these conditions by giving patients direct control of devices using their brain activity. In particular, the use of non-invasive techniques like electroencephalography (EEG) has demonstrated the invaluable clinical potential of BMIs for such patients (Birbaumer et al., 1999), avoiding the need of invasive surgery with all its associated risks. Early BMI studies using EEG have demonstrated that humans are capable of relying on feedback to shape neural activity and increase task performance (Vidal, 1973; Wolpaw et al., 1991). Results from such studies were vital for identifying EEG activity based on simple decoders that can be voluntarily modulated, and for documenting the possible applications of non-invasive BMI techniques, as well as their limitations.

However, during the last decade, developments in the field of machine learning have directed the research of human BMI mostly towards improvements in the so-called decoder approach, where the algorithms are optimized to decode pre-existing natural brain patterns to control an external device. In these cases, a mathematical model is generated linking the subject's recorded neural activity to a particular action (e.g. a physical or imagined limb movement). The model is then used to predict movements based on the neural activity alone (Carmena, 2013) which can be linked to specific task commands (e.g. movement of a cursor or an avatar). Throughout the task, the subject is required to produce the same activity in a stable and consistent way, so that the model robustly recognizes those patterns and converts them into the appropriate commands. A typical implementation of this approach in human BMI can be found in the modulation of sensorimotor rhythms (SMR) recorded over the sensorimotor regions during movement execution, imagined movement or movement preparation (Birbaumer et al., 1999; McFarland and Wolpaw, 2017; Pfurtscheller and Neuper, 2001; Roberts et al., 1989)

These studies, however, commonly neglect the subject's capacity to learn (Lotte et al., 2013; McFarland and Wolpaw, 2018; Perdikis et al., 2018). The fact that the subject is not required to learn new neural patterns but instead to produce existent and stable EEG signals, even when environmental conditions change, has played a critical role in the reliability of such approaches. In the presence of noisy, non-stationary signals, current algorithms fail to robustly extract the information needed to identify long-lasting patterns. Consequently, many studies often require daily changes to their algorithm, involving new calculations of activity patterns. These changes can lead to inconsistent BMI performances and to the BCI-illiteracy phenomenon observed in many studies (Blankertz et al., 2010; Guger et al., 2003; 2009).

Here, we introduce a novel human EEG-based BMI task with an operant learning approach that contrasts with the prevalent decoder methods. Subjects are required to voluntarily modulate their brain activity to learn a new neuroprosthetic skill in order to control a cursor on a screen and increase task performance. We implement a fixed mathematical transformation (*transcoder*) that converts neural activity into cursor position. We propose the term *transcoder* for the mathematical transformation of neural activity with the operant learning approach, in order to differentiate it from the conventional decoder approaches. By using a fixed transcoder, we relate any changes that occur throughout the training to changes in the subjects' neural activity alone. We design the task so that subjects need to be in continuous control of the activity in multiple EEG frequency bands in order to direct the cursor to the correct target. This differs from the traditional neurofeedback approaches of changing the baseline activity level of an EEG pattern that relates to a particular state. Moreover, by not decoding the initial activity from a specific natural plan, we reduce the possibility that the BMI control can be attained solely by changing a mental state or motor image. This approach requires that the subjects learn a new abstract skill, which cannot be accomplished by simply increasing the frequency selection of pre-existent state.

Our results show that subjects learn to modulate their EEG activity to continuously control the cursor and increase task performance over training. We also show that this learning is consolidated and can be readily recalled in each training day, as well as after a long intermission in training. The continuous control of cursor position is seen in multiple task measures, showing a refinement of the activity throughout training. Moreover, we observe that the EEG activity is modulated in all of the four EEG bands that are fed into the transcoder. Overall, here we introduce a new and alternative approach to EEG-based BMI, where subjects learn an arbitrary transcoder with long-lasting effects and without the need for signal classification or machine learning algorithms.

RESULTS

We collected behavioral and EEG data over the motor and prefrontal cortices from 15 subjects during a self-paced, closed feedback loop BMI task, **Fig. 2.1A**. The fixed transcoder, which transformed activity into cursor position, used a ratio that included four EEG bands: delta [1-4Hz], theta [4-8Hz], beta [14-25Hz] and gamma [30-80Hz], from five specific channels. This ratio of bands followed several requirements such as varying smoothly in time and showing low contamination from motor artifacts. We tested the influence of facial muscle activity and eye movement, and saw no significant changes in the result of the transcoder (*cf.* Methods) An index made of these four activity bands had also previously been found to be correlated with behavioral states in rodents (Costa et al., 2006), further suggesting it as a good candidate for a transcoder in an operant learning task. The change in cursor position provided the subject with continuous, real-time visual feedback. The task was run during 10 consecutive weekdays, each day (session) consisting of three 10-minute runs with feedback of the cursor position. Following the three runs, another 10-minute run without feedback was performed each day, which served as an experimental control of the task, **Fig. 2.1B**. During the no-feedback run the subjects simply looked at the screen which displayed a still frame of the task.

In feedback runs, subjects had to modulate their activity to maintain the cursor in the region between the two innermost lines (base area) for 2 consecutive seconds (i.e. 8 timesteps) in order to start a new trial. Once started, the trial type was indicated with an up or down arrow, displayed in a pseudo-random sequence indicating that the objective was to reach either the top or bottom horizontal target, respectively, **Fig. 2.2A**. Each trial could end in one of three possible ways: correct, incorrect or timeout if no target was reached within a set time limit of 30 seconds.

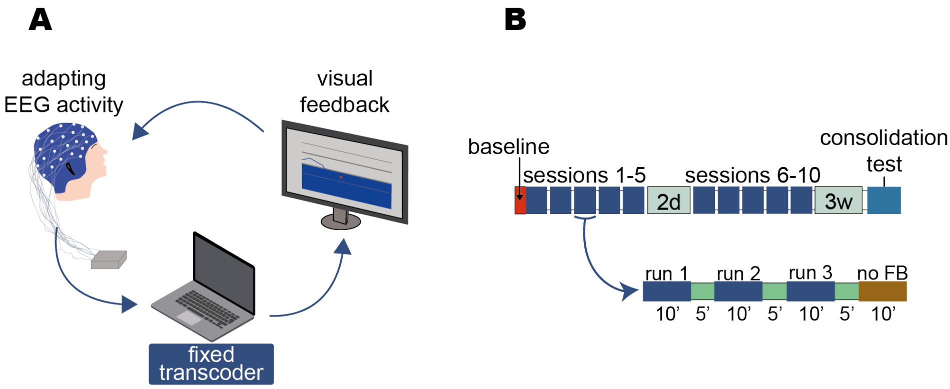

Fig. 2.1 | Closed-loop operant EEG-based BMI task with visual feedback. (A) Schematic of the BMI task. The subject's EEG activity was recorded and transformed using a fixed transcoder into cursor position on a screen. Visual feedback was given in near real-time and the subject needed to adapt EEG activity in order to correctly position the cursor on screen and increase task performance. **(B)** Task protocol. Each subject performed the experiment during ten consecutive weekdays, with a 2-day interval in the middle of training. Each day (session) consisted of three feedback runs of 10 minutes (blue), each separated by 5 minutes of interval (green). At the end of each session, a run without feedback of EEG activity (no FB, brown) was performed. A consolidation test session was run 3 weeks after the last day of training to assess capacity to recall learning of the abstract skill (light blue). Before starting the task on the first day, a short channels selection and target calculation session (red, panel D for detail). Throughout the rest of training, the transcoder, the electrode positions and the target positions remained constant.

During the trial, visual reinforcements were displayed to the subjects when they crossed the base limit (inner-lines) in the correct direction (as a lighter patch displayed on the screen) or crossed the correct target (as a darker patch). Besides having constant feedback of cursor position, these reinforcements further indicated that the recorded neural activity was moving the cursor towards the correct target.

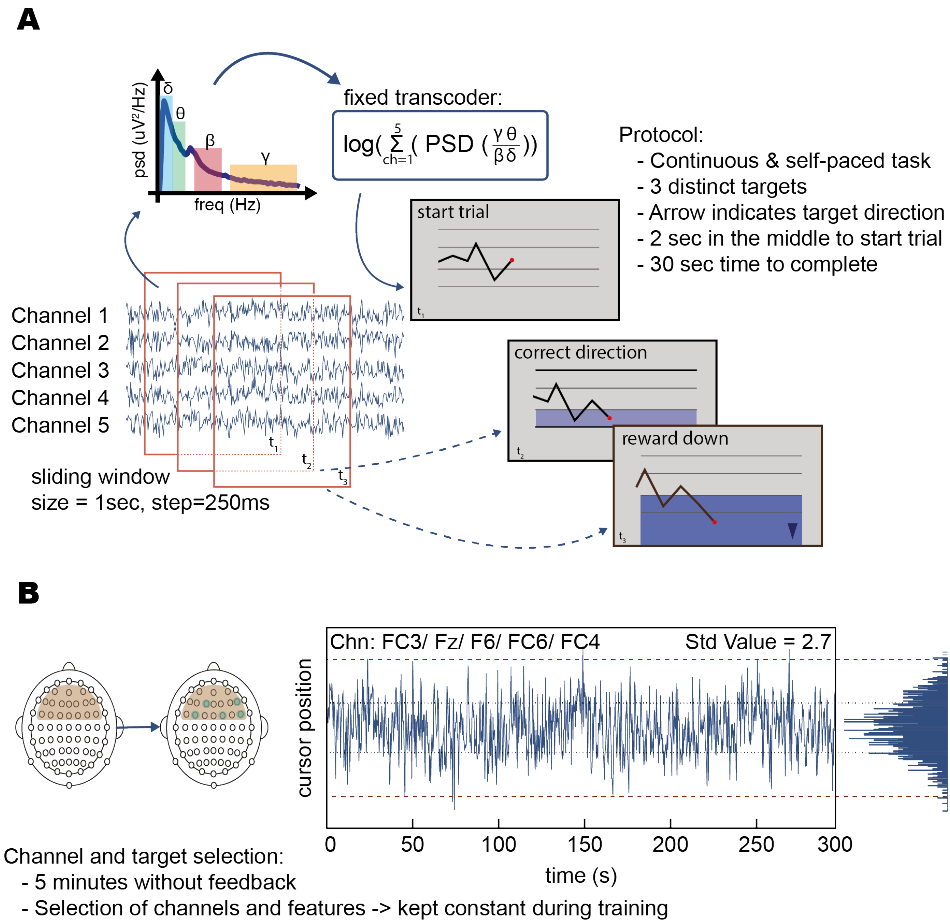

Fig. 2.2 | Schematic of the BMI paradigm in task and selection of channels. (A) EEG channel activity was recorded and processed in near real-time. For each 1 second-window, the activity of the five selected electrodes was converted to power spectral density (PSD) and the average activity of each specific frequency band was fed into the transcoder that outputted a new cursor position. In order to start a new trial the cursor needed to be kept in the base area (between the two inner lines) for two consecutive seconds. Once a new trial started, an arrow was displayed randomly on the right-hand side of the screen, pointing up or down. The objective was to direct the cursor to cross the top- or bottom target, respectively. Positive reinforcement in the shape of a colored patch was shown when EEG activity translated into a cursor position that crossed the

first horizontal line in the direction of the target. In the rarer events of a correct target hit, a darker colored patch was shown and the trial finished. Crossing an incorrect target ended the trial, which was classified as incorrect but there was no display of a negative visual feedback besides cursor position. **(B)** Channels selection and target calculation session. Five minutes of EEG data were collected in the beginning of the first training day. This data was used to calculate target positions, base limits and select 5 channels out of a pool of 17 possible electrodes. All these parameters were maintained constant throughout the rest of the training.

Each subject underwent a short channel selection and target calculation session, which took place on the first day before starting the training. In this session we chose 5 electrodes from an initial pool of 17 possible positions above the motor and frontal cortices and calculated the position of the horizontal base limits and targets for the task, **Fig. 2.2B** (cf. *Methods*).

Performance in Brain-Machine Interface task increases with training

We started by investigating whether subjects were able to modulate their activity to direct the cursor to reach a specified target, and increase task performance over training. Over the course of 30 training runs, subjects exhibited marked improvement in the percentage of trials in which the cursor crossed the correct target as opposed to the incorrect one, **Fig. 2.3A** (n=15; Nonparametric one-way repeated ANOVA **,p=0.0047). This finding contrasts with the performance for runs without feedback as well as with Monte Carlo simulations using the recorded data of the feedback runs (*cf. Methods*), neither of which showed significant change over the course of training (no feedback: n=15; Nonparametric one-way repeated ANOVA ns, p=0.2434). The percentage of correct trials increased significantly from the first to last session of training, **Fig. 2.3D left panel** (Mixed model $F_{1.7,22.8}$ = 11.2 ***,p=0.0007; post hoc analysis (Tukey): first vs last session ***, p=0.0008).

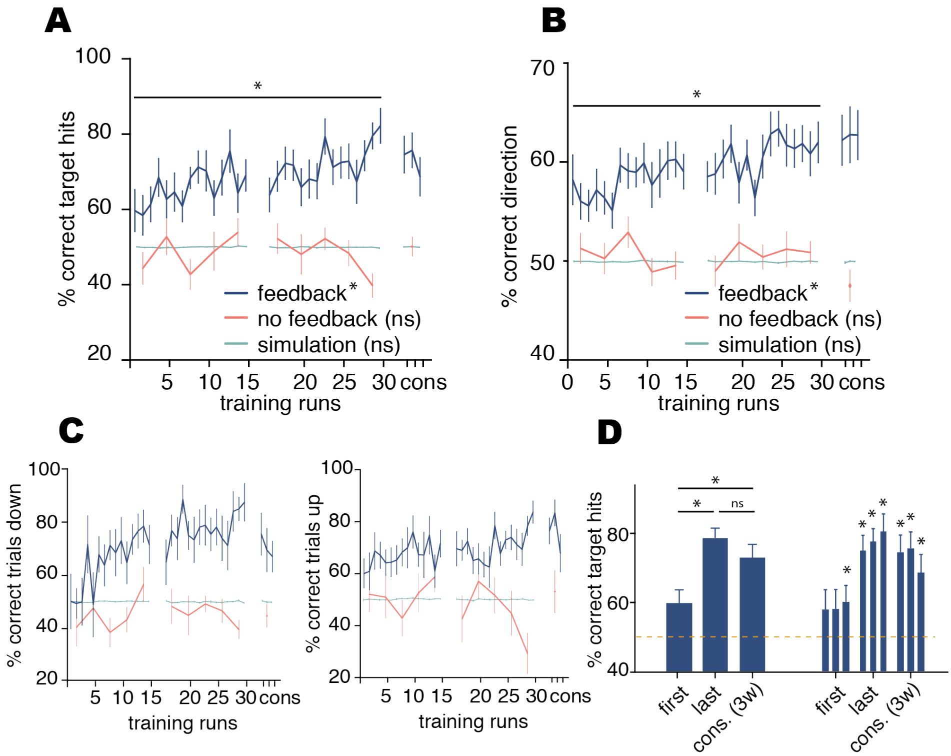

Fig. 2.3 | Subjects learn to volitionally control an EEG-based BMI abstract skill. (A) Mean percentage of correct target crosses for all subjects across training runs 1-30 and consolidation runs 1-3. Performance increases over training during feedback runs (blue), while it is kept at 50% chance level for no feedback runs (red) and for Monte Carlo simulations using the original feedback data (green). **(B)** Mean percentage of correct base limits (central horizontal lines in task display) crosses for all subjects across training. As seen in (A), the percentage of correct base limits crosses also increases over training for feedback runs (blue), showing no difference from chance level for runs without feedback (red) and for Monte Carlo simulations (green). **(C)** Mean percentage of correct crosses for down **(left panel)** and up **(right panel)** arrow trials. Performance in both directions is seen to increase during training under feedback condition. Again, runs without feedback and Monte Carlo simulations show no improvement in performance. **(D)**

Percentage of correct trials for the first and last sessions of training, as well as for the consolidation test following 3 weeks without training (**left**). Performance increases significantly from first to last session and is maintained during consolidation test. This profile is also seen when looking at the results per run on each of these training sessions (**right**). Error bars represent s.e.m., *p<0.05

We showed that the transformation was rapidly learned, starting at chance level 50%, in run 1 and run 2 of session 1, **Fig. 2.3D right panel** (run 1 ns,p=0.1054; run 2 ns,p=0.1319; run3 *,p=0.0276) and quickly becoming significantly (trial 11) different than chance **Fig. 2.4 inset** (one sample t-test (chance 50%) for trials 1-10,15,16 ns,p>0.05 and for trials 11-14,17-30 *,p<0.05), and then increased throughout the rest of the training, **Fig. 2.4 main** (longitudinal regression model, **,p=0.03).

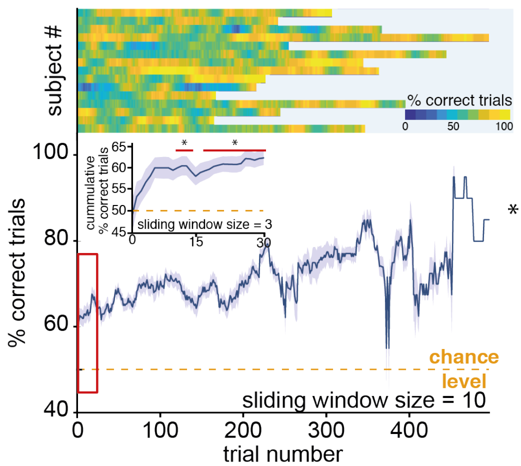

Fig. 2.4 | Individual subject performance across all training trials (average of a 10-trials sliding window, top panel). Mean percentage of correct trials across all trials. Performance is seen to increase across training (**main** – sliding window size, 10 trials). As expected, performance starts at 50% chance level when focusing on the first 30 trials of training (**inset** – note that the sliding window size is reduced to 3 trials to increase resolution and the y-axis shows the cumulative percentage of correct trials).

We also found an increase in the percentage of correct base limit crosses (i.e. when the cursor crosses one of the two innermost horizontal lines in the target's direction), indicating that learning in the task is not restricted to the target crossings, **Fig. 2.3B** (n=15; Nonparametric one-way repeated ANOVA **,p=0.00123). Furthermore, for both up and down directions (longitudinal regression model up: ****,p<0.0001; down: ****,p<0.0001), the fraction of correct trials improved from first to last day of training, **Fig. 2.3C left panel** (n=15; Wilcoxon test, *, p=0.0156) and **right panel** (n=15; Wilcoxon test, *, p=0.0125), respectively. For every measure analyzed, we found the performance to be significantly above chance level on the last day of training for the feedback runs, **Fig. 2.3A–C (2.3A:** one sample t-test (chance 50%) (run 28)****p<0.0001,(run 29) ****p<0.0001, (run 30) ****p<0.0001; **2.3B:** one sample t-test (chance 50%) (run 28)****p<0.0001,(run 29) ***p=0.0002, (run 30) ****p<0.0001; **2.3C left:** (run 28)***p=0.0007; (run 29) ****p<0.0001; (run 30) ***p=0.0002; **2.3C right:** (run 28) **p=0.0075; (run 29) ****p<0.0001; (run 30) ****p<0.0001).

One of the major caveats of using EEG is that it's signal can capture the facial muscles and ocular activity, which can have much higher amplitudes than the typical neural activity. In this study, we took several measures to ensure that facial muscle activity and ocular activity from eye movement did not explain task success. We selected a transcoder that depended on a ratio of four bands, which made the transformation robust to noise since a signal affecting the bands in the numerator and denominator of the transcoder would be evened out. In cases where there would be specific muscular or ocular activity in a particular frequency band, its effect is also felt less strongly in the outcome of the transcoder than using only one band, since the other 3 frequency bands would still be contributing with the non-contaminated signal. We performed a series of tests when choosing the transcoder and verified that even in situations of uncommon, very high muscular and ocular activity, the result of the transcoder would still be kept within acceptable values, **Fig. 2.5**. We also instructed the subjects to not rely on any kind of muscular activity to control the cursor, and not to perform movements that could lead to noticeable changes in the cursor position.

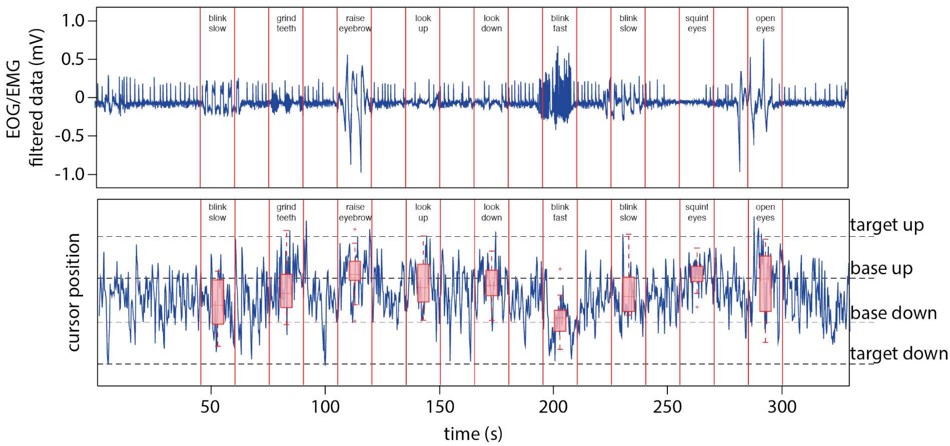

Fig 2.5 | Testing decoder resistance to major muscular and ocular activity. A test of 320 seconds was run where we asked subjects to perform major facial and eye movements while recording the activity and investigating the influence to the outcome of the transcoder. The subject was instructed to blink slowly, grind their teeth, raise eyebrows, look up, look down, blink fast, blink slowly again, squint the eyes and open eyes widely **(top)** Activity recorded from an external electrode placed on top of the right eye of the subject. Signal is filtered from 0.5-200Hz for display purposes. **(bottom)** Cursor position, calculated during the test with the activity of the 5 electrodes of the subject. We can observe that the activity is kept mostly within the target positions, does showing robustness of the transcoder.

We measure the EMG and EOG signal using external electrodes in a subset of the subjects and confirmed that the activity measured did not explain target reaches (*cf. Methods* and **Fig 2.12A-B**). Moreover, in order to ascertain that there was no influence of external muscular or ocular activity, we also conducted a new, subset of control experiments, **Fig 2.13**, where the cursor position was not updated in the presence of any facial muscle or ocular activity, identified with the use of external electrodes placed around the subjects' eyes, **Fig. 2.14A-B**. Similar to the results previously described, we found that subjects performed above chance. Taken together, these results show that human subjects are able to learn a new EEG pattern by controlling a cursor displayed on a screen in an operant learning task providing positive reinforcement for selecting the desired activity.

Learning is consolidated and performance does not decrease after long training intermission

Having analysed performance during training, we investigated consolidation of the learning to see if it could be recalled after a long period of training intermission. We ran a consolidation test session three weeks after the last training session, where subjects had to perform a similar test to the one during training. We found that the percentage of correct trials was above chance in all runs of the session, **Fig. 2.3D right panel** (one sample t-test (chance=50%), cons_run1 ***,p=0.0003; cons_run2 ***,p=0.0001; cons_run3 **,p=0.0035). We also observed a significantly higher performance during the consolidation session when compared to the first day of training, but not when compared to the last training session, **Fig. 2.3D left panel** (One-way ANOVA $F_{1.722,\ 22.39} = 10.87$; ***p= 0.0008; posthoc analysis (Tukey): first vs consolidation session *, p= 0.0362 and last vs consolidation session ns, p= 0.3463).

Moreover, the effect of learning consolidation could also be seen in all other performance measures (last 3 points on the right of **Fig. 2.3A–C**). Performance in no-feedback runs during consolidation testing was again not significantly different from chance.
We also ran another follow-up consolidation test, where we retested four of the original subjects after more than two years after training. The results suggested that the effects of learning were still present even after an extensive training intermission (mean percentage of correct trials was 66.9 ± 6.7% (sem)).
These results show that the learning of the transcoder is consolidated and can be recalled by subjects readily when asked to perform the same task even after stopping the training for a long period of time.

More than target reaching: Task-relevant EEG patterns are refined throughout learning

To further characterize the improvement in performance throughout training, we evaluated how cursor position distribution evolved throughout training. We divided each run into three different task periods: up trials, down trials and pre-trial periods, **Fig. 2.6A**. During the pre-trial periods, the subjects had to keep the cursor inside the base (region between the two innermost lines) for 2 consecutive seconds in order to start a new trial (*cf. Methods*). For every run, we fitted a normal distribution to the histogram of cursor position in each set and evaluated the evolution of these distributions within three different training phases: early- (runs 1-6), mid- (runs 13-18) and to late-training (runs 25-30). We found that the distributions of cursor position for up and down trials overlapped for the early-training phase, **Fig. 2.6B left panel**, but became more distinct as training progressed into mid and late phases, **Fig. 2.6B middle and right panels**, respectively. The distribution of cursor position during up and down trials were significantly different in mid (2way ANOVA repeated measures (direction x bins) $F_{1,5} = 10.70$, *, $p=0.0220$) and late training (2way ANOVA repeated measures (direction x bins) $F_{1,5} = 10.70$, **, $p=0.0086$), but not during early-training (2way ANOVA repeated measures (direction x bins) $F_{1,5} = 0.046$, ns, $p=0.8389$).

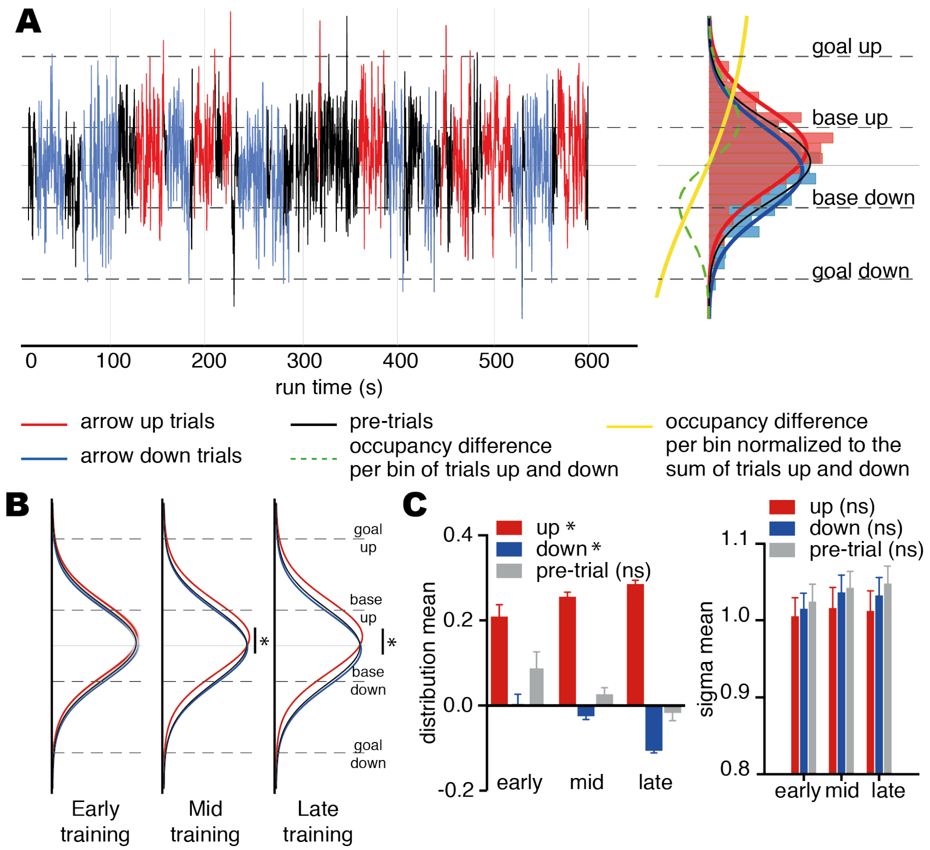

Fig. 2.6 | Distributions of transcoded EEG activity for the 3 different periods on the feedback runs (up and down trials and pre-trial periods). (A) Illustration of a representative cursor position during a 10-minute run. **(Left)** Sequences of up (red), down (blue) and pre-trial (black) periods are shown. **(Right)** The cursor position is represented for up (red binned histogram) and down (blue binned histogram) trials. Bin size represents average time spent in each bin position during the run. A Gaussian function was fitted to the histograms of cursor position distribution for the up (red line), down (blue line) and pre-trial (black line) periods. The difference in cursor position distribution between up and down trials was calculated (green dashed line) and was normalized to the sum of the up and down distributions (yellow line, see methods). **(B)** The distributions of position for up and down trials became more distinct with training, from early (runs 1-6), to mid (runs 13-18) and to late training phases (runs 25-30). **(C)** Mean position of up trial distributions increased across training phases while mean position of down trial distributions decreased across training phases **(left).** Standard deviation of distributions did not change across training phases **(right).**

When evaluating the means of these distributions, we observed an increase during up trials (nonparametric one-way repeated ANOVA *,$p=0.0289$) and a decrease during down trials (nonparametric one-way repeated ANOVA **,$p=0.0055$). The distribution mean in pre-trial periods remained unchanged (nonparametric one-way repeated ANOVA ns, $p=0.1416$), **Fig. 2.6C, left panel**. The difference in distributions was not due to a change in the shape of the distribution, as the standard deviation was unchanged throughout training (up trials: nonparametric one-way repeated ANOVA ns, $p=0.9563$; down trials: nonparametric one-way repeated ANOVA ns, $p=0.1416$; pre-trials: nonparametric one-way repeated ANOVA ns, $p=0.1840$), **Fig. 2.6C, right panel**.

Having found a change in the distributions across trial type during different training phases, we then sought to establish a quantification of the evolution of cursor position distributions for up and down trials throughout training. For each run, we calculated the normalized difference between up and down trial distributions. This quantity represented the difference in time spent at each point of the screen between up and down trials (*cf. Methods*). We plotted these differences for each of the 30 runs of training, **Fig. 2.7A**. We found that the closer to the upper target the more positive the normalized difference was, meaning that cursor was in that position more often for up trials than down trials. Inversely, the closer to the lower target, the more negative the normalized difference was, and so the cursor occupied those positions more often during down trials than up trials. In the middle of the screen, the normalized difference was close to zero, meaning that the time spent at this position was the same for up and down trials. This analysis also revealed that the longer into the training, the higher was the magnitude of the normalized difference closer to the extremities, and thus the cursor stayed longer in that position during the corresponding trials. Moreover, it is important to point out that the value of the normalized difference in the center of the screen did not vary with training, showing that the time spent in around that position was similar for up and down trials throughout training. Importantly, this profile in cursor position distribution is directly linked to a refinement of the EEG pattern over training. The overall EEG pattern becomes closer to the optimal pattern to reach the target, even during the periods when the target had not been reached.

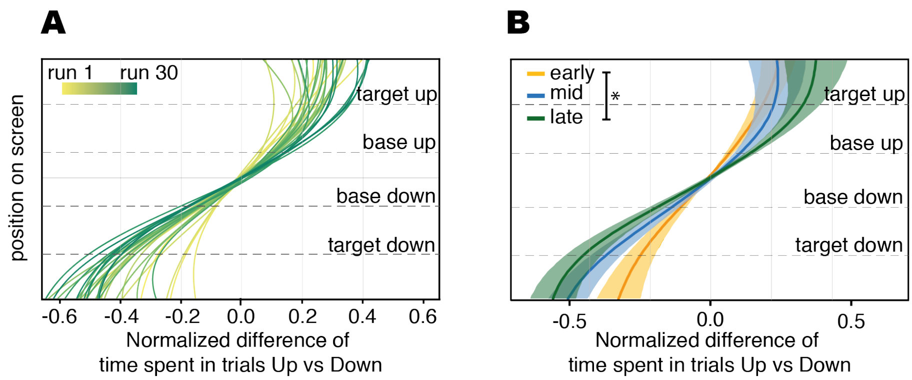

Fig 2.7 | Normalized difference of up and down cursor position distributions. (A) Normalized difference of cursor position distributions for runs 1-30. While values in the extremes of the screen (above target up and below target down) increased, in magnitude, as training progressed, there was no difference between time spent in up and down trials in the middle section of the screen. **(B)** Normalized difference of cursor position distributions for early-, mid- , and late-training phases. Same effect as in (A) can be seen when training is divided in three different phases.

The same analysis was also performed for early-, and late-training, **Fig 2.7B**. The normalized difference increased from early to late training phases around target up positions (2-way ANOVA repeated measures (training phase x bins), main effect (training) $F_{1,14} = 6.77$, *,p=0.0210) and decreased for the same phases around target down positions (2-way ANOVA repeated measures (training phase x bins), main effect (training) $F_{1,14} = 18.47$, ***,p=0.0007). Again, this meant that the cursor was occupying more often those positions during the corresponding up and down trials, respectively.

EEG activity is modulated in four target bands in order to control cursor position on screen

Next, we investigated how the recorded EEG activity changed as the cursor crossed the correct target. To do that, we divided each run into three distinct periods: up, down, and pre-trial. We considered the last second of each correct trial, corresponding to EEG data inputted to the transcoder that made the cursor position hit the target in the correct direction. Since pre-trial periods were longer than 1 second, we selected randomly 1 second of data during that period.

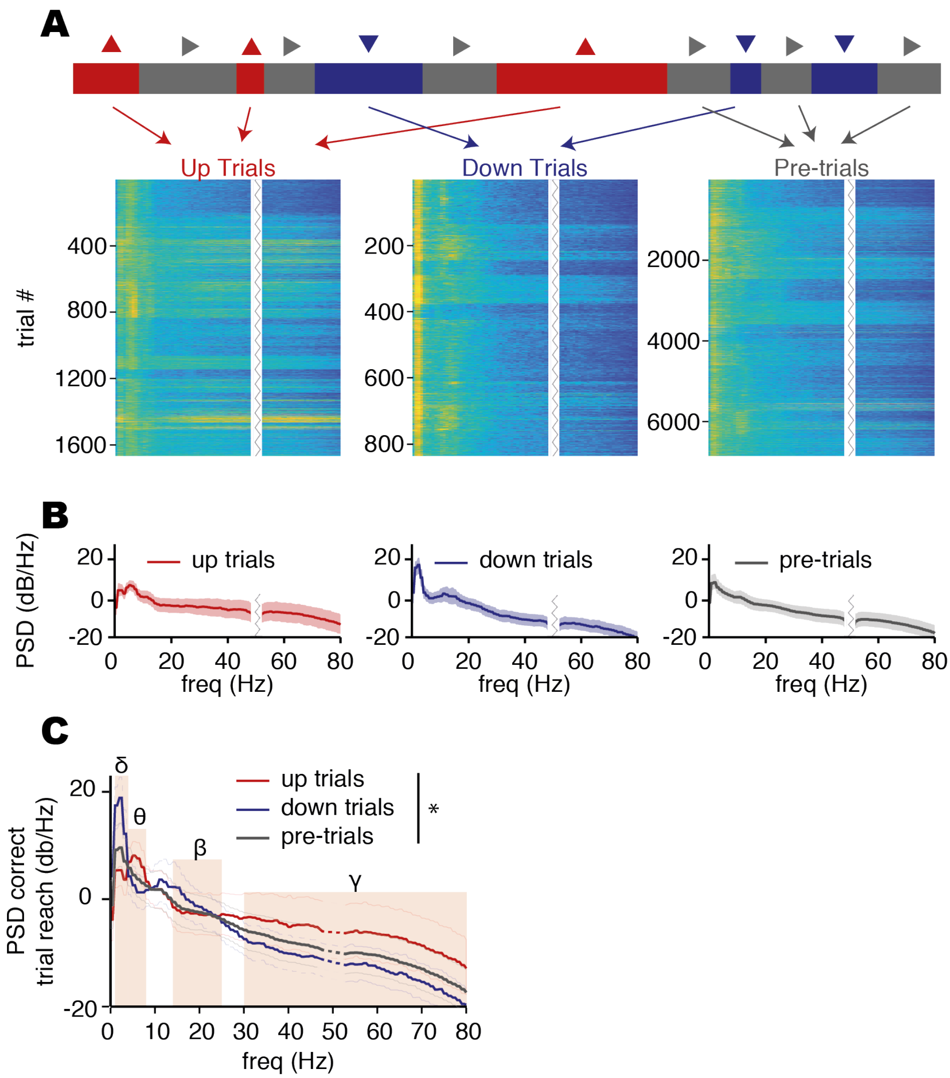

Fig. 2.8 | Correct targets are reached by modulating all four EEG frequency bands. (A) (Top) Segmentation of a run into 3 distinct periods: up (red), down (blue) and pre-trial (grey) periods; **(Bottom)** Trial's Power Spectral Density (PSD) for all trials and all subjects for the corresponding periods of a run. Data is color coded from blue (-30dB/Hz) to red (30dB/Hz). White band represents notch filter ~50Hz to remove grid noise interference. **(B)** Median of PSD for all trials, corresponding to the data and periods represented above. **(C)** Comparison of mean PSD per period. Signal changes from pre-trial to up and down trial types in multiple EEG frequencies.

We evaluated the mean power spectral density (PSD) of the five electrodes used by each subject for all trials during these periods, **Fig. 2.8A**. For this analysis, we considered the frequency range used in the transcoder (1–80 Hz). We found discernible differences in the average PSD of all trials when comparing up, down periods and ore-trial periods (2-way ANOVA repeated measures (trial type x frequency), main effect (trial type) $F_{1.803, 19.83} = 5.82$, *,p=0.012), **Fig. 2.8B-C**.

We then sought to find out which EEG bands showed differences in modulation when comparing up and down trial types. Both up and down targets could have been reached by modulating a subset of the four EEG bands used in the transcoder. However, modulating all bands to move the cursor in the target's direction would minimize the modulation needed for each band. We started by normalizing the up and down data sets to the pre-trial periods of the same run and plotting the resulting ratio. We observed changes in the PSD profile for the up and down trial types across all 4 EEG frequency bands when normalized to the pre-trial period, **Fig. 2.9A**. These changes were seen in the direction that facilitated the cursor's displacement to the correct target, e.g., for the up trials, we saw an increase in the transcoder result when compared to the pre-trial period. This increase resulted from an increment in PSD of the theta and gamma bands and a decrease in the delta and beta bands in comparison to the pre-trial periods. We found the inverse result for down trials compared to pre-trials. In contrast, we did not find such evident changes when analyzing similar periods during the no-feedback runs, **Fig. 2.9B**.

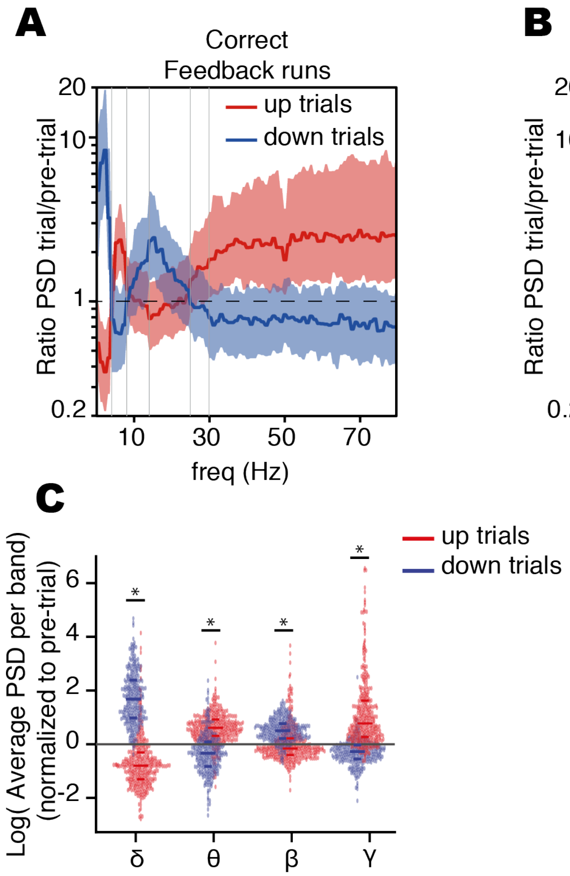

Fig 2.9 | PSD changes from correct up (red) and correct down (blue) trials to pre-trials, during the last second window of trial data. (A) Changes in PSD in comparison to pre-trial period for correct feedback runs. The changes are noticeable in all 4 bands of the transcoder, and happen in the direction that facilitates cursor movement to the correct target. **(B)** Changes in PSD during no-feedback runs are not evident in the transcoder frequencies. **(C)** Average PSD changed from up and down trials to pre-trial. Also in this case the differences between up and down trial can be noticed.

Next, we evaluated the mean PSD for each of these bands, since the transcoder used the mean activity in each band. We found that for each band, the averages PSD for up and down trials were significantly different, further demonstrating that the subjects were able to modulate their EEG activity in all bands in order to control the cursor on the screen (paired t-test, ****,$p<0.0001$ for all bands), **Fig 2.9C**.

Taken together, we observed a modulation of the EEG signal in all frequency bands in order to achieve the task objectives. Although the subjects could have had reached the targets by modulating the EEG profiles in many different ways, this particular frequency profile requires the least variation in each EEG band, which could be interpreted as an efficient way of attaining the task objectives.

DISCUSSION

In this study we investigated human subjects' capacity to learn a rare complex pattern of neural activity to directly control a cursor on a screen. Through a EEG-based Brain-Machine Interface (BMI), using an operant-learning task, subjects needed to learn to continuously control a multiband EEG pattern. This novel approach to human BMI expands on recent findings from animal studies that demonstrate the capacity of the brain to create *de novo* circuits to perform neuroprosthetic actions when executing operant-learning BMI tasks (Athalye et al., 2018; Ganguly and Carmena, 2009; Koralek et al., 2012; Neely et al., 2018). We showed that subjects increase task performance over a two-week period, becoming more in control of a pattern that relies on the modulation of a fixed multi-band EEG transcoder. We also tested subjects' capacity to recall learning after a three-week training intermission during a consolidation test, showing that the task performance does not drop after the long training break and can readily be recalled. We further showed that the learning can be seen in multiple measures of performance, including significant changes in the distributions of cursor position throughout training. In these cases, the cursor position distributions for up and down trials started overlapping in the beginning of training but were shown to separate as training progressed. This separation demonstrates a continuous control of the EEG pattern and shows that the EEG patterns become more refinement with training, even during the periods when the targets were not being reached. Finally, we showed that the modulation of the activity when reaching the targets happens on the all four bands of the transcoder, which correspond to a strategy where the least amount of changes had to occur in each band for the trial to be successful.

The majority of human-BMI studies have implemented the decoder approach focusing on machine learning (ML) techniques and signal processing. These techniques identify pre-existent EEG patterns and mostly require that the subjects produce stable, consistent signals to match the ML-learnt decoder. Despite significant progress using this approach, several downsides have been identified and proved difficult to overcome, e.g. recognizing input commands from EEG signals that are intrinsically noisy and being able to classify them as task actions, or relying on the subjects' capacity to generate stable and consistent neural signals across days.

In order to deal with these issues, researchers typically rely on implementations that are known to generate more consistent and reliable EEG signals such as motor imagery, motor planning or movement execution (Blefari et al., 2015; Perdikis et al., 2014; Wolpaw and McFarland, 2000). In these cases, subjects are asked to think of specific motor actions, such as moving the left or right arm, while the corresponding neural activity is classified and used later in the BMI paradigm. For the most part, however, these studies neglect the users' capacity to learn to generate and adapt their own neural activity (Lotte et al., 2013; Perdikis et al., 2018). Interestingly, even in studies where the decoder approach was implemented, using pre-existent natural activity as features, e.g. changes in sensorimotor area's BOLD activity, it was shown that allowing the subjects to develop their own strategy revealed higher learning effects than following the researcher's instructions (Sepulveda et al., 2016).

Additionally, research in EEG-based BMI in humans, that rely on neurofeedback, have mostly targeted control of pre-existent EEG activity (typically one or two EEG bands such as mu or low beta). These approaches usually rely on identifying specific properties in that band (or set of bands) that can discriminate task conditions from the start of the training, e.g. an increase/decrease in the amplitude of a band is assigned to an increment in the up/down movement direction of a cursor in a 1D task (Wolpaw et al., 1991). Control in such tasks can be attained by managing to change the activity in relation to a baseline and is usually accomplished by evoking a pre-acquired action that relates to that targeted neural activity e.g. or changing an emotional state like being more relaxed or more focused. Although demonstrating control of neural activity, the patterns of activity evoked during those BMI tasks mostly need to be similar to those evoked during the BMI algorithm training and do not require the generation and learning of new links between neural patterns and actions in task.

Previous studies have shown that animals' neural activity changes during BMI tasks (Carmena et al., 2003; Ganguly and Carmena, 2009; Ganguly et al., 2011) and that animals learn to more frequently enter arbitrary patterns of activity that lead to reinforcements (Athalye et al., 2018; Clancy et al., 2014; Fetz, 1969; Koralek et al., 2012). These studies have shown that cortico-striatal plasticity is necessary for the learning of new BMI skills (Koralek et al., 2012; 2013; Neely et al., 2018). As learning progresses, task relevant cortical patterns are gradually more refined and are optimized to achieve outcomes more directly. Task-relevant neuronal population activity increases its covariance throughout training, while indirect neurons variability decreases with training (Athalye et al., 2018; 2017).

Changes happening during operant BMI learning are similar to what is seen during motor learning (Barnes et al., 2005; Costa et al., 2004; Jin and Costa, 2010; Karni et al., 1998; Yin et al., 2009), thus indicating that BMI and motor learning implicate the similar neural strategies.

The paradigm we implemented in this chapter expands on the studies in animal models, presenting an alternative to the existing human, non-invasive implementations in several fundamental ways: 1) the transcoder encompasses multiple EEG bands, and is selected independently of any link to a natural plan, suggesting that the transformation needs to be learned *de novo* and the pattern re-entered and refined; 2) subjects have to be in control of the activity to reach three specific targets (up and down targets and stay in the base area for two seconds); 3) the task is self-paced and does not rely on cues, increasing the dependence on the constant control of EEG activity; 4) neural modulation learned in task is readily recalled every day, and during a consolidation test after long training intermission task performance is maintained, indicating long lasting effects of BMI learning,

In summary, these findings offer an alternative to the conventional human BMI approaches by implementing a complex fixed transcoder with multiple EEG bands. The implemented task reinforced the learning of a challenging EEG pattern, initially unrelated to any pre-existing motor or mental action. In order to increase task performance subjects needed to modulate EEG activity to more often enter the rare pattern. We showed that learning of such pattern was possible and that subjects re-entered it more efficiently throughout training. The continuous control of the EEG pattern was also refined throughout training, leading to improvement in performance measures related to task objectives, even during the periods when the targets had not yet been reached. Imposing the generation and learning of a new link between neural activity and actions in the task opens up the extent of possible applications of BMI systems, since the subjects are not constrained by previous acquired skills and neural activity.

METHODS

Subjects

15 volunteers (9 female and 6 male; mean age 29.4 years old, SD 7.7years old, Table S1 in Supplementary Materials) took part in the study without any type of monetary compensation. Subjects reported no history of psychiatric or neurological disorders, nor did they report chronic use of medication. Subjects had not participated in any prior brain-machine interface experiments. All subjects were asked to keep a similar schedule during the two weeks of experiment and if at all unavoidable to keep a regular schedule in the hours prior to the experiment on each day. No physiological sleep disruptions were reported by the subjects during the experimental period. Informed consent was obtained from all subjects.

Subject	***Age***	***Electrodes Used***
A	*42*	*FC1; AF4; Fz; FC6; FC4;*
B	*27*	*AF3; F3; F5; Fz; FC6;*
C	*31*	*F5; F4; F6; FC6; FCz;*
D	*28*	*AF3; FC5; FC6; FC2; FCz;*
E	*33*	*F3; F5; FC1; AF4; AFz;*

Subject	***Age***	***Electrodes Used***
F	*37*	*F1; F5; FC1; AF4; AFz;*
G	*24*	*F1; AF4; F2; F4; F6;*
H	*25*	*AF3; F2; F4; FC4; FC2;*
I	*24*	*FC3; FC1; AF4; F4; FC6;*
J	*46*	*F3; FC5; FC6; FC4; FCz;*

Subject	***Age***	***Electrodes Used***
K	*35*	*F1; FC3; AF4; FC2; FCz;*
L	*23*	*F3; FC5; FC1; F2; F4;*
M	*21*	*F3; F5; FC5; Fz; FC6;*
N	*23*	*F5; AFz; F2; FC6; FCz;*
O	*22*	*F5; FC5; Fz; F6; FC6;*

Table 2.1 | Electrode locations for the 15 subjects.

Experimental Design

All subjects were assigned the same experimental protocol with a duration of 10 consecutive weekdays (Monday to Friday, for two weeks). Every day during the two weeks, subjects were requested to allocate one hour and thirty minutes to the experiment, enough time to prepare and set up the EEG recording system, perform the experiment session and clean after the experiment. Subjects were also requested to allocate the same 1.5 hours three weeks after the last training session, with the objective of performing another session to re-test if there had been consolidation and retaining of learning. Each training and consolidation sessions consisted of 3 runs of 10 minutes with 5 minutes breaks in between. In each of these runs, subjects were comfortably seated in a chair while their EEG data was recorded and transformed with a transcoder. The subjects were asked to try to control a cursor displayed on a screen approximately 1.5m away from them, at eye-level. No indication or strategy were given on how to execute the task. At the end of these 3 runs, a fourth run was recorded, during which the subjects were shown a still frame taken from the task and thus were not given any feedback of their EEG activity. This last run was used as a control setting to assess performance without feedback.

Fixed Transcoder

The fixed transcoder that converts neural activity into cursor position is a mathematical function of four specific EEG frequency bands. This particular index of bands was previously found to be correlated with dopamine-related states in rodents (Costa et al., 2006). In this specific transcoder the average power in the previous second of the theta (4-8Hz) and gamma (30-80Hz) bands had the opposite effect in the cursor position to the average power in the delta (1-4Hz) and beta (14-25Hz) bands. An increase in average power per electrode in theta and gamma, as well as a decrease in power in the delta and beta bands led to a higher cursor position, while a decrease in the former two bands and an increase in the latter two bands led to lower cursor position. The mathematical transformation to calculate the position at time t was given by:

$$p(t) = log\left(\sum_{i=1}^{5} \frac{\overline{\gamma^{i}_{[t-1,t]}}}{\overline{\beta^{i}_{[t-1,t]}}} \frac{\overline{\theta^{i}_{[t-1,t]}}}{\overline{\delta^{i}_{[t-1,t]}}}\right) \tag{2.1}$$

The ratio is calculated for each electrode i and summed over all 5 electrodes chosen for each subject. The result is then log-transformed, which transforms the output in a normal distribution. Every 250ms a new cursor position was calculated and displayed on the screen by taking into account the last 1 second of EEG data from the 5 chosen electrodes, **Fig. 2.2A**. The mathematical expression for the transcoder in **Eq. 2.1** was the same for all 15 subjects, while the 5 electrodes were picked specifically for each subject from a pool of 17 electrodes located above the motor and frontal cortices (AF, Fp, F, C locations in the modified international 10-20 system (Klem et al., 1999)), *cf. section Channel Selection and Calculation of Target Positions.* This selection was done before the first training session, during a short channel selection and target calculation session which took into account the EEG activity at rest during 5 minutes.

Task description and objectives

Subjects were informed their EEG activity was going to be recorded, processed and transmitted to the computer, so that the cursor on the screen would change its vertical position according to the transformed EEG activity. Subjects were shown a still frame of the task in order to explain its layout, **Fig 2.10A**. The subjects were told that the blue line before the cursor represented the history position of the cursor during the five timesteps prior to the current position, which represented 1.25seconds in total. The current position was represented by a red circle, displayed horizontally in the center of the screen, but allowed to move vertically. The four horizontal lines on the screen represented important positions for the task: The top and bottom lines represented the targets to be crossed in the cases of up and down trials, respectively, **Fig. 2.10A-F**. The inner-up and inner-down lines represented the base area, in between which the subject had to maintain the cursor for two seconds in order to start a new trial. Every time a new trial was started an arrow was displayed on the top- or bottom-right side of the screen, indicating in which direction the subject should direct the cursor to.

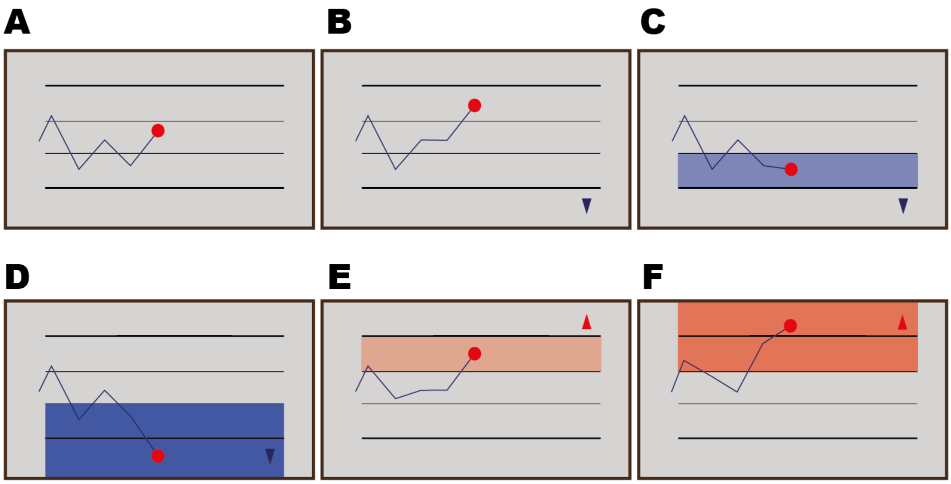

Fig. 2.10 | Example of situations occurring during one run of the task. (A) During pre-trial periods no arrow is shown and the subject needs to direct the cursor to the middle of the screen where it needs to stay for 2 consecutive seconds in order to start a trial; **(B)** Trial down, indicated by blue arrow in the bottom corner, Cursor is crossing the base area in the wrong direction, no feedback is given besides cursor position; **(C)** Cursor crosses the base area in the correct direction during a trial down. Light patch of color appears reinforcing the action; **(D)** Down target is reached during trial down. Darker patch of color is displayed, trial is considered correct and arrow disappears shortly after; **(E)** and **(F)** same as (C) and (D) but exemplified for an up trial.

The generation of trial direction was done in a random way and, in order to avoid a biased performance, we limited the number of consecutive trials to the same side to four, after which we would force the trial target to be in the opposite direction. We also explained to the subjects that each trial had a maximum of 30 seconds during which three possible outcomes were allowed: 1) the trial ended correctly if the subject reached to the desired target; 2) the trial ended incorrectly if the subject reached the opposite target, and 3) the trial ended as a timeout if during 30 seconds no target had been reached. After the end of each trial, the arrow disappeared and the subject had to return the cursor to the base area for two seconds to start a new trial. Subjects were informed that they were going to receive a visual feedback every time they were going in the desired direction. If the cursor crossed the first horizontal line, i.e. left base area, in the desired direction of the trial a short and light color patch was displayed on the screen between the first and second lines in that direction, **Fig. 2.10C,E**. On the other hand, if the cursor passed the first line in the opposite direction, no negative visual feedback was shown to the subject, **Fig. 2.10B**. In the cases that the cursor crossed the top/bottom goal line, a darker and larger patch of light was displayed indicating that the trial had been successfully completed, **Fig. 2.10D,F**. If the cursor crossed the incorrect target line, the arrow disappeared and the trial was classified as incorrect.

Channel Selection and Calculation of Target Positions

After setting up the EEG system and before starting the training on the first session, the subjects were informed about the experiment's protocol and its objectives. The subjects were asked to sit on a chair and look at the computer screen for 5 minutes, which displayed a still frame taken from the task they were about to perform, **Fig. 2.10A**. Subjects were informed that an EEG reference signal was going to be recorded and were asked to avoid movement as much as possible in order not to contaminate the recorded signal. After the 5-minute period of EEG signal collection, a script was run to calculate the most suitable electrodes and the corresponding horizontal targets for the specific subject using the transcoder. A flow diagram of the channel selection and target position calculation can be seen in **Fig. 2.11**. All the combinations of five electrodes, out of the 17 initial electrodes located above the motor and frontal cortices **Fig. 2.2B**, were taken into consideration and the EEG signals from each ensemble of five electrodes were transformed with the transcoder to calculate the arrays of cursor positions for the 5 minutes.

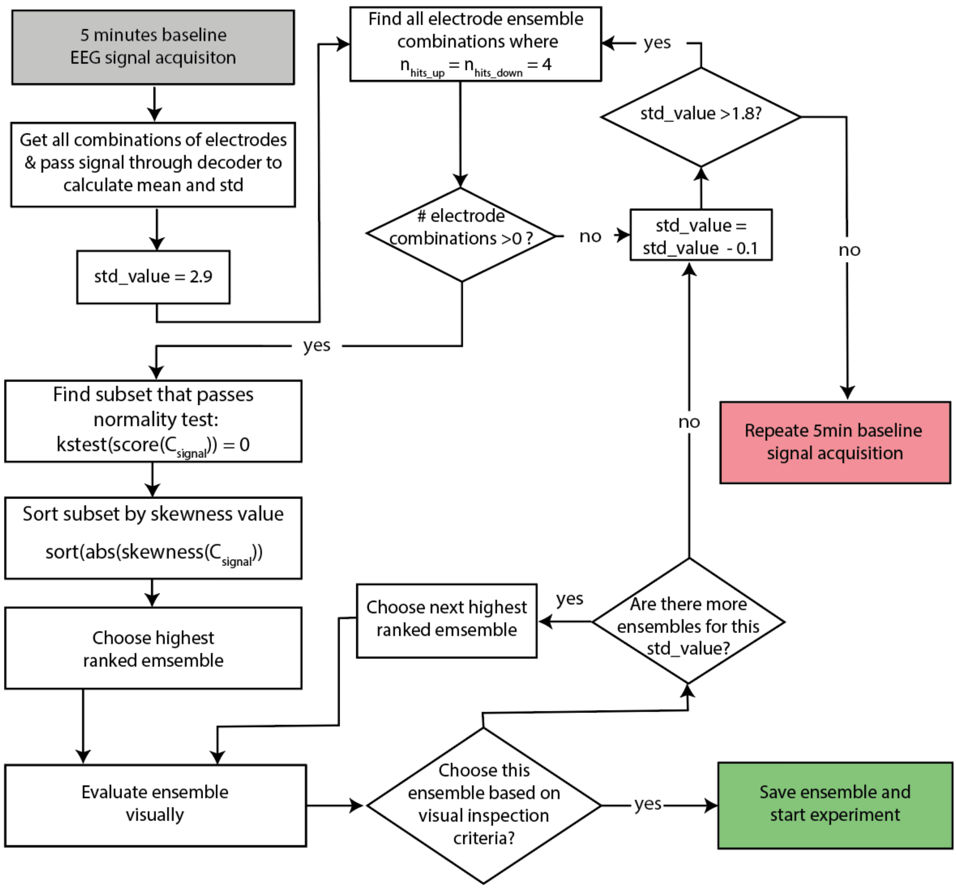

Fig. 2.11 | Flow diagram illustrating the procedure for channel ensemble selection and target position calculation before the beginning of first training session.

The electrodes and targets were then chosen to guarantee that over the 5-minute reference activity the distribution of cursor position would follow a Gaussian distribution and that naturally the subject would be able to reach both targets the same number of times, thus making sure that the distribution was unbiased and attainable, **Fig. 2.2B - right panel**.

The number of target crossings during the 5-minute period was set to 4 on each target. The reasoning behind this value was to make these events possible to reach but rare enough that would allow feedback to reinforce the behavior. The proposed value was considered to be not too small (which could lead to a lack of enough correct trials and loss of motivation) nor too high (which could result in a greater amount of correct but also incorrect trials), which in both cases would render the task more difficult to learn. The limits of the base area were set at the position calculated by:

$$B_{pos}^{up/down} = \overline{p(t)_{t=[1,300]}} \pm \sigma\left(p(t)_{t=[1,300]}\right) \qquad (2.2)$$

where, $\overline{p(t)_{t=[1,300]}}$ is the mean of the reference signal acquired during the 5 minutes (300 seconds) and $\sigma\left(p(t)_{t=[1,300]}\right)$ is the standard deviation of the distribution. The target positions were calculated by:

$$T_{pos}^{up/down} = \overline{p(t)_{t=[1,300]}} \pm \mathcal{K} * \sigma\left(p(t)_{t=[1,300]}\right) \qquad (2.3)$$

Where $\mathcal{K}$ is a constant calculated in the first day of training, *cf.* **Fig. 2.11**, that guarantees a fixed and balanced number of target crossings within the 5 minutes, as explained above. The target positions as well as the limits of the base area were then linearly scaled into pixel position on the screen so that they would always be displayed in the same absolute position to the subject. Once the parameters were set, the rest of the first session was designed to be the same as the remainder trainings session.

The parameters obtained during the first day, were kept constant throughout the experiment which allowed us to link any changes in performance exclusively to changes in recorded activity. Nevertheless, during each run, the distribution of position was evaluated every 3 minutes. In the rare cases that the mean of the position distribution during the previous 3 minutes shifted more than a pre-defined threshold given by:

$$\overline{p(t)_{[t-180,t]}} > \left|0.5 * (T_{last}^{up} - \overline{p_{last}})\right| \tag{2.4}$$

both targets and base area limits were realigned by $\Delta = (\overline{p(t)_{[t-180,t]}} - \overline{p_{last}})$. This realignment was implemented to prevent any bias to a specific side and making sure that the task would continue to present the same level of difficulty towards the up and down targets.

Equipment and Signal transformation

EEG signals were acquired using an ActiveTwo measurement system (BioSemi Instrumentation, Amsterdam, Netherlands), with a sampling frequency of 2048Hz. EEG was recorded using 64 electrodes arranged in the modified 10/20 international standard (Klem et al., 1999). Electrooculogram (EOG) and facial electromyogram (EMG) signals were synchronously acquired using four external electrodes with the same system for 6 subjects (S9 - S15). The external electrodes were placed next to the left and right canthi of the eyes as well as above and below the subject's left eye, in order to capture both horizontal and vertical EOG components. The data was collected under Ubuntu Linux 10.04 Operating System and the recording was done based on the CNBI Toolkit (CNBITK) framework for BCI, developed in the CNBI lab at EPFL which implemented a standardized communication interface based on the Tools for Brain Computer Interaction (TOBI) project (Müller-Putz et al., 2011). The EEG data was filtered and processed online in steps of 250 ms taking into account the last 1 second of data (or 2048 points). The EEG signal of the 64 electrodes was bandpass filtered between 1-80Hz (zero-phase Butterworth, 4th order) using a zero-phase filter and a notch filter was applied to the signal at 50Hz, second-order Infinite Impulse Response (IIR) filter. We then calculated the power spectral density (PSD) using the Welch's method (*pwelch* function implemented in *MATLAB*) of the 5 chosen electrodes for the subject. The Welch's method segmented the time windows into 8 different intervals with a 50% overlap. Each segment was windowed with a Hamming window and a modified periodogram was computed for these segments where the resulted values were averaged to obtain the PSD estimate. The average PSD per frequency band was calculated and input in the transcoder to obtain the cursor position according to **Eq. 2.1.**

Data Analysis

Analyses were performed in MATLAB (Mathworks) with custom-written routines. For the feedback and no-feedback results in **Fig. 2.3A-C**, the performance of the corresponding run for all subjects was averaged and the standard error of the mean was calculated.

The Monte Carlo simulations were performed using the feedback data of each 10-minute run, but reconstructing a new cursor position array from that data as follows: 1) the initial element of the array was the cursor position of the feedback run at a random time *t;* 2) the following elements in the array corresponded to the original cursor positions to the end of the run; 3) the remaining data, which corresponded to the interval [0, t-1], was concatenated to the end of the array, resulting in a new 10-minute vector with the same number of data points as the original array. This method was preferred to randomly sampling a new data array from the original 10-minute cursor position, to prevent the loss of temporal information. The performance of the simulated run was calculated considering the new array of cursor positions and following the same protocol as if a normal feedback run was being conducted.

In **Fig. 2.3D**, the performance for each of the three represented sessions corresponded to the mean ± s.e.m. of the respective three runs in the session, for all subjects. The right panel data is the same as represented in the corresponding runs in **Fig. 2.3A.**

For **Fig. 2.4**, the trial-by-trial analysis was performed using a sliding window length of 10 trials in the main panel and a sliding window of 3 trials for the inset panel. This difference in the window size was used to show how the performance started at chance level during the first few trials. This detail result could not be captured with the original 10-trial window size due to the fast rise in performance above chance in early training.

In **Fig. 2.6A** we showed how a typical run is divided into 3 periods: up and down trials and pre-trial. For each of the subjects' runs we performed the same analysis. We started by subtracting the mean cursor position of the run so that the runs for all subjects were centered around the same value. We then fit a normal distribution to the distributions of cursor position for each of the periods (using the functions *fitdist() and normpdf()* in MATLAB). We subtracted the fitted distributions for the up and down periods to obtain the difference in cursor position distribution for the two different trials (green dashed line). We then normalized this result to the sum of the two fitted distributions to obtain a visual representation of the change in cursor distribution per trial type (yellow solid line). In **Fig. 2.6B** we averaged the distributions of each period for three different training phases, early- (runs 1-6), mid- (runs 13-18) and late-training (runs 25-30) and present the average for all subjects ± s.e.m highlighted. The average of the means and average of standard deviations of the fitted distributions is displayed in **Fig. 2.6C**. Finally, in **Fig. 2.7A** we show normalized difference of the cursor position distributions for up and down trials, as explained above. Each line represented the average of each run over all subjects. **Fig. 2.7B**, shows a similar analysis but, instead, averaged over the runs of the corresponding period.

In **Fig. 2.8**, we analysed the EEG data during the last second of the correct trials. This one second window of EEG data corresponded to the transformed signal that when passed through the transcoder allows the cursor to reach the up or down targets. For all panels in this figure, the analyses were run on all the trials of all subjects, concatenated together. For each trial (up or down) the mean PSD corresponding to the five used electrodes was calculated and a PSD profile within 1-80Hz was represented in each line of **Fig. 2.8A.** To maintain the same number of data points going into each analysis, for pre-trial periods we randomly selected 1 second window from the data when the subject had to start a new trial. The median of all trials was then calculated and is represented in Fig. 2.7B-C. Shaded areas of the plots represent the 25% and 75% quantiles.

In **Fig. 2.9**, the PSD for up and down trials were divided by the pre-trials to obtain the profile of change between these different periods. The calculation of each ratio was performed for the corresponding run, e.g. PSD of up trials in run 1 of subject A was normalized by the PSD of pre-trials in the same run 1 of subject A. This was done to avoid contamination mixing the signal from different subjects and different runs, which could have a different baseline from the start. The same analysis was run for the runs without feedback. Although the subject was not receiving any feedback of the cursor position, the simulation was still running in the back and by chance targets would be reached, see **Fig 2.2** for chance level performance of no feedback runs. **Fig. 2.9C** resulted from evaluating the mean PSD of each band from the data of **Fig. 2.9A**.

Testing external EMG/EOG activity

Measuring EMG/EOG activity during BMI task

We recorded electrooculogram (EOG) and facial electromyogram (EMG) signals synchronously with the EEG signal for 6 of the 15 subjects (J–O, **Table 2.1**). We analyzed the data around the target crossing events for the correct and incorrect trials in order to evaluate if there was a link between the activity registered with the external channels and that particular period of the task. **Fig 2.12** shows the median EEG activity in a window of five seconds before and after target crossings for correct, **Fig. 2.12A**, and incorrect, **Fig. 2.12B**, trials. We calculated the range of signal activity in a window [-3 s, -1 s] before the target crossing window for the four recording electrodes. This window was taken because it was a period that we knew the cursor had not crossed the target. The activity was deemed statistically significant when more than 20 ms bins (40 consecutive data points) within the 1 s target window laid outside the [1%, 99%] of activity at the intervals [-3 s, -1 s]. Although there is a clear change in activity after the event, this change is not noticeable during the event window. Taken together, these results allow us to conclude that the use of external artifacts was not necessary for task performance.

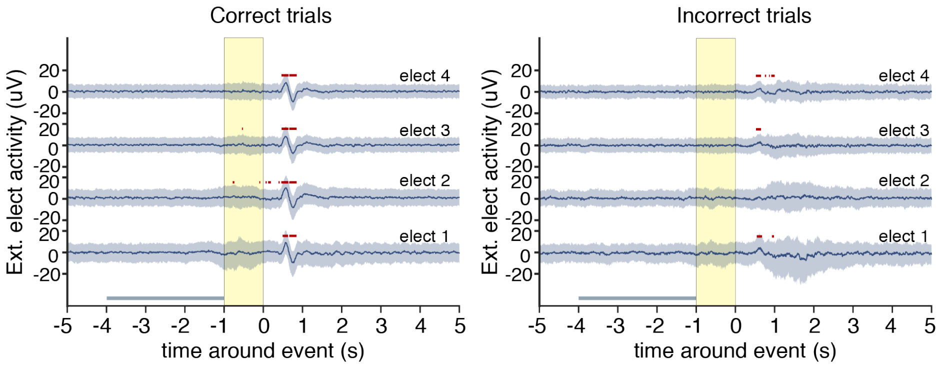

Fig 2.12 | EOG/EMG activity measured around event. **(A)** Activity measured with the four externals electrodes around correct target crossings and **(B)** incorrect target crossings.

Subset of experiments with enforced artefact detection and avoidance

We designed and conducted a subset of experiments to probe BMI performance under stricter task rules. In these experiments we analyzed the data recorded with the external electrodes in real time while the subjects were performing the task. We established an online rule that allowed us to identify whether a source of external muscular or ocular activity was being used. Because we were mostly interested in artifacts that could be related to eye movement and blinks, the detection of artefacts was done by assessing the skewness of the distribution of the recorded signal on the electrode placed above the right eye, during 1 s windows. Before each subject began the BMI task, we evaluated the minimum and maximum skewness values that would detect artefacts. We selected specific values for each subject, so that the detection was very conservative **Fig. 2.13A, left panel**. We opted to have a conservative method and increase the number of false positives detected, making the task more difficult to control. During training, every time the activity was recorded outside the limits of the criteria, we triggered a flag on the BMI code that prevented the update of the cursor position for 1 second and subjects saw a continuation of the last allowed cursor position, **Fig. 2.13A, right panel**.

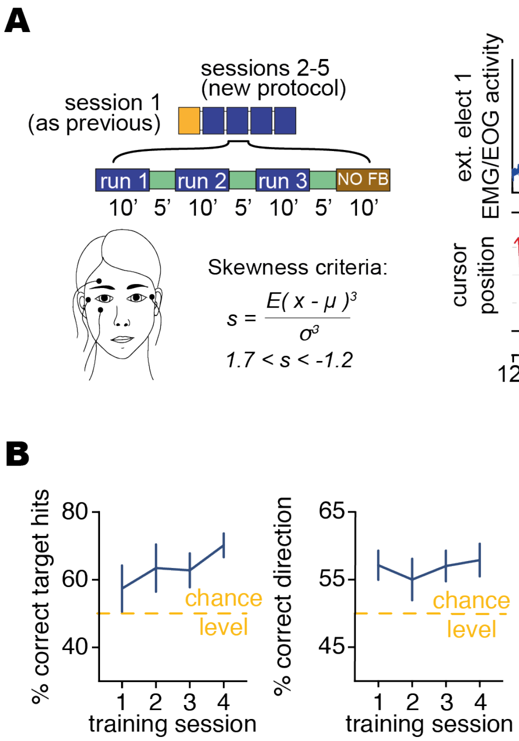

Fig 2.13 | Subset of experiments with enforced artefact detection and avoidance. (A) Protocol of experiment; **(left)** In the first day of training the experiment was the same as the subjects had already trained on. From days 2-4 the new protocol was implemented. In this case the EMG/EOG signal recorded with electrodes around the eyes was evaluated in real-time and if the skewness of the signal in 1 s window was outside the indicated criteria the cursor position would not be updated **(right). (B)** Even with much stricter rules than in the original experiment, performance in task was above chance for both the percentage of correct target hits and the percentage of correct base limits crosses (central horizontal lines in task display) for all subjects across training.

CHAPTER 2

The cursor would maintain the position constant for 1 s after the last activity outside the criteria had been verified. When the signal was back to permitted activity, the ball position would be updated again. No reinforcements were displayed during the periods when the flag was on. Even in such challenging conditions for the subjects, we found that performance was above chance, **Fig. 2.13B**.

Fig. 2.14 shows the activity measured around event for correct **(A)** and incorrect **(B)** target crossings, during this subset of experiment. The analysis was conducted as before, and again we see no statistical differences during the 1 s window of target crossings and the 3s windows of baseline considered.

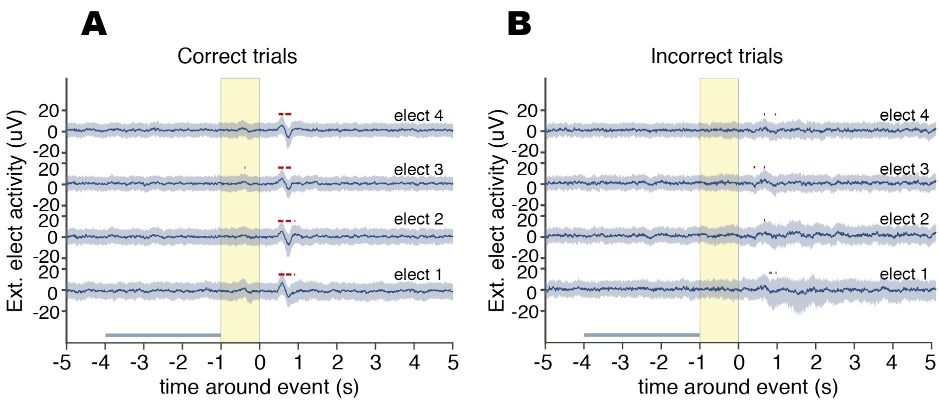

Fig 2.14 | EOG/EMG activity measured around event during task to enforced artefact detection and avoidance. B**A)**Activity measured with the four externals electrodes around correct target crossings and **(B)** incorrect target crossings.

Fig	Description	Statistical test	Values
2.3A	Feedback; n=15	Nonparametric one-way repeated ANOVA	**p=0.0047
	No Feedback; n=15	Nonparametric one-way repeated ANOVA	ns, p=0.2434
	Three last runs	one sample ttest (chance = 0.5)	(run 28)****p<0.0001,(run 29) ****p<0.0001, (run 30) ****p<0.0001
2.3B	Feedback; n=15	Nonparametric one-way repeated ANOVA	**p=0.00123
	No Feedback; n=15	Nonparametric one-way repeated ANOVA	ns; p=0.8834
	Three last runs	one sample ttest (chance = 0.5)	(run 28)****p<0.0001,(run 29) ***p=0.0002, (run 30) ****p<0.0001
2.3C	Down Feedback; n=15	Longitudinal regression model	beta_1 = 0.91± std_error = .018; ****,p<0.0001
	Down Feedback; First vs Last Session n=15	Wilcoxon test (non-parametric)	*p=0.0156
	Up Feedback; n=15	Longitudinal regression model	beta_1 = 0.34± std_error = .12; ***,p<0.004
	Up Feedback; First vs Last Session n=15	Wilcoxon test (non-parametric)	*p=0.0125
	Down Feedback, Three last runs	one sample ttest (chance = 0.5)	(run 28)***p=0.0007; (run 29) ****p<0.0001; (run 30) ***p=0.0002
	Up Feedback, Three last runs	one sample ttest (chance = 0.5)	(run 28) **p=0.0075; (run 29) ****p<0.0001; (run 30) ****p<0.0001
2.3D	First Session vs last session vs Re-test session	One-way ANOVA	F (1.722, 22.39) = 10.87; ***p=0.0008
	First Session vs Last Session	Multiple Comparisions Tukey corrected	** p=0.0013
	First Session vs Consolidation Session	Multiple Comparisions Tukey corrected	* p=0.0362
	Last Session vs Consolidation Session	Multiple Comparisions Tukey corrected	ns, p=0.3463
	first 3 runs vs chance	one sample ttest (chance = 0.5)	run1, ns p=0.1054; run2, ns, p=0.1319; run3, *p==0.0276
	last 3 runss vs chance	one sample ttest (chance = 0.5)	run28, ****p<0.0001; run29, ****p<0.0001; run30, ****p<0.0001
	Consolidation runs vs chance	one sample ttest (chance = 0.5)	cons_run1, ***p=0.0003; cons_run2, ***p=0.0001; cons_run3, **p=0.0035
2.4	Main	Longitudinal regression model	beta_1 = 0.057± std_error = .01921; **,p=0.003
	Inset	one sample ttest (chance = 0.5)	trials 1-10,15,16 ns,p>0.05 and for trials 11-14,17-30 *,p<0.05
2.5B	Early: Up vs Down	2way ANOVA repeated measures (direction x bins)	F(1,5) = 0.046, ns, p=0.8389
	Mid: Up vs Down	2way ANOVA repeated measures (direction x bins)	F(1,5) = 10.70, *p=0.0220
	Late: Up vs Down	2way ANOVA repeated measures (direction x bins)	F(1,5) = 17.54, **p=0.0086
2.5C	Mean up: early vs mid vs late (left panel)	Nonparametric one-way repeated ANOVA	*p=0.0289
	Mean down: early vs mid vs late (left panel)	Nonparametric one-way repeated ANOVA	**p=0.0055
	Mean pre-trial: early vs mid vs late (left panel)	Nonparametric one-way repeated ANOVA	ns; p=0.1416
	Sigma up: early vs mid vs late (right panel)	Nonparametric one-way repeated ANOVA	ns; p=0.9563
	Sigma down: early vs mid vs late (right panel)	Nonparametric one-way repeated ANOVA	ns; p=0.1416
	Sigma pre-trial: early vs mid vs late (right panel)	Nonparametric one-way repeated ANOVA	ns; p=0.1840
2.6B	Early vs Late: center to top screen	2way ANOVA repeated measures (training phase x bins)	Main effect (training) F(1,14)=18.47 ***,p=0.0007;
			Bin effect F(39, 546)=29.94 ****,p<0.0001;
			Interaction training x bin F(39,546) =10.11, ****,p<0.0001
	Early vs Late: center to bottom screen	2way ANOVA repeated measures (training phase x bins)	Main effect (training) F(1,14) = 6.77 *,p=0.0210;
			Bin effect F(40, 560)= 13.85 ****,p<0.0001;
2.7C	PSD of all trials for up down and pre-trial	2way ANOVA repeated measures (trial type x frequency)	Main effect (trial type) F(1.803,19.83)=5.82 *,p=0.0120;
			frequency effect F(1.116, 12.28)=21.28 ***,p=0.0004;
			Interaction frequency x trial type F(1.118, 12.30) =14.34 , **,p=0.0020
2.8C	Log average PSD up vs down trials, normalized to pre-trial	paired t-test	delta, **** p<0.0001
			theta, **** p<0.0001
			beta, **** p<0.0001

Table 2.2 | Statistical analysis and results.

AUTHOR CONTRIBUTIONS

N.J.L. and V.B.P performed the behavioral and recording experiments and analyses. N.J.L., V.B.P and R.M.C. designed the experiments. N.J.L. and R.M.C. wrote the manuscript.

REFERENCES

Athalye, V.R., Santos, F.J., Carmena, J.M., and Costa, R. (2018). Evidence for a neural law of effect. Science *359*, 1024–1029.

Athalye, V.R., Ganguly, K., Costa, R.M., and Carmena, J.M. (2017). Emergence of Coordinated Neural Dynamics Underlies Neuroprosthetic Learning and Skillful Control. Neuron *93*, 955–970.e955.

Barnes, T.D., Kubota, Y., Hu, D., Jin, D.Z., and Graybiel, A.M. (2005). Activity of striatal neurons reflects dynamic encoding and recoding of procedural memories. Nature *437*, 1158–1161.

Birbaumer, N., Ghanayim, N., Hinterberger, T., Iversen, I., Kotchoubey, B., Kübler, A., Perelmouter, J., Taub, E., and Flor, H. (1999). A spelling device for the paralysed. Nature *398*, 297–298.

Blankertz, B., Sannelli, C., Halder, S., Hammer, E.M., Kübler, A., Müller, K.-R., Curio, G., and Dickhaus, T. (2010). Neurophysiological predictor of SMR-based BCI performance. NeuroImage *51*, 1303–1309.

Blefari, M.L., Sulzer, J., Hepp-Reymond, M.-C., Kollias, S., and Gassert, R. (2015). Improvement in precision grip force control with self-modulation of primary motor cortex during motor imagery. Frontiers in Behavioral Neuroscience *9*, 18.

Carmena, J.M. (2013). Advances in neuroprosthetic learning and control. PLoS Biol *11*, e1001561.

Carmena, J.M., Lebedev, M.A., Crist, R.E., O'Doherty, J.E., Santucci, D.M., Dimitrov, D.F., Patil, P.G., Henriquez, C.S., and Nicolelis, M.A.L. (2003). Learning to control a brain-machine interface for reaching and grasping by primates. PLoS Biol *1*, E42.

Clancy, K.B., Koralek, A.C., Costa, R.M., Feldman, D.E., and Carmena, J.M. (2014). Volitional modulation of optically recorded calcium signals during neuroprosthetic learning. Nature Publishing Group *17*, 1–4.

Costa, R.M., Cohen, D., and Nicolelis, M.A.L. (2004). Differential corticostriatal plasticity during fast and slow motor skill learning in mice. Curr. Biol. *14*, 1124–1134.

Costa, R.M., Lin, S.-C., Sotnikova, T.D., Cyr, M., Gainetdinov, R.R., Caron, M.G., and Nicolelis, M.A.L. (2006). Rapid alterations in corticostriatal ensemble coordination during acute dopamine-dependent motor dysfunction. Neuron *52*, 359–369.

Fetz, E.E. (1969). Operant Conditioning of Cortical Unit Activity. Science *163*, 955–958.

Ganguly, K., and Carmena, J.M. (2009). Emergence of a stable cortical map for neuroprosthetic control. PLoS Biol *7*, e1000153.

Ganguly, K., Dimitrov, D.F., Wallis, J.D., and Carmena, J.M. (2011). Reversible large-scale modification of cortical networks during neuroprosthetic control. Nature Publishing Group *14*, 662–667.

Guger, C., Edlinger, G., Harkam, W., Niedermayer, I., and Pfurtscheller, G. (2003). How many people are able to operate an eeg-based brain-computer interface (bci)? IEEE Trans. Neural Syst. Rehabil. Eng. *11*, 145–147.

Guger, C., Daban, S., Sellers, E., Holzner, C., Krausz, G., Carabalona, R., Gramatica, F., and Edlinger, G. (2009). How many people are able to control a P300-based brain–computer interface (BCI)? Neuroscience Letters *462*, 94–98.

Jin, X., and Costa, R.M. (2010). Start/stop signals emerge in nigrostriatal circuits during sequence learning. Nature *466*, 457–462.

Karni, A., Meyer, G., Rey-Hipolito, C., Jezzard, P., Adams, M.M., Turner, R., and Ungerleider, L.G. (1998). The acquisition of skilled motor performance: Fast and slow experience-driven changes in primary motor cortex. Proceedings of the National Academy of Sciences *95*, 861–868.

Klem, G.H., Lüders, H.O., Jasper, H.H., and Elger, C. (1999). The ten-twenty electrode system of the International Federation. The International Federation of Clinical Neurophysiology. Electroencephalogr Clin Neurophysiol Suppl *52*, 3–6.

Koralek, A.C., Costa, R.M., and Carmena, J.M. (2013). Temporally precise cell-specific coherence develops in corticostriatal networks during learning. Neuron *79*, 865–872.

Koralek, A.C., Jin, X., Long, J.D., Costa, R.M., and Carmena, J.M. (2012). Corticostriatal plasticity is necessary for learning intentional neuroprosthetic skills. Nature *483*, 331–335.

Lotte, F., Larrue, F., and Mühl, C. (2013). Flaws in current human training protocols for spontaneous Brain-Computer Interfaces: lessons learned from instructional design. Front Hum Neurosci *7*, 568.

McFarland, D.J., and Wolpaw, J.R. (2017). EEG-Based Brain-Computer Interfaces. Curr Opin Biomed Eng *4*, 194–200.

McFarland, D.J., and Wolpaw, J.R. (2018). Brain–computer interface use is a skill that user and system acquire together. PLoS Biol *16*, e2006719.

Müller-Putz, G.R., Breitwieser, C., Cincotti, F., Leeb, R., Schreuder, M., Leotta, F., Tavella, M., Bianchi, L., Kreilinger, A., Ramsay, A., et al. (2011). Tools for Brain-Computer Interaction: A General Concept for a Hybrid BCI. Front Neuroinform *5*, 30.

Neely, R.M., Koralek, A.C., Athalye, V.R., Costa, R.M., and Carmena, J.M. (2018). Volitional Modulation of Primary Visual Cortex Activity Requires the Basal Ganglia. Neuron *97*, 1356–1368.e4.

Perdikis, S., Leeb, R., Williamson, J., Ramsay, A., Tavella, M., Desideri, L., Hoogerwerf, E.-J., Al-Khodairy, A., Murray-Smith, R., and Millan, J.D.R. (2014). Clinical evaluation of BrainTree, a motor imagery hybrid BCI speller. J. Neural Eng. *11*, 036003.

Perdikis, S., Tonin, L., Saeedi, S., Schneider, C., and Millan, J.D.R. (2018). The Cybathlon BCI race: Successful longitudinal mutual learning with two tetraplegic users. PLoS Biol *16*, e2003787–28.

Pfurtscheller, G., and Neuper, C. (2001). Motor imagery and direct brain-computer communication. Proc. IEEE *89*, 1123–1134.

Roberts, L.E., Birbaumer, N., Rockstroh, B., Lutzenberger, W., and Elbert, T. (1989). Self-Report During Feedback Regulation of Slow Cortical Potentials. Psychophysiology *26*, 392–403.

Sepulveda, P., Sitaram, R., Rana, M., Montalba, C., Tejos, C., and Ruiz, S. (2016). How feedback, motor imagery, and reward influence brain self-regulation using real-time fMRI. Hum. Brain Mapp. *37*, 3153–3171.

Vidal, J.J. (1973). Toward direct brain-computer communication. Annu. Rev. Biophys. Bioeng. *2*, 157–180.

Wolpaw, J.R., and McFarland, D.J. (2000). Brain-computer interface research at the Wadsworth Center. IEEE Transactions on Rehabilitation Engineering *8*, 222–226.

Wolpaw, J.R., McFarland, D.J., Neat, G.W., and Forneris, C.A. (1991). An EEG-based brain-computer interface for cursor control. Electroencephalogr Clin Neurophysiol *78*, 252–259.

Yin, H.H., Mulcare, S.P., Hilário, M.R.F., Clouse, E., Holloway, T., Davis, M.I., Hansson, A.C., Lovinger, D.M., and Costa, R.M. (2009). Dynamic reorganization of striatal circuits during the acquisition and consolidation of a skill. Nat. Neurosci. *12*, 333–341.

3

APPLICATIONS OF THE OPERANT LEARNING, EEG-BASED BMI

"We are stuck with technology when what we really want is just stuff that works."

Douglas Adams in
The Salmon of Doubt: Hitchhiking the Galaxy One Last Time

SUMMARY

This chapter discusses applications of what we learned in chapter 2, and is divided into two main sections. In section A, we describe a proof of concept of the EEG-based Brain-Machine Interface (BMI) using operant learning control introduced in chapter 2. BMIs have been tested in a wide range of applications, from controlling computer cursors to wheelchairs and neuroprosthetic arms. In this work, we expanded on such applications and assessed if a pilot could use a BMI to control an aircraft successfully. For this purpose, we combined the operant learning BMI approach discussed in chapter 2 with a custom-designed flight controller to provide control over a light airplane's flight path. We tested the system in a fixed base flight simulator, where we conducted several pilot-in-the-loop experiments. The output of the flight controller allowed for horizontal airplane motion in different operational and laboratory tasks. This section discusses the main results of the approach and the lessons learned from such an application scenario. In section B, we present on-going work on the development of a dry-electrode EEG headset, that records neural activity and implements the operant learning BMI paradigm directly on the headset, sending the output command wirelessly to control a device. The system presented in this section opens up a range of applications and allows a wider reach of the BMI technology.

SECTION A - Proof of concept of the operant learning bmi paradigm: controlling an airplane[1]

The dream of flying has been linked to human history for millennia. With mentions dating back to the Babylonians and Ancient Greece, history is full of curious descriptions of flying machines and airplanes, and their flying attempts. We have demonstrated our ability to fly machines consistently over the last century. However, the way we input our commands and intentions to the machine is still very much the same as when we first started flying. Presently, autonomous flying has been replacing many of the conventional control tasks in aircraft, and Unmanned Air Vehicles (UAV) are currently widely used in situations where human lives could be at risk. However, even in such cases, keeping a human in the loop, either as a pilot or a remote operator, is crucial for the success of the flight. A pilot's manual operation of an aircraft, using hands and feet, is still commonplace today. We seem far from the *mind-controlled* airplanes seen in science-fiction books and movies such as *Firefox*, where an airplane is controlled in part by the pilot's EEG signals (Eastwood, 1982). The possibility to accurately by-pass the manual inputs to the airplane and directly control its behavior using neural signals would be a breakthrough in the field of aviation.

[1] All experiments and data discussed in this chapter were collected in collaboration with the Department of Institute of Flight System Dynamics of the Technical University of Munich

Under the FP7 Project BRAINFLIGHT (FP7 European Commission, 2015) we proposed to implement a Brain-Machine Interface (BMI) controlled airplane without the need for physical interaction with the controls. The main goal of the project was to assess the performance of this concept and encourage a long-term vision of enabling physically disabled people to control a General Aviation (GA) aircraft, spreading the access to general aviation. In order to accomplish this goal, we combined an EEG-based BMI operant learning approach, *cf.* Chapter 2, with a custom-developed flight controller to control the inputs to an airplane simulator. Given the characteristics of the project, the experiments in the simulator were exploratory, with an emphasis on understanding and engineering appropriate flight-control parameters to translate the neural activity into useful aircraft controls. In this chapter, we describe a subset of the experiments and analysis performed under the BRAINFLIGHT project and the FCT-DAAD collaborative project with the Technical University of Munich (TUM). The results discussed in this Chapter are limited to the experiments conducted with the implementation of a BMI system using an operant learning approach. As part of the BRAINFLIGHT project, a BMI with a Motor Imagery (MI) approach to control the aircraft simulator was also tested in a collaboration between the Technical University of Munich and Technical University of Berlin. The results from those studies can be found in (Zander et al., 2014) and (Fricke and Holzapfel, 2014). Other studies have also reported on the use of MI for the control of virtual (Doud et al. 2011) and physical drones (LaFleur et al, 2013) in three-dimensional spaces. These studies attest to the control of a drone using BMIs, but require the use of proxy commands for the control since subjects needs to imagine movement of the arms, foot or tongue to control different flight dimensions. These methods contrast with the control through an abstract approach, as detailed in chapter 2, which would allow a direct control of the dimensions of flight without the need for proxies through imagined movements.

The details about the experiments in this Chapter are published in (Fricke et al., 2015), co-authored by N.J.L. A comparison between the MI and operant learning approaches in the control of the aircraft can be found in (Fricke, 2017).

Results

All the experiments reported in this chapter were conducted in the DA42 flight simulator at the TUM's Institute of Flight System Dynamics, **Fig. 3.1A**. The flight simulator was a real-size, two-seat cockpit of an actual DA42 aircraft, built by Diamond with the original aircraft components. The original DA42 airplanes, as depicted in **Fig. 3.1B**, use a mechanical control system, where displacements of a center stick and rudder pedals are translated into control surface movements by rods and wires. (Diamond Aircraft Industries, 2009).

A B

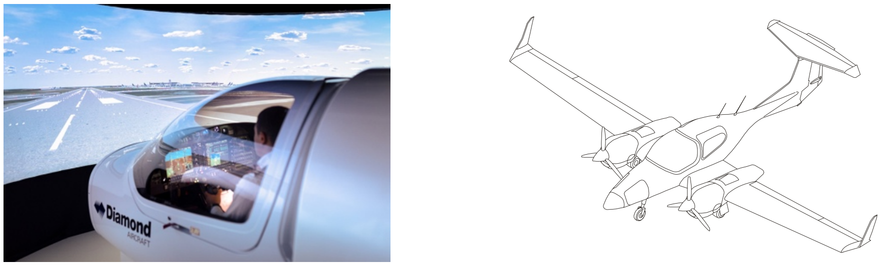

Fig 3.1 | Schematic of the DA-42 and its simulator counterpart. (A) Diamond DA42 aircraft, reproduced from (Diamond Aircraft Industries, 2009); **(B)** DA42 Flight simulator at the TUM's Institute of Flight System Dynamics, reproduced from (Diamond Aircraft Industries, 2019)

The actual displacement of control surfaces was simulated in a virtual world created in the flight simulator. The inputs to the simulator and flight dynamics implemented in the system were designed to be an accurate representation of a real flight. Around the cockpit, a three-channel External Visual System (EVS) projected a simulation of the world on a 180° cylindrical screen. The simulator, **Fig. 3.1A**, was certifiable up to Flight Training Device (FTD) level 5 as defined by the Federal Aviation Administration (FAA) (Federal Aviation Administration, 2006) and was frequently used in the training and preparation of commercial pilots for Lufthansa Airlines. **Fig. 3.2** shows a representation of the flight simulator and its typical configuration for the BMI control protocol.

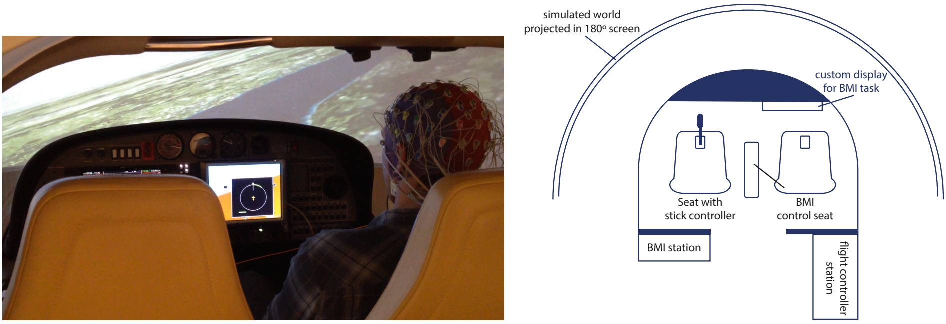

Fig 3.2 | Experimental setup on the DA42 aircraft simulator. (left) Pilot controls the aircraft while seated on the right-hand side of the cockpit during experiment. Visual feedback of the task is provided to the subject through a custom-built display. **(right)** Schematic of the experimental apparatus. It includes the BMI station and the Flight controller station.

Aircraft visual feedback

During the experiments, the subject had, at all times, two visual feedback reports of the inputs that were sent to the aircraft simulator. The first was the simulated world in the EVS and the traditional four aircraft instruments onboard the cockpit (airspeed indicator, attitude indicator, altimeter and magnetic compass). The second means of feedback was provided by a custom-made screen that was placed on the dashboard of the cockpit in front of the subject, **Fig. 3.3**. In this screen, the background displayed an artificial horizon, and other parameters such as airspeed, altimeter and heading were displayed in the foreground in a standard T configuration as is usual in aircraft. The rate of turn was displayed as a magenta arc on top of the compass rose. In the example shown, the airplane is flying at an altitude of 5000ft, pitched up by about 2.0°, banked 25° to the right, and with an indicated airspeed of 120 kt. The aircraft is currently crossing the heading 244º at a rate of turn higher than the standard turn rate of 3º/s.

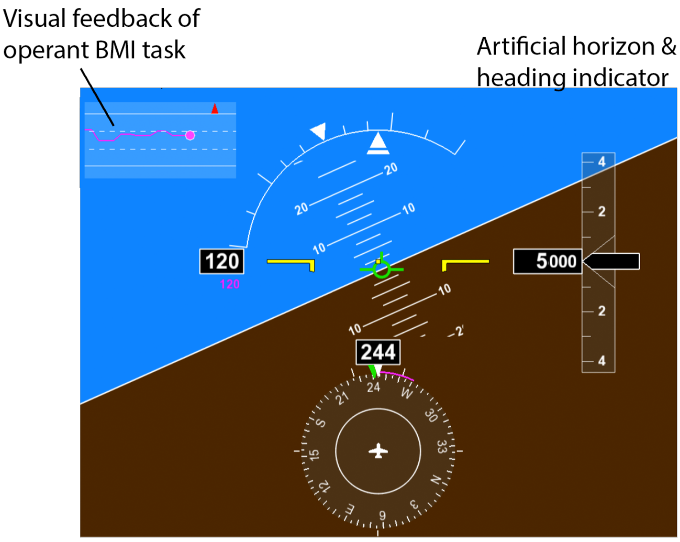

Fig 3.3 | Custom built display indicating main control parameters of the aircraft and BMI task

The visual feedback from the operant learning BMI task was also displayed on the top left corner of the screen so that the subject was able to relate the feedback regarding the aircraft's outputs and the BMI feedback trained previously (*cf.* Chapter 2). In that display, the ball position in relation to the horizontal lines indicated the strength of the command being sent to the flight controller, scaled linearly to [-1,1] (*cf.* BMI control section in Methods). The cursor's tail, displayed in magenta to the left of the ball, indicated previous commands up to 1.5 seconds into the past. The movements of the ball in the upward/downward directions were translated to left/right commands sent to the aircraft.

The target heading was indicated with a heading bug, which was red when the difference between the current heading and the target was above 10º, it turned yellow when it was between 5º and 10º error and was green when the error was below 5º. These values follow the requirements for pilot license flight tests (Joint Aviation Requirements Flight Crew Licensing, 2006).

During a flight, there are many external factors that may affect the flight direction of an aircraft, e.g. winds and gust, air space regulations, deviating from other in-route aircraft. One of the main onboard instruments available to a pilot is the magnetic compass, **Fig. 3.4**. It allows the pilot to know in which heading the aircraft is flying and whether changes to that heading are needed to keep a specific direction of flight. In this work, we took advantage of the information displayed on the magnetic compass and designed an experiment where the pilot needed to turn the aircraft to a designated heading on the compass using the signal provided by the BMI.

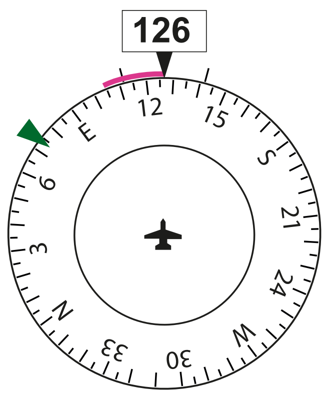

Fig. 3.4 | Example of aircraft compass displayed during the BMI task. Aircraft is flying on the magnetic heading 126º and the target heading to turn the aircraft to is 074º. The pink arc on the top of the compass indicates the speed at which the aircraft is currently turning to the left.

We divided the experimental setup into two main tasks. In the first task, the objective was to direct the aircraft to an indicated fixed heading on the aircraft's compass and once reached keep the aircraft flying in that direction. In the second task, the goal was to follow a heading bug that would be in continuous motion, thus constantly turning the aircraft into a designated direction.

For both tasks, the flight controller received input commands from the BMI station which was connected to the EEG system. The activity recorded by the EEG system was transformed in near-real-time with a fixed transcoder, as explained in chapter 2. The resulting output command from the BMI was sent to the flight controller that further transformed the signal into appropriate commands to control the aircraft simulator. The flight controller was engineered to implement specific transfer functions that translated the commands sent by the BMI station into different control strategies to displace the aircraft laterally. For each transfer function implemented, different parameters were tuned to better accomplish the goals of the designed tasks. Several tests were run with three main configurations implementing three types of transfer functions (*cf.* Methods). Below we describe the main results for each of the tasks.

Task A – Turning the aircraft to a fixed heading

The first task's objective was to simulate potential real flight situations where changes in an aircraft heading are issued by the controller, for example by an airfield tower. In such cases the pilot needs to turn the aircraft to the new heading indicated on the magnetic compass. In this experiment, each trial can be divided into two different phases: reaching the target heading, followed by maintaining that same heading. During flight, each target heading was indicated by a green heading bug on the compass on top of the corresponding magnetic heading, **Fig. 3.4**. The pilot was advised to always choose the shortest turn to acquire the next heading and to turn with standard rate of turn (3^{o}/s), if possible. After a period of time, a new target heading was calculated using **Eq. 3.1**, where the heading variations $\Delta\psi$ could be any integer multiple of 10^{o} to the left or right direction.

$$\psi_{tg} = \psi_t + \Delta\psi \quad (3.1)$$

These arbitrarily chosen values ensured that the next target was always unpredictable. The maximum time allowed to reach the target, as calculated by **Eq. 3.2**, was a function of the heading variations $\Delta\psi$ and of the standard turn rate (3^{o}/s). This rate of turn is typical in flight control because it allows the pilot sufficient time to cross-check the flight instruments and avoid drastic changes to the aerodynamic forces being exerted on the aircraft.

$$t = \frac{\Delta\psi}{3°/s} + 63s \quad (3.2)$$

The constant in the end accounted for time to maintain the target heading and enough time for turn initiation and termination.

The first transfer function we implemented in the flight controller, Y_A, was a double integrator which changed the turn rate by 1.5º/s, every second the command would be at a maximum input, **Eq. 3.3**.

$$Y_A = K_A \cdot \frac{1}{s^2} = \frac{1.5° . \pi/180°}{s^2} = \frac{0.0262}{s^2} \tag{3.3}$$

A high-level filter like the double integrator was chosen for an initial attempt because it corresponded to the control of the rate of rate of turn of the aircraft. This meant that once a turn was initiated with a correct rate of turn, the subject would only have to keep close to zero input values until the turn was finished. Zero input command meant constant rate of turn. The result of the use of this transfer function is shown in **Fig. 3.5A**. The target heading is represented in green and the steps indicate the arbitrary changes in heading which happened after specific periods given by **Eq. 3.2**. The blue line represents the flight path of the aircraft during the run. With this transfer function we saw that the aircraft was flown with constant turn rates and smooth paths, which can be seen by the straight lines in the plots. However, controlling the rate of rate of turn made the aircraft less responsive and less agile, as can be seen by the small amount of inflexions of the blue curve during the run.

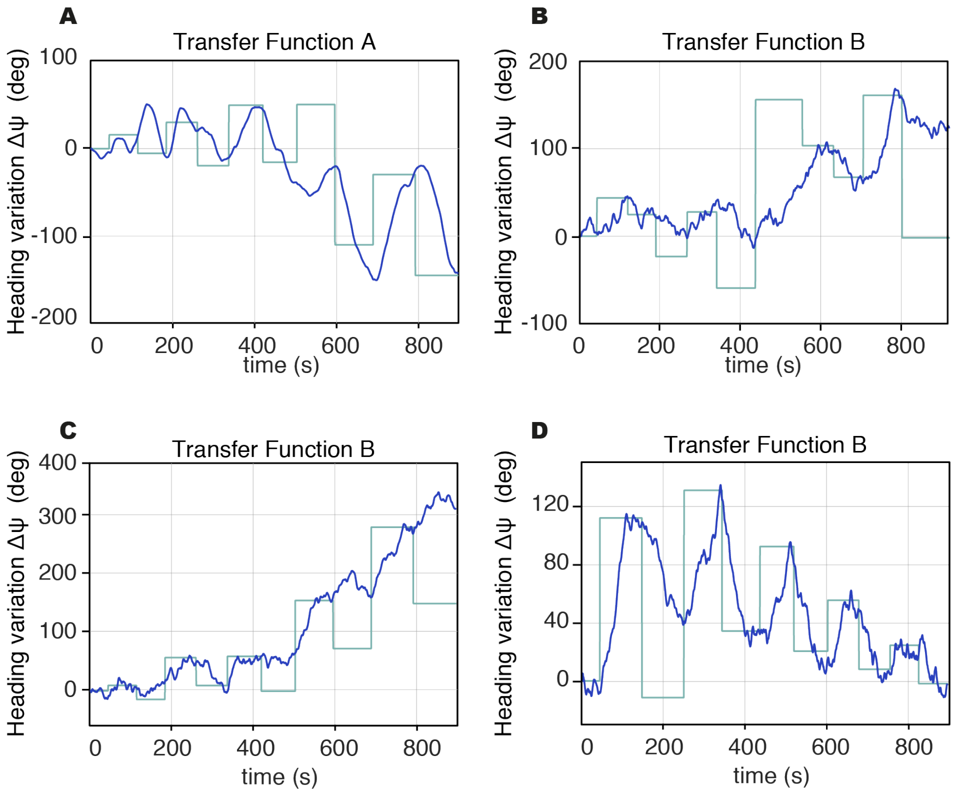

Fig 3.5 | Aircraft heading during Task A. The target heading changes at variable time intervals as a function of the initial heading separation (see **Eq. 3.2**). Flight controller transfer function Y_A was used on the top left plot while Y_B ,with different time constants, was used for the other three runs.

This lack of agility demanded for an anticipation of the end of turn much earlier than with a reactive filter, which resulted in a higher mental effort to predict when to start undoing a turn. Furthermore, the turns were difficult to start and finish, which resulted in overshooting some of the targets.

In order to introduce more maneuverability to the control, one of the poles in Y_A was changed from a pure integrator to a first-order filter, **Eq. 3.4**.

$$Y_B = K_B \frac{1}{(T_B s+1)s} = \frac{0.1}{(3.82s+1)s} \tag{3.4}$$

The values of T_B and K_B were set after a few training turns, to assess which values would provide the best feeling of control to the subject. Even though the aircraft was more reactive with this new filter, it also demanded constant non-zero control inputs during turns. This resulted in more jitter during the control of the aircraft, in particular during the first attempts, **Fig. 3.5B**.

Even in such cases the control still felt sluggish to the subject, which led to a further decrease of time constant in the first-order lag to $T_B = 1.5$, **Fig. 3.5C,** and later to $T_B = 1.2$, **Fig. 3.5D**. In these attempts, we see a definite increase in performance over training, benefiting from the adjustment of the parameters discussed previously, which can be translated into faster reaches and staying longer in the target heading. Still, we see some that some of the turns were not easy to maintain, in particular on the three last right turns of **Fig. 3.5C**.

A third transfer function was attempted to reduce jitter in the flight path while maintaining the responsiveness and maneuverability of the system. In order to do this, we filtered the signal obtained from the BMI station with a low-pass filter, **Eq. 3.5,** before applying Y_B from **Eq. 3.4** with the same parameters as described above. The resulting transfer function was called Y_C.

$$Y_{filt} = \frac{1}{s+1} \tag{3.5}$$

With this new transfer function, the aircraft was more responsive and the targets could be more easily reached. Changes in direction were also easier to perform, **Fig. 3.6A,B**. The introduction of the filter, however, also introduced considerable lags into the control. All in all, this was still seen as a good compromise to the other transfer functions tested.

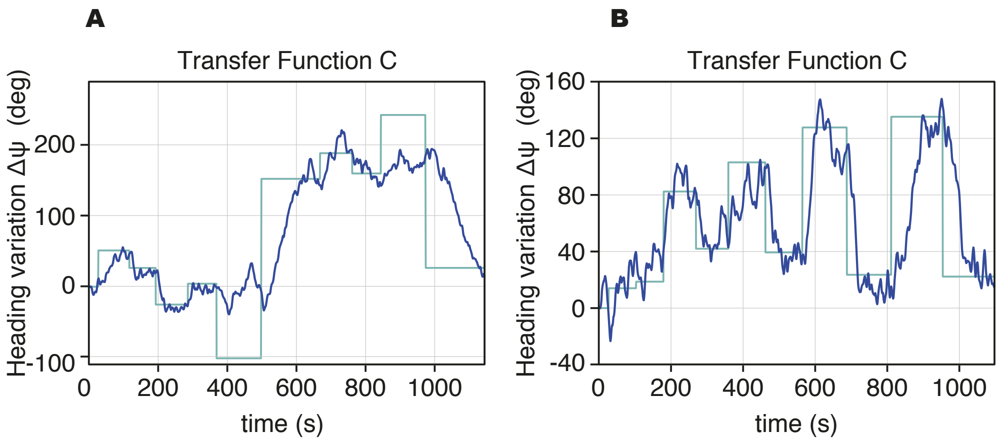

Fig 3.6 | Aircraft heading during Task A. Flight controller transfer function Y_C was used for both plots.

Task B — Heading Bug tracking

For task B, we explored the capacity of the pilot to control the lateral maneuverability of the aircraft by continuously tracking a moving heading bug. The continuous displacement of the heading bug was given by **Eq. 3.6**.

$$\psi_{tg} = \sum_{i=1}^{10} A_i \sin(\omega_i t) \tag{3.6}$$

where ω_i and A_i changed according to **Table 3.1**.

For this task we used transfer function Y_C, since it was the one providing the best results in task A. Fig **3.7A,B** shows the results of the continuously tracking of a moving heading bug for two runs (target represented in green and actual flight path represented in blue).

Frequencies ω_i [Hz]	Frequencies ω_i [rad/s]	Amplitudes A_i [º]
1/300	0.0209	5
2/300	0.0419	5
3/300	0.0628	5
4/300	0.0838	5
7/300	0.147	5

Frequencies ω_i [Hz]	Frequencies ω_i [rad/s]	Amplitudes A_i [º]
12/300	0.251	5
21/300	0.44	0.5
34/300	0.712	0.5
57/300	1.19	0.5
95/300	1.99	0.5

Table 3.1 | Components of Eq. 3.6 to calculate the continuous displacement of the heading bug.

Due to the nature of the task and constant changes in the heading bug direction, the difficulty of this task was much higher than in task A. We can observe that although very few attempts to the task were performed, the subject was able to track the heading bug continuously, improving performance from first to second attempt and maintaining the angle to the target within a few degrees. In the second attempt although there was a sudden deviation of 50º from the target, the subject was able to return to the desired path just before the finish of the run.

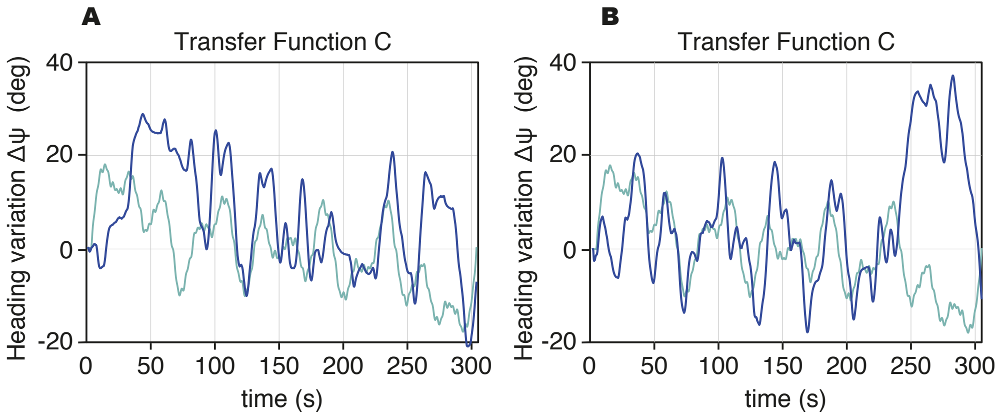

Fig 3.7 | Aircraft heading during Task B. Flight controller transfer function Y_C was used for both plots.

Discussion

The objective of the work described in this chapter was to showcase a real-world application of the operant learning BMI paradigm that was introduced in Chapter 2. The outcome of this project was successful in reporting that the control of an aircraft can be attained. By engineering specific control functions that translated the BMI output commands into control commands to the aircraft flight controller, we were able to show that targeting specific fixed headings and performing slight changes of heading to track a moving object are possible with BMI control. The results obtained during this project should, however, be validated in follow-up experiments, including a higher number of subjects and longer training sessions to evaluate changes in performance with training. Previous work has demonstrated BMI control of virtual and physical drones using motor imagery (MI) approaches (LaFleur et al., 2013; Doud et al. 2011). Under the BRAINFLIGHT project a MI-based BMI approach was also used to control the DA42 simulator (Zander et al., 2014; Fricke and Holzapfel, 2014). Comparison of the different BMI approaches is important to evaluate under which circumstances each technique plays a more relevant role. The current results, however, are difficult to compare with previous literature results since the tasks performed are not the same and the metrics to evaluate performance change. In order to compare the approaches and their results, future work should it would develop a standardized experiment with different BMI control methods and establish pre-defined measures of performance.

Methods

Participant

Here we report the experimental results conducted with one subject (male, 27 years old). The main goal of the project was to provide a proof of concept that the aircraft control with operant learning BMI was possible. The efforts in this project were concentrated in developing and tuning parameters to prove the concept. The flight simulator location was far away from the BMI laboratory (a 3-hour flight between Munich and Lisbon), which rendered the experiments more infrequent than would have been necessary to conduct an experimental protocol that could be tested and replicated with several subjects and more sessions. The subject that performed the experiment reported in this chapter had a valid private pilot license and was familiarized with the aircraft instruments that were used during the experiments. The subject had also undergone significant training using the BMI operant learning paradigm that was implemented to control the aircraft.

EEG equipment and Signal Transformation

EEG signals were acquired using an ActiveTwo measurement system (BioSemi Instrumentation, Amsterdam, Netherlands), with a sampling frequency of 2048Hz. EEG was recorded using 64 electrodes arranged in the modified 10/20 international standard (Klem et al. 1999).

The data was collected under Ubuntu Linux 10.04 Operating System and the recording was done based on the CNBI Toolkit (CNBITK) framework for BCI, developed in the CNBI lab at EPFL which implemented a standardized communication interface based on the Tools for Brain Computer Interaction (TOBI) project (Muller-Puftz et al. 2011). The EEG data were filtered and processed online in steps of 250 ms taking into account the last 1 s of data (or 2048 points). The EEG signal of the 64 electrodes was bandpass filtered between 1-80Hz (zero-phase Butterworth, 4th order) using a zero-phase filter and a notch filter was applied to the signal at 50Hz (second-order Infinite Impulse Response (IIR) filter). For each segment of 1 s., we calculated the power spectral density (PSD)) of the 5 chosen electrodes for the subject, using the Welch's method (*pwelch* function implemented in *MATLAB)*. The PSD was then used to calculate the resulting signal for the BMI control and sent to the aircraft flight controller, as described below.

BMI control

The BMI ran on a standalone computer, i.e., BMI station, that was connected via Ethernet to the flight controller. The neural activity recorded with the EEG system was transmitted to the BMI station in real-time and a fixed transcoder was used to convert the signal into an input command to the flight controller, where it was further modified to actuate on the aircraft controllers. The transcoder was a mathematical function of the four specific EEG frequency bands described in Chapter 2. The average power spectral density (PSD) of the theta (4-8Hz) and gamma (30-80Hz) bands had the opposite effect of the ones in the delta (1-4Hz) and beta (14-25Hz) bands. An increase in the average power per electrode in theta and gamma, as well as a decrease in power in the delta and beta bands, led to a command that changed the aircraft's roll angle more to the left, while a decrease in the former two bands and an increase in the latter two bands led to a command to change the aircraft's roll angle to the right, as follows:

$$Y_{BMI} = log \left(\sum_{chn=1}^{5} \frac{\overline{\gamma_i}\,\overline{\theta_i}}{\overline{\beta_i}\;\overline{\delta_i}} \right) \tag{3.7}$$

The ratio of band powers was calculated and summed for the 5 electrodes chosen for the subject, and it was log-transformed in the end so that the variation of output commands would follow a Gaussian distribution. Every 250ms (4Hz), an output command was calculated taking into account the last 1sec of EEG data from the 5 chosen electrodes. The result of **Eq. 3.7** was then scaled linearly, so that a value of Y_{BMI} = $target_{UP}$ on the original task would be converted and sent to the flight controller as Y_{BMI_sent} = 1; and a value Y_{BMI} = $target_{DOWN}$ would be sent to the flight controller as Y_{BMI_sent} = -1. The flight controller would then take the Y_{BMI_sent} value received and pass it through an engineered

CHAPTER 3

transfer function, tailored to increase maneuverability of the aircraft (*cf.* Flight controller transfer function)

Section Acknowledgments

We thank Florian Holzapfel for the discussions and valuable suggestions during the task development in the DA42 airplane simulator. This research was supported by the INDP Graduate Programme and an FCT fellowship to N.J.L, and an FCT-DAAD joint project grant.

Author Contributions

N.J.L. and V.B.P. designed and conducted the experiments with the EEG and BMI systems. Tim Fricke (T.F.) designed the flight controller and adapted the BMI task to the DA42 simulator at the Technical University of Munich. N.J.L. and T.F. implemented the communication protocols between the BMI station and the flight controller.

SECTION B – Development of a dry-electrode EEG headset for operant learning BMI

Electroencephalography (EEG) systems typically provide a wide range of advantages that make them attractive to be used in BMI applications, when comparing to other recording techniques (*cf.* chapter 1). However, EEG systems that provide good quality recordings and are used in research and clinical applications, like the ones used in chapter 2 and section A of this chapter, still have some disadvantages. In particular, these systems can be time-consuming to assemble and require a specialist to set them up. The typical implementation of an EEG system requires the use of conductive gel, necessitating the need to shower after each utilization, require dedicated hardware and software to process the data, and transform it to be used for a BMI application, etc. Several companies have started addressing these problems by providing systems that are easier to set up, use semi-dry or dry electrodes and may provide wireless transmission of raw EEG data. Among others, *Neuroelectrics* (*https://www.neuroelectrics.com/), Bitbrain (https://www.bitbrain.com/*) *Cognionics* (https://www.cgxsystems.com/), and *mBrainTrain* (*https://mbraintrain.com/)* have been developing interesting solution that provide solutions to some the issues mentioned above.

In this section we briefly present on-going work on the development of a novel, wireless EEG system that is portable and easy-to-use while providing high-quality signals. The system is a headset with five active, dry EEG electrodes placed above the motor and frontal cortices, that record and amplifying the signal locally, **Fig. 3.8**. The processing of the recorded signals is fully done within the headset via a transcoder that is programmable in hardware, thus avoiding the need for extra, proprietary software for signal processing. The result of the programmable transcoder is directly and wirelessly sent to any external device to be controlled.

The headset can be used directly with an operant learning task that runs in the user's phone or other devices and allows them to learn to voluntarily control specific EEG patterns, through an approach similar to the one described in chapter 2. The system is versatile, allowing the implementation of adaptive algorithms that enable changes in the transcoder, thus making it more adapted to the user and the specific device to control. Together with the headset, we developed an Android app and a Virtual Reality (VR) game that serve as show cases for the technology.

Fig. 3.8 | Design of the portable EEG headset. (Left) Computer generated render of the headset; **(Right)** Working 3D printed protoype built from the specifications of the rendered design.

Headset specifications

EEG SENSORS

5 Channels: Active electrodes C3, Cz, C4, F3, F4

2 References: Passive electrode: Bias - left mastoid A1

Reference - right mastoid A2

Sensor material:

Active electrodes - Currently using Flexible dry electrode Cognionics;

Passive electrodes - Biomedical Sensor Pads - H124SG

EEG SIGNAL

Sampling method: Sequential sampling, single ADC

Sampling rate: 500 SPS or 1kSPS (user configured)

Resolution: 24 bits with 1 LSB = 0.012µV

Bandwidth: 0.1 – 80Hz

Filtering: Built in digital 5th order butterworth filter bandpass; Digital notch filters at 50Hz or 60Hz

Dynamic range (input referred): 100mV(pp)

MOTION SENSORS

Accelerometer: 3-axis +/-2g

Sampling rate: 100 Hz

Resolution: 12 bits

CONNECTIVITY

Wireless: Bluetooth 2.1

Wireless Range: 10 meters

POWER

Battery: Internal Lithium Polymer battery 1200mAh

Battery life: up to 6 hours

Charger method: MicroUSB

Section Acknowledgments

We thank Filipe Carvalho and Artur Silva for the discussions and suggestions on requirements and development of the EEG electronics.

Author Contributions

The developments and tests discussed in this chapter are the result of a collaborative work with VisionVolt, David Gonçalves. R.M.C., N.J.L. and V.B.P. established the requirements to be implemented in the hardware and software. N.J.L. and V.B.P. supervised the hardware developments and design of the headset.

REFERENCES

Diamond Aircraft Industries (2009). DA 42 NG (support.diamond-air.at).

Diamond Aircraft Industries (2019). Flight Simulator Website.

Doud, A.J., Lucas, J.P., Pisansky, M.T., and He, B. (2011). Continuous Three-Dimensional Control of a Virtual Helicopter Using a Motor Imagery Based Brain-Computer Interface. PLoS ONE 6, e26322.

Eastwood, C., (1982) Firefox [Motion Picture] (Malpaso Productions).

Federal Aviation Administration (2006). 14 CFR Part 60.

FP7 European Commission (2015). *FP7 BRAINFLIGHT Project*.

Fricke, T. (2017). Flight Control with Large Time Delays and Reduced Sensory Feedback. Ph.D. Dissertation.

Fricke, T., and Holzapfel, F. (2014). Applying Brain-Machine Interfaces to Aircraft Control-Potentials and Challenges. Deutsche Gesellschaft Fur Luft-Und Raumfahrt.

Fricke, T., Paixão, V., Loureiro, N., Costa, R.M., and Holzapfel, F. (2015). Brain Control of Horizontal Airplane Motion-A Comparison of Two Approaches. American Institute of Aeronautics and Astronautics 207.

Joint Aviation Requirements Flight Crew Licensing (2006). 1, Amendment 7, 1 December 2006. Lovdata.No.

Zander, T.O., Fricke, T., Holzapfel, F., and Gramann, K. (2014). Applying Brain-Computer Interfaces outside the lab – Piloting a plane with active BCI. pp. 384–387.

LaFleur, K., Cassady, K., Doud, A., Shades, K., Rogin, E., and He, B. (2013). Quadcopter control in three-dimensional space using a noninvasive motor imagery-based brain-computer interface. J. Neural Eng. 10, 046003.

4

DISCUSSION

The purpose of this research was to 1) develop a novel non-invasive Brain-Machine Interface (BMI) with a fixed transcoder to continuously control a device and 2) test if human subjects can learn and consolidate a transformation between a complex EEG pattern and an effector.

The approach to BMI required that the subjects operantly learned to modulate their neural activity establishing a new link between the activity and the intended control action. In order to do so, subjects had to enter the neural pattern of the transcoder more efficiently. We showed that subjects learned a fixed, complex BMI transform, increasing their task performance throughout training. The learning was consolidated and recalled after a long training intermission. The findings within this thesis advance our understanding of non-invasive human BMI, opening up a range of possibilities for the implementation of new BMI transcoders and their application in real-world scenarios.

The goal of a Brain-Machine Interface is to reliably and robustly convey enough intent from the central nervous system (CNS) to accurately control an effector such as a prosthetic device, a computer or even our own muscles. Ideally, controlling a BMI should be as seamless and natural as controlling one's own limb, and the control should be stable and last for long periods of time.

The first experiments with brain-machine interfaces were conducted over half a century ago (Fetz, 1969; Kamiya, 1969). Since then, different technical implementations of BMIs have demonstrated the potential to restore communication and movement in patients with neurological injuries and movement disorders (Benabid et al., 2019; Birbaumer et al., 1999; Collinger et al., 2013; Donati et al., 2016; Hochberg et al., 2012). BMIs have also played an essential role in fundamental neuroscience and in our understanding of how the brain changes during learning, in particular, how neural activity is shaped when acquiring new abstract skills and perfecting them (Athalye et al., 2018; 2017; Ganguly and Carmena, 2009). Despite these many advances, there are still barriers to the development of BMIs that prevent their widely accessible implementations. In particular, current non-invasive BMI performance is still far from the practical efficacy necessary to be used on a daily basis.

We can categorize the current challenges of the field into two main classes. The first class has to do with the quality of signal information that a non-invasive device can acquire. Although the most extensively used non-invasive BMI technique has been the electroencephalography (EEG), these systems still provide a low signal-to-noise ratio (SNR) when compared to invasive (Ball et al., 2009) and other non-invasive techniques (Goldenholz et al., 2009) and require complex and cumbersome equipment. The primary source of the EEG is the synchronous activity of thousands of cortical neurons, reducing the spatial resolution of the recorded signal. Additionally, by recording the activity on the scalp, the EEG is affected by artifacts and outside noise, further affecting the quality of the signal. The second class of challenges has to do with high inter- and intra-subject signal variability when subjects perform BMI tasks. Signal variability has proven to be one of the most difficult BMI challenges to overcome. With the rise in popularity of the field of Machine Learning, many studies have proposed highly complex algorithms capable of classifying and linking neural activity to the subject's intentions (Lotte et al., 2018; Müller et al., 2008). However, the lack of consistency in the recorded signal over time hinders the algorithms' performance, which negatively affects the control of a device through the BMI. Our work and this dissertation have mainly addressed the second limitation, proposing an alternative approach to BMIs in chapter 2. Moreover, in chapter 3, we also briefly addressed some of the concerns of the first challenge, and we return to that discussion at the end of this chapter.

As described in chapter 1, a closed-feedback BMI loop typically comprises three main components: The sensors (collecting neural activity from the subject's brain), the processor (that implements mathematical transformations of the neural activity through specific algorithms) and lastly the device that is to be controlled. The subject's transformed neural activity is sent to actuate on the device, changing its state. A closed-loop is then established by providing the subject with visual or sensory feedback of these changes in near-real-time. For a closed-feedback BMI loop to operate correctly, there needs to be adaptation within the control loop. This adaptation is a critical step of a BMI to guarantee that the subject's intentions match the appropriate control changes on the device. Within the control loop, there are two places where the adaptation can occur: the algorithm and the subject. Depending on where in the control loop, the adaptation happens, we can either have a decoder (adaptation of the algorithm) or a learning (adaptation of the subject) approach to the BMI (Carmena, 2013).

In chapter 2, we described the task and results of an operant learning approach to BMI, where subjects learned a fixed transcoder to continuously control a cursor on a screen. However, most brain-machine interfaces, and in particular the non-invasive ones, have focused on the decoder approach. This approach's goal is to decode a natural plan in the neural signals. A mathematical model is trained to decode and categorize the subject's neural activity of pre-existing natural plans and relate it to specific control actions on a device. Examples of natural plans for BMI control are the imagination, planning, or execution of specific motor commands or limb movements. Additionally, the modulation of a mental state such as relaxed/meditative or attentive/aroused can also be natural plans used for a BMI. These plans can be decoded by analyzing shifts in the amplitudes of the signal or specific EEG frequency bands.

Although the decoder approach has shown remarkable performance results, it has also underlined some of its issues. In particular, authors have recently started to question the attention paid to the development of the classification algorithms of natural plans while overlooking the subject's role in the BMI loop (Lotte et al., 2013; McFarland and Wolpaw, 2018; Perdikis et al., 2018). Decoding pre-existent natural plans comes with a few problems. The first is the assumption that the intended plan is always generated in a similar way, and expressed by similar neural activity. The task's performance will depend on the stability of the natural plan and its corresponding brain activity. As long as the activity is kept sufficiently constant, the algorithm will be able to classify it according to the categories it was trained on. However, as soon as it changes, the algorithm will no longer be able to recognize it and will need to be retrained. Changes from day to day in the EEG when performing the natural plans are frequent, thus affecting the decoder's performance and requiring its recurrent adaptation. A second problem is more fundamental and arises from the actual design approach to BMIs. When subjects use a BMI to receive continuous feedback of activity and accomplish a goal in a neuroprosthetic task, e.g., moving a cursor on a screen, they are readily confronted with the fact that the neuroprosthetic is not the natural limb or mental state that they are used to control. In fact, the neuroprosthetic is an entirely novel limb, and the brain needs to learn to adapt to this new situation (Carmena et al., 2003; Ganguly and Carmena, 2009; Ganguly et al., 2011). If a neuroprosthetic skill is similar to introducing a novel limb in the system, then why would we require the subjects to control it through pre-established natural plans? We know that animals have the striking capacity to adapt to their environment, selecting neural activity that shapes actions that are optimized to increase rewards (Athalye et al., 2018; Costa, 2011). Then, why not exploit this capacity and design BMIs that fully capitalize on this property of our brains? This is where the learning approach can be essential.

The learning approach takes on these two problems of the decoder approach by shifting the role of adaptation to the subject. As introduced in chapter 1, the learning approach uses a fixed transcoder that needs to be learned by the brain. This transcoder is an entirely new pathway between activity and a prosthetic skill. Since it is not selected for its link to an *a priori* natural motor plan the brain needs to adapt to the transcoder and the transformation needs to be learned *de novo* (Carmena, 2013; Costa, 2011). Learning to establish a new link between the brain activity and the control of an effector through a fixed transform is much like having a new spinal cord directing the transformed brain activity to a new limb. Previous studies have shown that animals can learn a fixed, arbitrary transcoder of neural activity (Athalye et al., 2018; Clancy et al., 2014; Koralek et al., 2012). These studies have implicated brain structures such as the motor cortex, and striatum as playing important roles in establishing new neural patterns in BMI tasks, similar to what happens during motor skill learning (Barnes et al., 2005; Costa et al., 2004; Jin and Costa, 2010; Karni et al., 1998; Yin et al., 2009). In one of these studies (Koralek et al., 2012), animals learned to modulate the pitch of a speaker, i.e., the neuroprosthetic skill, which is dependent on the differential activity of two ensembles of cells in the motor cortex, in order to get sucrose or pellet rewards. Our work expands on the results of those studies, implementing a similar operant learning approach in a human BMI task using EEG.

Here, we developed a task that uses a fixed transcoder, constructed from an original rare EEG pattern that depends on four frequency bands. The transcoder was not initially related to any mental or motor task and thus had to be learned *de novo* in order to increase rewards in the task. We showed that subjects increased task performance over two weeks, i.e., learned the transcoder, and became more in control of the arbitrary EEG pattern. We showed that there was a phase of rapid improvement in early training, followed by a phase of slower learning. This learning profile is also typically observed in motor skill learning (Costa et al., 2004; Karni et al., 1998), further strengthening the link between the BMI learning approach and the learning of a new motor skill. As expected, learning could not be seen when subjects were not provided with the feedback of their transformed activity.

We also demonstrated subjects' capacity to recall the learning after a three-week training intermission during a consolidation test, showing that task performance did not drop after the long training break and could be readily recalled. This last result is important for two reasons. Firstly, it shows how this BMI approach can be valuable for real-life scenarios. Being able to recall a learned skill and having it readily available would be paramount if we want to introduce such technology in the daily control of devices. Retraining a classifier to account for pattern changes after training intermission is not ideal for such applications. Secondly, the fact that the learned transcoder was able to be recalled after a long training intermission gives confidence to the robustness of the consolidation. This can be important when other transcoders are introduced and need to be learned. Being able to keep the consolidated learning of the first transcoder is crucial if we want BMIs to achieve the control of multiple degrees of freedom. Additionally, the results of the re-test after more than two years of training intermission, despite the few subject points, suggested that learning could still be recalled, further supporting the robustness of the consolidation.

Importantly, we observed no significant changes in EMG signals before and during target reach, as measured by external electrodes around the eyes with a subset of the subjects during the experiment. We do see, however, evident changes in EMG after target reach, as subjects relax and prepare to start a new trial. Furthermore, when conducting a subset of experiments where the cursor position would not be updated if the algorithm identified an artifact condition, we still observed the subjects' capacity to perform the task. These data suggest that subjects do not rely on physical movements to learn the task and continuously control the cursor. However, it is difficult to exclude the possibility that subjects use some movement to generate neural activity and drive the cursor. A possible way of testing such a scenario would be to perform the task in patients with complete locked-in syndrome (CLIS) and evaluate whether the increase in performance could still be seen.

We also evaluated how the subjects performed the task. For that, we tested different performance measures that had not been stated as the primary task objective, but still could be thought to be related to task performance. Studies have shown that brain activity is refined with training (Athalye et al., 2018; 2017; Costa, 2011). The basal-ganglia reinforces inputs to the cortex, which lead to the co-activation of task-relevant neurons, and the refining of their dynamics (Koralek et al., 2012). Task-unrelated activity, on the other hand, is not reinforced as much and is thus seen to decrease with training (Athalye et al., 2018; Ganguly and Carmena, 2009). In this study we showed that with training subjects were able to increase the percentage of time spent in the correct direction. This result helped to understand that the control of the EEG pattern happens even when targets had not been reached. We could also further test this observation by analyzing the changes in cursor position distribution. In these analyses, we showed that the difference in cursor position distributions between up and down trials became more distinct with training, moving into the direction of the target. Increasing the separation of the distributions implies that the learning of the EEG pattern becomes more refined with training. Being able to understand the subject's intent during the trial, even at times when the correct target has not been reached, could play a significant role in the use of BMI for real-world application. This would be particularly important if one were to move in the direction of mutual learning, where both the subject and the algorithm adapt (Carmena and Cohen, 2013; Dangi et al., 2014; 2013; Kim et al., 2006; Gilja et al., 2012; Perdikis et al., 2018). For example, (Dangi et al., 2013) proposed the implementation of a closed-loop decoder adaptation (CLDA) that uses information about the task objective to fit the decoder to the subject's activity patterns. Using such approaches, the transcoder could be tweaked to approximate the subjects' intentions during the trial without largely affecting the performance and learning of the subject.

Combining operant-learning with decoder adaptation and even with shared-control between the algorithm and the subject (Kim et al., 2006) could lead to increased performance in tasks, and provide the practical efficiency needed for real-world implementations. As described in chapter 1, however, one possible difficulty in this approach is to understand when to change and how to change the decoder parameters without affecting the subject's capacity to modulate their neural activity and still increase task performance. The combination of the adaptation in both agents (algorithm and subject) in such BMI closed-loops needs to be carefully considered in order to account for the problem of the moving-target and allow for robust and high-performing BMIs.

Another important topic to discuss within this dissertation is the choice of the transcoder. All subjects used the same transformation of neural activity to the cursor position, changing only the electrodes used for each subject and the position of the targets. Both properties were calculated before the first day of training and maintained constant throughout training; as mentioned before, the target position was allowed to change as an offset in very particular conditions, but their distance to the center was always constant, thus not changing the task and maintain it unbiased. Was there anything specific to this transcoder that led to the positive results we reported? Would subjects have learned any other transcoder?

We can address each of the questions independently. For that, we must first review the reasons that led to the choice of this particular transcoder. When choosing the transcoder we established a few *a priori* requirements:

1) the decoder should be robust and shouldn't depend on the power of only one frequency band, which could probably be controlled by changes of mental state, 2) it should change smoothly in time, providing relevant feedback to the user, 3) it should be resistant to significant motor artifacts, such as moving the head, chewing or moving the eyes, and 4) if possible, it shouldn't need the use of noise extraction during online control, such as Independent Component Analysis (ICA) (Delorme et al., 2007; Makeig et al., 1996). Although different transcoders were tested at first, the transcoder we ended up using met the above criteria. Additionally, previous findings had reported that Local Field Potentials (LFP) measured in the motor cortex and striatum of rodents showed a strong correlation of the gamma*theta/delta*beta index with dopaminergic activity (Costa et al., 2006). Given that this particular index is a naturally occurring frequency in the brain and is correlated with dopaminergic activity, which has been linked to motivation and learning (Berke, 2018), there is a higher likelihood that subjects would be able to learn this transcoder.

Regarding the question of whether subjects could have learned a different transcoder, it is difficult to answer without further investigations. However, to the best of our knowledge, there is nothing particular in this transcoder that would make it unique. Thus, we would assume we can find other decoders that meet the requirements stated above and that subjects could also learn. Targets for different decoders would still need to be calculated so that the operant learning protocol would provide enough rewards to reinforce the learning. With this transcoder, we observed that when reaching the targets, the four EEG frequency bands were modulated differently from the EEG activity during pre-trial periods, and each of the bands was modulated in the direction that facilitated target crossing. This was not seen, however, during runs without feedback. It would be interesting to evaluate if subjects would still be able to learn the transcoder if some of the bands were inverted, or if their frequency ranges changed.

Despite pointing out in chapter 1 that BMIs can hold a promise for patients suffering from neurological injuries and movement disorders, this topic was not fully addressed in this thesis. Our experiments in chapter 2 were conducted with healthy individuals. In chapter 3, we demonstrated the practical use of our approach with a healthy subject in an application that would probably not have the highest demand by patients suffering from neurological disorders that limit their mobility, as discussed in chapter 1. Further work on this topic would benefit from investigating whether this approach can be used as an alternative to the currently implemented non-invasive BMI methods for patients with movement disorders. In particular, testing the paradigm with locked-in syndrome (LIS) and complete locked-in syndrome (CLIS) patients would be instrumental in understanding whether these patients can learn a new EEG skill. Studies have reported that patients that attempted to used BMIs after they had entered CLIS state were not able to generate consistent voluntary signals to control the BMI (Birbaumer, 2006). Our paradigm has shown stability across days and is independent of motor activity, which would be an essential property for application with LIS and CLIS patients. Event related potentials (ERP) measured in CLIS patients show reactions to different stimuli, suggesting that some processing modules are still intact (Hinterberger et al., 2005a; 2005b; Wilhelm et al., 2006). However, motor imagery tasks conducted with such patients do not always seem to result in high performing control (*ibid.*). One possible explanation is that by not being able to move, these patients may lose the contingency between physiological behavior and its consequences. In such cases, extinction can set in due to the lack of reinforced activity. It would thus be interesting to test whether these patients could still be able to acquire BMI skills through an operant learning approach as the one described above.

In chapter 3, part A, we showed a practical demonstration of the operant learning BMI paradigm. The main objective was first to prove that the paradigm could be used in the airplane simulator. For that, we engineered flight controller parameters that would appropriately translate the outcome from the learned transcoder into a command to control the airplane simulator. The demonstration was successful, showing control over several runs to direct the aircraft to specific fixed headings and to track a heading bug. These demonstrations offered a useful proof of concept but would need to be replicated to evaluate the extent of control and the generalization to other subjects and flight profiles. Nevertheless, we were able to show the generalization of the learned transcoder to other tasks and control of a different dimension of movement than the one that had been trained initially (horizontal in the aircraft vs. vertical in the BMI training).

In chapter 3, part B, we briefly described on-going work related to the development of a new EEG headset. The currently available EEG systems that provide acceptable SNR for research and real-world applications are still cumbersome and expensive. Our objective with this development is to facilitate access to high-quality signals without the requirement of complex systems that require long setups and dedicated software. We described an EEG headset using active dry-electrodes, capable of processing EEG data in real-time on the headset through a fixed transcoder like the one described in chapter 2. The transformed signal is sent wirelessly to a device to be controlled without the need for extra analysis software. We predict such systems may open the access to EEG data to the general public, and the use and improvement of EEG-based BMIs.

Summing up, the findings in this dissertation show that operant learning of an EEG-based task is possible and that it can be consolidated and recalled after long training intermissions. We also showed an application of this BMI approach in a real-world scenario of controlling an aircraft. Finally, we described the on-going development of an EEG headset capable of providing high-quality EEG signals and processing them locally in the system. This work thus expands on the currently available non-invasive BMI paradigms and opens up the possibility for future investigations in this field.

REFERENCES

Athalye, V.R., Santos, F.J., Carmena, J.M., and Costa, R. (2018). Evidence for a neural law of effect. Science 359, 1024–1029.

Athalye, V.R., Ganguly, K., Costa, R.M., and Carmena, J.M. (2017). Emergence of Coordinated Neural Dynamics Underlies Neuroprosthetic Learning and Skillful Control. Neuron 93, 955–970.e955.

Ball, T., Kern, M., Mutschler, I., Aertsen, A., and Schulze-Bonhage, A. (2009). Signal quality of simultaneously recorded invasive and non-invasive EEG. NeuroImage 46, 708–716.

Barnes, T.D., Kubota, Y., Hu, D., Jin, D.Z., and Graybiel, A.M. (2005). Activity of striatal neurons reflects dynamic encoding and recoding of procedural memories. Nature 437, 1158–1161.

Benabid, A.L., Costecalde, T., Eliseyev, A., Charvet, G., Verney, A., Karakas, S., Foerster, M., Lambert, A., Morinière, B., Abroug, N., et al. (2019). An exoskeleton controlled by an epidural wireless brain–machine interface in a tetraplegic patient: a proof-of-concept demonstration. The Lancet Neurology 1–11.

Berke, J.D. (2018). What does dopamine mean? Nat. Neurosci. 21, 787–793.

Birbaumer, N., Ghanayim, N., Hinterberger, T., Iversen, I., Kotchoubey, B., Kübler, A., Perelmouter, J., Taub, E., and Flor, H. (1999). A spelling device for the paralysed. Nature 398, 297–298.

Birbaumer, N. (2006). Breaking the silence: brain-computer interfaces (BCI) for communication and motor control. Psychophysiology 43, 517–532.

Carmena, J.M. (2013). Advances in neuroprosthetic learning and control. PLoS Biol 11, e1001561.

Carmena, J.M., and Cohen, L.G. (2013). Brain-machine interfaces and transcranial stimulation: future implications for directing functional movement and improving function after spinal injury in humans (Elsevier B.V.).

Carmena, J.M., Lebedev, M.A., Crist, R.E., O'Doherty, J.E., Santucci, D.M., Dimitrov, D.F., Patil, P.G., Henriquez, C.S., and Nicolelis, M.A.L. (2003). Learning to control a brain-machine interface for reaching and grasping by primates. PLoS Biol 1, E42.

Clancy, K.B., Koralek, A.C., Costa, R.M., Feldman, D.E., and Carmena, J.M. (2014). Volitional modulation of optically recorded calcium signals during neuroprosthetic learning. Nature Publishing Group 17, 1–4.

Collinger, J.L., Wodlinger, B., Downey, J.E., Wang, W., Tyler-Kabara, E.C., Weber, D.J., McMorland, A.J.C., Velliste, M., Boninger, M.L., and Schwartz, A.B. (2013). High-performance neuroprosthetic control by an individual with tetraplegia. Lancet 381, 557–564.

Costa, R.M. (2011). A selectionist account of de novo action learning. Curr. Opin. Neurobiol. 21, 579–586.

Costa, R.M., Cohen, D., and Nicolelis, M.A.L. (2004). Differential corticostriatal plasticity during fast and slow motor skill learning in mice. Curr. Biol. 14, 1124–1134.

Costa, R.M., Lin, S.-C., Sotnikova, T.D., Cyr, M., Gainetdinov, R.R., Caron, M.G., and Nicolelis, M.A.L. (2006). Rapid alterations in corticostriatal ensemble coordination during acute dopamine-dependent motor dysfunction. Neuron 52, 359–369.

Dangi, S., Gowda, S., Moorman, H.G., Orsborn, A.L., So, K., Shanechi, M., and Carmena, J.M. (2014). Continuous closed-loop decoder adaptation with a recursive maximum likelihood algorithm allows for rapid performance acquisition in brain-machine interfaces. Neural Comput 26, 1811–1839.

Dangi, S., Orsborn, A.L., Moorman, H.G., and Carmena, J.M. (2013). Design and Analysis of Closed-Loop Decoder Adaptation Algorithms for Brain-Machine Interfaces. Neural Comput 25, 1693–1731.

Delorme, A., Sejnowski, T., and Makeig, S. (2007). Enhanced detection of artifacts in EEG data using higher-order statistics and independent component analysis. NeuroImage 34, 1443–1449.

Donati, A.R.C., Shokur, S., Morya, E., Campos, D.S.F., Moioli, R.C., Gitti, C.M., Augusto, P.B., Tripodi, S., Pires, C.G., Pereira, G.A., et al. (2016). Long-Term Training with a Brain-Machine Interface-Based Gait Protocol Induces Partial Neurological Recovery in Paraplegic Patients. Sci Rep 6, 30383.

Fetz, E.E. (1969). Operant Conditioning of Cortical Unit Activity. Science 163, 955–958.

Ganguly, K., and Carmena, J.M. (2009). Emergence of a stable cortical map for neuroprosthetic control. PLoS Biol 7, e1000153.

Ganguly, K., Dimitrov, D.F., Wallis, J.D., and Carmena, J.M. (2011). Reversible large-scale modification of cortical networks during neuroprosthetic control. Nature Publishing Group 14, 662–667.

Gilja, V., Nuyujukian, P., Chestek, C.A., Cunningham, J.P., Yu, B.M., Fan, J.M., Ryu, S.I., and Shenoy, K.V. (2012). A brain-machine interface control algorithm designed from a feedback control perspective. Conf Proc IEEE Eng Med Biol Soc 2012, 1318–1322.

Goldenholz, D.M., Ahlfors, S.P., Hämäläinen, M.S., Sharon, D., Ishitobi, M., Vaina, L.M., and Stufflebeam, S.M. (2009). Mapping the signal-to-noise-ratios of cortical sources in magnetoencephalography and electroencephalography. Hum. Brain Mapp. 30, 1077–1086.

Hinterberger, T., Birbaumer, N., and Flor, H. (2005a). Assessment of cognitive function and communication ability in a completely locked-in patient. Neurology 64, 1307–1308.

Hinterberger, T., Wilhelm, B., Mellinger, J., Kotchoubey, B., and Birbaumer, N. (2005b). A Device for the Detection of Cognitive Brain Functions in Completely Paralyzed or Unresponsive Patients. IEEE Trans Biomed Eng 52, 211–220.

Hochberg, L.R., Bacher, D., Jarosiewicz, B., Masse, N.Y., Simeral, J.D., Vogel, J., Haddadin, S., Liu, J., Cash, S.S., van der Smagt, P., et al. (2012). Reach and grasp by people with tetraplegia using a neurally controlled robotic arm. Nature 485, 372–375.

Jin, X., and Costa, R.M. (2010). Start/stop signals emerge in nigrostriatal circuits during sequence learning. Nature 466, 457–462.

Kamiya, J. (1969). Operant control of EEG alpha rhythm and some of its reported effects on consciousness. In Allered States of Consciousness, C.T. Tart, pp. 507–517.

Karni, A., Meyer, G., Rey-Hipolito, C., Jezzard, P., Adams, M.M., Turner, R., and Ungerleider, L.G. (1998). The acquisition of skilled motor performance: Fast and slow experience-driven changes in primary motor cortex. Proceedings of the National Academy of Sciences 95, 861–868.

Kim H.K., Biggs S.J., Schloerb D.W., Carmena J.M., Lebedev M.A., Nicolelis M.A.L. and Srinivasan M.A. (2006) Continuous shared control stabilizes reach and grasping with brain-machine interfaces. IEEE Transactions on Biomedical Engineering 53(6), pp. 1164-1173.

Koralek, A.C., Jin, X., Long, J.D., Costa, R.M., and Carmena, J.M. (2012). Corticostriatal plasticity is necessary for learning intentional neuroprosthetic skills. Nature 483, 331–335.

Lotte, F., Bougrain, L., Cichocki, A., Clerc, M., Congedo, M., Rakotomamonjy, A., and Yger, F. (2018). A review of classification algorithms for EEG-based brain–computer interfaces: a 10 year update. J. Neural Eng. 15, 031005–031029.

Lotte, F., Larrue, F., and Mühl, C. (2013). Flaws in current human training protocols for spontaneous Brain-Computer Interfaces: lessons learned from instructional design. Front Hum Neurosci 7, 568.

Makeig, S., Bell, A.J., Jung, T., and Sejnowski, T.J. (1996). Independent component analysis of electroencephalographic data.

McFarland, D.J., and Wolpaw, J.R. (2018). Brain–computer interface use is a skill that user and system acquire together. PLoS Biol 16, e2006719.

Müller, K.-R., Tangermann, M., Dornhege, G., Krauledat, M., Curio, G., and Blankertz, B. (2008). Machine learning for real-time single-trial EEG-analysis: From brain–computer interfacing to mental state monitoring. J. Neurosci. Methods 167, 82–90.

Perdikis, S., Tonin, L., Saeedi, S., Schneider, C., and Millan, J.D.R. (2018). The Cybathlon BCI race: Successful longitudinal mutual learning with two tetraplegic users. PLoS Biol 16, e2003787–28.

Wilhelm, B., Jordan, M., and Birbaumer, N. (2006). Communication in locked-in syndrome: Effects of imagery on salivary pH. Neurology 67, 534–535.

Yin, H.H., Mulcare, S.P., Hilário, M.R.F., Clouse, E., Holloway, T., Davis, M.I., Hansson, A.C., Lovinger, D.M., and Costa, R.M. (2009). Dynamic reorganization of striatal circuits during the acquisition and consolidation of a skill. Nat. Neurosci. 12, 333–341.

ITQB-UNL | Av. da República, 2780-157 Oeiras, Portugal
Tel (+351) 214 469 100 | Fax (+351) 214 411 277

www.itqb.unl.pt